

# SRI International 0574

Distribution Unlimited

Final Report • October 1997

## CHEMICAL MECHANISMS OF SHOCK INITIATION OF NTO

Prepared by:

D. F. McMillen, David C. Erlich, Chun He,  
Christopher H. Becker, and Donald A. Shockey  
Molecular Physics Laboratory  
SRI International

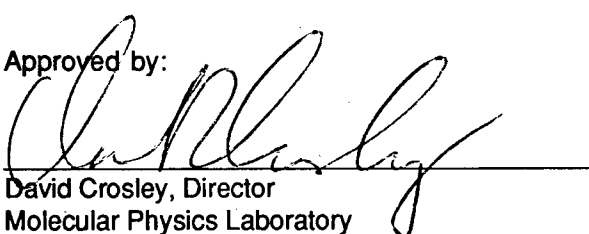
Contract No. F49620-94-C-0055  
MP 97-109

Prepared for:

Air Force Office of Scientific Research  
Building 410  
Bolling Air Force Base  
Washington, DC 20332-6448

Attn: Dr. Michael R. Berman  
Director of Chemistry and Material Sciences

Approved by:

  
David Crosley, Director  
Molecular Physics Laboratory

19971103 099

**DISTRIBUTION STATEMENT A**

Approved for public release;  
Distribution Unlimited

DTIC QUALITY INSPECTED 3

# REPORT DOCUMENTATION PAGE

Form Approved  
OMB No. 0704-0188

Public reporting burden for this collection of information is estimated to average 1 hour per response, including the time for reviewing instructions, searching existing data sources, gathering and maintaining the data needed, and completing and reviewing the collection of information. Send comments regarding this burden estimate or any other aspect of this collection of information, including suggestions for reducing this burden, to Washington Headquarters Services, Directorate for Information Operations and Reports, 1215 Jefferson Davis Highway, Suite 1204, Arlington, VA 22202-4302, and to the Office of Management and Budget, Paperwork Reduction Project (0704-0188), Washington, DC 20503.

1. AGENCY USE ONLY (Leave blank)		2. REPORT DATE 970900	3. REPORT TYPE AND DATES COVERED Final 940615-970614	
4. TITLE AND SUBTITLE  Chemical Mechanisms of Shock Initiation of NTO			5. FUNDING NUMBERS  F49620-94-C-0055	
6. AUTHOR(S) Donald F. McMillen, David C. Erlich, Chun He, Christopher H. Becker, and Donald A. Shockey			61102F 2303/ES	
7. PERFORMING ORGANIZATION NAME(S) AND ADDRESS(ES)  SRI International 333 Ravenswood Avenue Menlo Park, CA 94025-3493			8. PERFORMING ORGANIZATION REPORT NUMBER  PYU-6134	
9. SPONSORING/MONITORING AGENCY NAME(S) AND ADDRESS(ES)  Air Force Office of Scientific Research Bolling Air Force Base Washington, DC 20332-6445			10. SPONSORING/MONITORING AGENCY REPORT NUMBER  NL	
11. SUPPLEMENTARY NOTES				
12a. DISTRIBUTION/AVAILABILITY STATEMENT  Distribution unlimited.			12b. DISTRIBUTION CODE	
13. ABSTRACT (Maximum 200 words) A powerful analytical tool has been developed for in-situ, real-time measurement of the thermally and mechanically induced transient decomposition processes of energetic materials, and has been applied to the new, insensitive high explosive, nitro-1,2,4-triazol-5-one (NTO). Modification of the vacuum chamber of a laser-desorption mass spectrometry apparatus has enabled us to perform simple-shear and compressive fracture of pressed pellets directly beneath the sampling region: fragments spontaneously emitted from fractured NTO pellets are measured by single-photon ionization (SPI) time-of-flight mass spectrometry. The fracture-induced fragments of NTO are dominated by a single peak, m/z 99, which is completely absent in either the thermal- or laser-desorption spectra obtained in the same apparatus. This difference suggests that under the marginal stress of subcritical mechanical fracture, intermediates of mass 100 and/or 101 are diverted to the closed-shell, relatively stable species at mass 99, which then tends to accumulate, rather than going on to produce a next generation of unstable intermediates at m/z 85, 71, and 43. Thus, in its first use, this combination of techniques has enabled identification of intermediates not previously observed in NTO decomposition and allowed us to propose a reasonable sequence of reactions that involves all of these intermediates, reconciles a substantial portion of previous slow thermal decomposition data, and potentially explains the initiation insensitivity of NTO as resulting from diversion to a relatively stable "dead-end" species.				
14. SUBJECT TERMS Energetic Materials Shock Initiation Stress-Induced Chemistry			15. NUMBER OF PAGES	
Explosives Laser Desorption			16. PRICE CODE	
Mechanisms Mass Spectrometry				
17. SECURITY CLASSIFICATION OF REPORT  UNCLASSIFIED	18. SECURITY CLASSIFICATION OF THIS PAGE  UNCLASSIFIED	19. SECURITY CLASSIFICATION OF ABSTRACT  UNCLASSIFIED	20. LIMITATION OF ABSTRACT  Unlimited	

UNCLASSIFIED

SECURITY CLASSIFICATION OF THIS PAGE

CLASSIFIED BY:

N/A since Unclassified.

DECLASSIFY ON:

N/A since Unclassified.

SECURITY CLASSIFICATION OF THIS PAGE

UNCLASSIFIED

## EXECUTIVE SUMMARY

The general objective of this project was to use laser desorption mass spectrometry (LDMS) and certain specially designed modifications to examine the sequence of chemical steps that results from the mechanical stress used to initiate the detonation of explosives. In support of that objective, we performed, for the first time, real-time molecular detection of intermediates during fracture-induced decomposition of the explosive NTO (3-nitro-1,2,4-triazol-5-one) and combined these results with those from slow- and rapid-heating thermal decomposition, obtained in the same apparatus.

Particles spontaneously emitted from NTO pellets sheared or compressively impacted *in situ* were measured by single-photon (118-nm) ionization (SPI) time of flight mass spectrometry, using a modified version of SRI's surface analysis by laser-ionization (SALI) apparatus. The substrate and major intermediates were ionized without photofragmentation: the mass spectra provided true relative concentrations of registered masses.

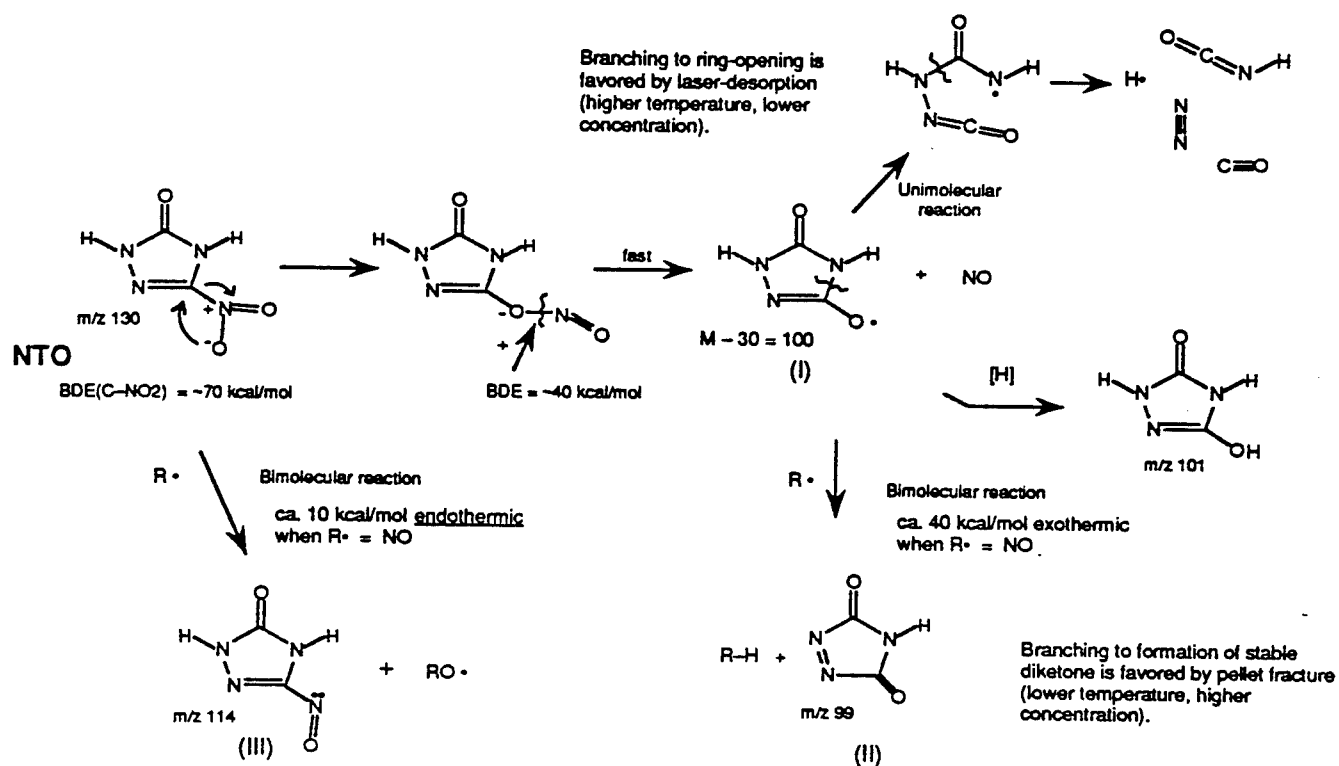
For comparison, we also obtained mass spectra under conditions of slow thermal decomposition and laser ablation-induced thermal decomposition. Comparisons of spectra obtained with and without laser desorption and as a function of temperature demonstrated that the sequences of ions observed under laser desorption conditions are the result of thermal decomposition, not fragmentation of the NTO molecular ion. As a result of this lack of ion fragmentation, the laser-desorption MS measurements, by themselves, produced a sequence of identifiable intermediates that have not previously been reported for NTO decomposition and that allow us to present a plausible explanation of a substantial amount of literature data on NTO decomposition that previously appeared to be in conflict.

The shear-induced- and compressive-impact-induced spectra, observed *in-situ* without laser desorption, are dominated by a peak at  $m/z$  99, which is related to peaks in the thermal decomposition LD-mass spectra, but does not itself appear in those spectra.  $M/z$  99 is assigned to the closed-shell triaza-diketone produced by a nitro-nitrite rearrangement of NTO, followed by NO loss and then by rapid *bimolecular* H-atom removal. The stability of the cyclic diketone intermediate thus generated could help to explain the shock insensitivity of NTO. Laser-desorption spectra were also obtained on samples recovered from marginally subcritical dropweight impact tests.

The sequence of thermally generated fragments is dominated by M-16, M-30, M-45, M-46, and M-59 (giving decomposition products/intermediates at 114, 99/100/101, 85, 84, and 71 Da).



This series suggests several decomposition pathways, all starting with the same nitro-nitrate rearrangement and NO loss as the shear-induced decomposition. However, under the lower-density, but higher temperature, thermal- or laser-desorption conditions, subsequent bimolecular H-atom removal to produce the closed-shell diketone is evidently slower than unimolecular ring-opening adjacent to the carbonyl group. Key aspects of this proposed decomposition network are shown in the abbreviated set of reactions in Scheme 1. We show how this sequence satisfactorily explains (1) the "initial" formation of CO<sub>2</sub> previously reported, (2) the results of nitrogen double-labeling experiments, and (3) the fact that neither NO<sub>2</sub> nor HONO has been seen as a substantial initial product of NTO decomposition.



Scheme 1. Principal reactions in proposed NTO decomposition sequence following a nitro-nitrite rearrangement.

In summary, we believe the capability developed and exploited in this project offers the potential for sensitive and very direct monitoring of the sequence of reactions that occurs as a result of mechanical energy input to various explosive and nonexplosive materials. The difficulty of fully elucidating the physical and chemical mechanisms of initiation remains. However, in the first use of this technique, we demonstrated (1) monitoring of a relatively new explosive under both thermal- and fracture-induced decomposition conditions, (2) observation of intermediates not previously detected, and (3) the use of these data to propose a reasonable sequence of reactions that

involves all these intermediates, reconciling a substantial portion of previous slow thermal decomposition data, and potentially explaining the initiation insensitivity of NTO.

Professional personnel contributing to the research effort this year included David C. Erlich, Chun He, Donald F. McMillen, Christopher H. Becker, and Donald A. Shockey.

Three publications were supported by this contract. The manuscript "Fracture-Induced and Thermal Decomposition of NTO Using Laser-Ionization Mass Spectrometry" is in press in the journal *Combustion and Flame*. The manuscript "Real-Time Photoionization Mass Spectrometry of Fracture-Induced Decomposition of a High Explosive" (Appendix B) has been prepared for submission to *Science*. The manuscript "Modification of a Laser-Desorption Time-of-Flight Mass Spectrometry apparatus for Real-Time Photoionization Mass Spectrometry of Fracture-Induced Decomposition" (Appendix C) has been prepared for submission to *Review of Scientific Instruments*.

## CONTENTS

EXECUTIVE SUMMARY.....	iii
INTRODUCTION AND OBJECTIVES.....	1
STATUS OF EFFORT.....	3
ACCOMPLISHMENTS.....	5
Background .....	5
General Experimental Approach .....	5
Test Procedure Rationale.....	6
<i>In-Situ</i> Simple Shear Testing with Millisecond Delay Times.....	6
<i>In-Situ</i> Simple Shear Testing with Microsecond Delay Times.....	9
<i>In-Situ</i> Compressive Impact Tests.....	9
Apparatus Modifications and Experimental Procedures .....	10
The SALI <i>In-Situ</i> Test Fixture .....	10
Fixture for <i>In-Situ</i> Simple-Shear Tests with Millisecond Delay Times.....	11
Fixture for <i>In-Situ</i> Simple-Shear Tests with Microsecond Delay Times.....	11
Fixture for <i>In-Situ</i> Compressive Impact Tests.....	15
NTO Sample Preparation.....	15
Diagnostic Tests for Pellet Fracture Fixtures .....	19
<i>In-Situ</i> Fracture Procedures.....	29
Test Results .....	31
Shear-Induced NTO Decomposition on the 100- $\mu$ s Time Scale .....	32
Compressive-Impact-Induced NTO Decomposition .....	35
Post-Examination of Subcritically Shocked NTO.....	39
General Mechanisms of Stress-Induced Chemical Reaction.....	40
CONCLUSIONS.....	45
REFERENCES.....	47
<b>Appendices</b>	
A    FRACTURE-INDUCED AND THERMAL DECOMPOSITION OF NTO USING LASER IONIZATION MASS SPECTROMETRY .....	A-1
B    REAL-TIME PHOTOIONIZATION MASS SPECTROMETRY OF FRACTURE-INDUCED DECOMPOSITION OF A HIGH EXPLOSIVE .....	B-1
C    AN APPARATUS FOR STUDY OF STRESS-INDUCED CHEMISTRY IN EXPLOSIVE AND NON-EXPLOSIVE MATERIALS .....	C-1

## FIGURES

1	Schematic view of <i>in-situ</i> test fixture on SALI apparatus for use in dynamic fracture tests .....	7
2	Detail of SALI <i>in-situ</i> test fixture for simple-shear tests with millisecond delay times .....	13
3	Detail of SALI <i>in-situ</i> test fixture for simple-shear tests with microsecond delay times.....	14
4	Detail of SALI <i>in-situ</i> test fixture for compressive impact tests.....	17
5	Cross-sectional view of NTO pressing fixture with conical die insert .....	20
6	High-speed video images of NTO SALI impact test and micro-photograph of conical NTO specimen tip.....	21
7	Displacement histories of spring-driven linear-motion feedthrough shaft for four velocity tests of shear fixture.....	24
8	High-speed video images of NTO dynamic shear test and photograph of fractured specimen .....	25
9	Timeline for events during <i>in-situ</i> dynamic shear test of NTO.....	28
10	Displacement histories of spring-driven linear motion feedthrough shaft in four SALI dynamic compression tests.....	30
11	Single-shot SALI spectrum of shear-induced fragment emission of NTO with nominal 30- $\mu$ s delay after crack completion .....	34
12	Single-shot SALI spectrum of compressive-impact-induced fragment emission of NTO with nominal 300- $\mu$ s delay after initial impact.....	36
13	Four-test average spectrum of compressive-impact-induced fragment emission of NTO .....	37

## REACTION SCHEMES

Scheme 1.	Principal reactions in proposed NTO decomposition sequence following a nitro-nitrite rearrangement.....	iv
Scheme 2.	Possible route to m/z 58 during fracture-induced decomposition.....	39

## INTRODUCTION AND OBJECTIVES

The overall objective of this project was to use laser-desorption mass spectrometry to identify the intermediates and pathways in the decomposition of the insensitive high explosive, NTO (3-nitro-1,2,4-triazol-5-one) so as to improve our understanding of the unusually low initiation sensitivity of this material. The specific objectives were to

- (1) Modify the laser desorption vacuum chamber so that the products of stress-induced decomposition could be monitored *in-situ*, in real time.
- (2) Subject NTO samples to a range of stresses, possibly including shear, tensile, and impact, while using laser desorption mass spectrometry (surface analysis by laser ionization, SALI) to identify and track the decomposition products generated in the stress-induced decomposition.
- (3) Perform post-examination, *ex-situ* experiments which the mechanical stress is much closer to threshold of initiation.
- (4) Determine, for comparison, the intermediates produced by slow and rapid heating in the mass-spectrometry chamber.
- (5) Use these data to clarify the NTO thermal decomposition mechanism and from that base to infer how various physical and chemical factors provide bottlenecks that limit the initiation sequence for NTO.

In the broadest terms, the objective was to use all of the above information to generalize about the characteristics of decomposition pathways that make a high explosive "insensitive."

These objectives were embodied in the Statement of Work, consisting of the following three tasks. Task 3 was to be performed as warranted by the results of the work in Year 1.

- Task 1: Prepare and stress NTO samples using techniques suitable for *in-situ* vacuum chamber operation and techniques for externally stressing samples for later spectroscopic examination.
- Task 2: Perform both *in-situ* and *ex-situ* analysis of stressed and shocked samples by a combination of SEM and SALI to provide subpicogram, 1- $\mu$ m resolution analysis of the products generated in hot spots.
- Task 3: Perform quantum mechanical calculations of nitroxyl radical or other selected product(s) identified in Task 2 as possible key intermediates in the hot spot ignition and growth processes.

## STATUS OF EFFORT

The results obtained in the project are described in three manuscripts included in this report as Appendices A, B, and C. The first of these manuscripts "Fracture-Induced and Thermal Decomposition of NTO Using Laser-Ionization Mass Spectrometry," is in press in the journal *Combustion and Flame*. The second and third manuscripts ("Real-Time Photoionization Mass Spectrometry of Fracture-Induced Decomposition of a High Explosive" and "Apparatus for Performing *in-situ* Real-Time Mass Spectrometry Measurements of the Products of Fracture-Induced Chemistry") will be submitted to the journals *Science* and *Review of Scientific Instruments*, respectively. The results described in these manuscripts are summarized in this report, together with some results not yet described in manuscripts for publication.

This effort was very successful in terms of (1) using laser desorption mass spectrometry (LDMS) to detect and identify intermediates of NTO thermal decomposition that had not been previously reported, (2) using these intermediates to suggest a decomposition mechanism that reconciles several sets of NTO literature data that otherwise seem inconsistent, (3) modifying the apparatus to obtain high signal-noise ratio spectra for fracture-induced decomposition, and (4) using these data to draw inferences about the origin of the unusual initiation insensitivity of NTO.

We extended this effort from shear tests at "long" delay times (milliseconds to seconds) to microsecond delay times with a modified shear orientation and to compressive impact, also with microsecond delay times. However, due to the greatly expanded time frame, we have not yet been able to determine the time-dependence of the fracture-induced emission as thoroughly on the microsecond scale.

The success so far achieved leaves very little doubt that single-photon-ionization, time-of-flight mass spectrometry represents the best way yet demonstrated to make real-time measurements of fracture-induced decomposition intermediates with high sensitivity and near-universal product detection capability and that this capability, when coupled with the more standard laser-desorption MS capability of the basic SALI system for following *thermal* decomposition, is a very powerful tool for understanding explosive decomposition and initiation.

## ACCOMPLISHMENTS

### BACKGROUND

The development of powerful and yet insensitive explosives is key to design of safer and more effective munitions. For nearly ten years, NTO (3-nitro-1,2,4-triazol-5-one) has been recognized as a potentially useful high explosive because of a calculated performance level approaching that of RDX, coupled with very low impact sensitivity and high kinetic thermal stability (Lee and Coburn, 1987). However, NTO's large failure diameter and the peculiar density-dependence of its detonation pressure in pressed formulations made it difficult to closely approach the calculated performance in early small-scale testing (Chapman, 1989). Apparently, the same physical and chemical factors that limit unwanted ignition and initiation can also make it difficult to achieve the detonation velocities and pressures that thermodynamic considerations indicate are possible.

Recently, Aubert (1994) showed that satisfactory performance levels can be achieved by using NTO of appropriate density. Nevertheless, the unusual behavior of NTO presents an opportunity to learn more about the kinetic bottlenecks that can prevent unwanted detonation but can also limit performance. Furthermore, a better understanding of the physical and chemical kinetic factors could substantially aid in formulating composites with other high explosives whose higher sensitivity might be reduced.

For an explosive, the coupling of mechanical energy to chemical decomposition and the ability of the ensuing chemical decomposition to generate enough energy to influence the flow and enhance the shock determine whether in any particular case an incident shock wave proceeds to a detonation. However, in spite of much effort over the years to examine the nature of "hot spots," scientists have not yet achieved a full understanding of the coupling of mechanical energy to chemical reaction. Moreover, for none of the organic explosive materials in common use has it yet been possible to determine the critical chemical steps that determine whether self-sustaining reaction is achieved.

### GENERAL EXPERIMENTAL APPROACH

In this project, we used a combination of mechanical stress and a state-of-the-art surface analysis technique to help determine the critical sequence of reactions for the insensitive explosive NTO. Our focus was on stress-induced chemistry, not only the initial reaction instigated by the

stress, but particularly the sequence of secondary reactions that either yield or fail to yield successful initiation. Because much less was known about the sequence of chemical intermediates generated during NTO decomposition than was known for other explosives, we also examined the thermal decomposition products of NTO, produced either by slow heating or by rapid heating during laser-desorption. For both the stress-induced and the thermally induced decomposition, we chose to use a mass spectrometric detection technique that is essentially "universal" in terms of product sensitivity and has the surface-selectivity desirable for examining exposed fracture surfaces, shear bands, and hot spots.

Surface analysis by laser ionization (SALI), developed at SRI (Becker and Gillen, 1984; Pallix et al., 1989) uses time-of-flight mass spectrometry to mass analyze material evolved from a sample surface under laser-desorption, thermal desorption, or argon- or gallium-ion sputtering. It differs from standard secondary-ion mass spectrometry (SIMS) principally in that, rather than relying on the so-called secondary ions generated in the highly energetic ion-beam- or laser-beam-ablation process, emitted neutral species are ionized by a 118-nm laser beam that passes directly over the sample surface and under the sampling cone. The 10.5-eV photons of this beam have enough energy to ionize almost any organic compound, but generally not enough excess energy to cause significant fragmentation. Furthermore, the ionization efficiencies differ very little from structure to structure, and SALI is not subject to the matrix effects that make for very large differences in sensitivities in SIMS analysis.

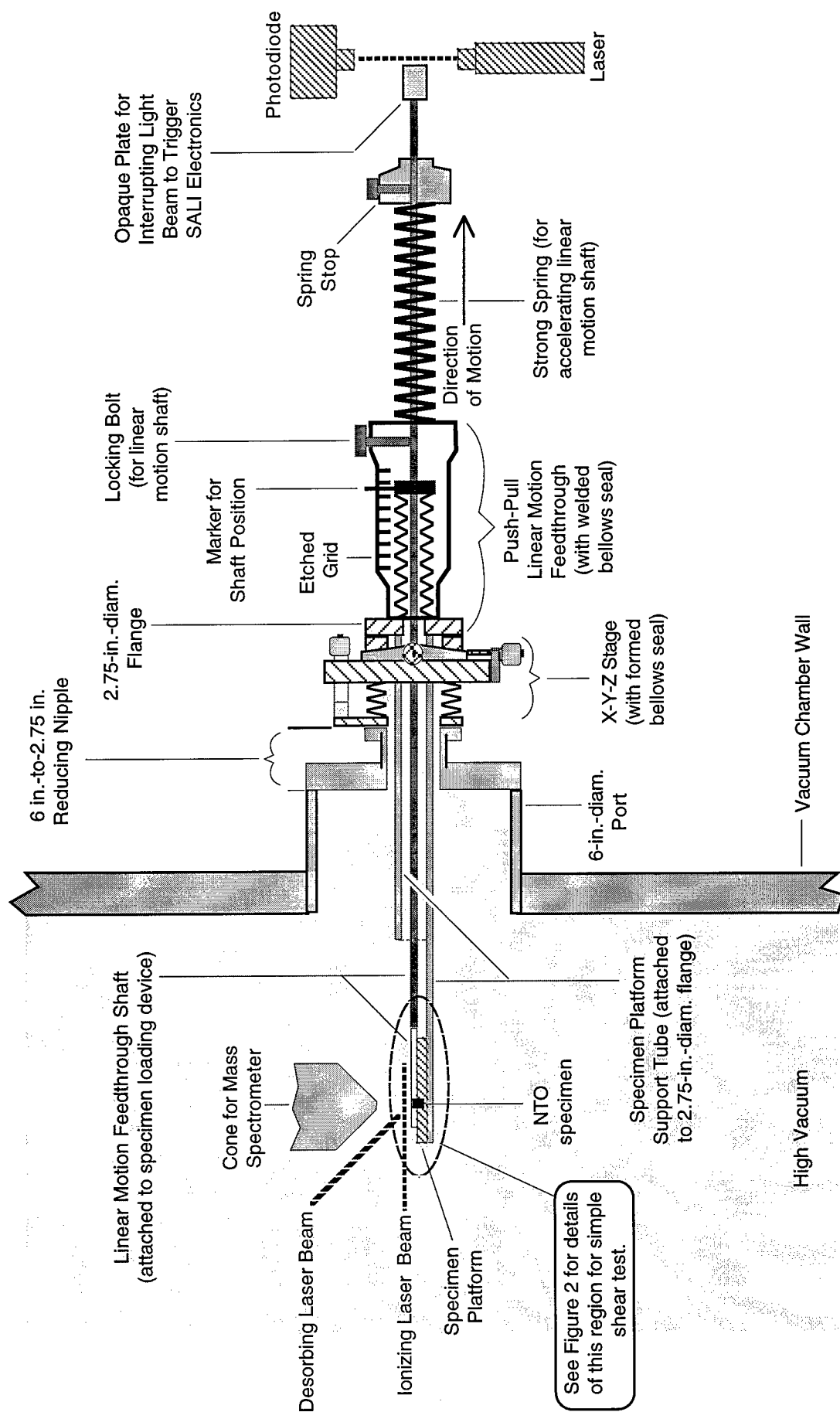
The SALI technique, as modified for measurement of *in-situ* shear-induced product measurement, is described in detail in Appendix C. Our discussion here is limited primarily to the modifications made and results achieved in the second and third years that enabled us to decrease the time delay between explosive pellet fracture and mass spectrum acquisition from the millisecond to the microsecond time scale and to perform *in-situ* fracture tests under conditions of compressive impact.

## TEST PROCEDURE RATIONALE

### *In-Situ* Simple Shear Testing with Millisecond Delay Times

For the first series of dynamic *in-situ* shear tests, as described in detail in Appendices A and C, the NTO specimens were placed beneath the ionizing laser beam and mass spectrometer cone with their axes in the vertical direction, and the cutting fixture, traveling at about 1.75 m/s, sheared a nearly horizontal slice through the specimen (see Figure 1). In this manner the new fracture surface was generated essentially perpendicular to the mass spectrometer flight axis; however, the cutter blade then had to clear the sheared face of the specimen before the ionizing





CAM-6134-5

Figure 1. Schematic view of *in-situ* test fixture on SALI apparatus for use in dynamic fracture tests.

Note: Both ionizing and desorbing laser beams enter at  $\approx 45^\circ$  from the plane of the paper.

laser could be triggered. Thus, the soonest we could begin taking SALI spectra was  $\approx 3$  ms after impact, which provided useful data for times  $\geq 3$  ms after impact, but allowed no observation of earlier evolution from the surface (molecular velocities in a high vacuum are of the order of mm/ $\mu$ s, so species that depart the fracture surface at the instant fracture is completed would travel beyond the mass spectrometer range in only a few microseconds).

The fact that the time constant for decay of the shear-induced emission is about 10 seconds suggests that some fragments were produced at substantial depths from the apparently monolithic fracture surfaces generated in these experiments. An expanded time window for fracture-induced spectra collection offered the opportunity to better understand the physical nature of the generation process as well as to learn as well how the distribution of NTO products may change throughout the microsecond to millisecond time range.

### ***In-Situ Simple Shear Testing with Microsecond Delay Times***

For the microsecond-delay *in situ* shear tests, the objective was to make SALI measurements as soon after impact as possible. We redesigned the test fixture so that we could observe the sheared face without having to wait for the shear cutter to clear the specimen.\* The cylindrical specimen (having the same dimensions as in the first series of tests) was now mounted beneath the ionizing beam and mass spectrometer cone with its axis in the horizontal, rather than the vertical, direction. The cutter sheared a nearly vertical slice through the specimen at a position directly below the ionizing laser and mass spectrometry cone, which meant that the line of sight from the crack to the ionization/extraction region was unobstructed almost immediately after the crack was formed, although mass spectrometer axis was almost  $90^\circ$  from normal to the new fracture surfaces. With this new configuration, we did not know whether the net effect on signal strength would be a loss of intensity because the MS axis was so far from normal, or a net increase, because we were examining the fracture so much earlier.

### ***In-Situ Compressive Impact Tests***

The simple-shear tests, in which a crack was caused to propagate across the specimen diameter, splitting the specimen roughly in half, involved relatively little energy being absorbed by the NTO specimen. The shear cutting fixture, traveling at around 2 m/s, loses negligible velocity,

---

\*Given that the blade speed required to clear the specimen in microseconds is roughly 1000 times faster than the currently achieved 2.25 m/s, faster than the speed of sound in air, and not practically achievable under the present conditions, the only option for acquiring data with shorter delay times was to view the pellet, in effect, from the side, as the end is sheared off. In any case, the crack moves much faster than the blade speed, and even if a substantially faster blade speed could have been achieved, it would not have resulted in a substantially more energetic crack propagation.

and hence negligible kinetic energy, as it drives a shear crack through the thin NTO specimen. The objective in the compressive tests was to substantially increase the energy absorbed by the specimen in the fracturing process. One way to achieve that is to impact the NTO specimen in a compressive (or crushing) mode, with the impactor coming to a complete stop during the process of fracturing the specimen, thereby imparting all its kinetic energy to the fracturing process.\* We therefore modified our *in-situ* fixture to allow for end-on impacts of the cylindrical NTO specimens. We decided on a conical shape for the impacted specimen end, judging that a cone would cause more surface fragmentation than impact on a flat-ended specimen.

## APPARATUS MODIFICATIONS AND EXPERIMENTAL PROCEDURES

### The SALI *In-Situ* Test Fixture

A diagram of the generalized *in-situ* test fixture is shown in Figure 1 above. The SALI apparatus has a 6-in.-diameter port approximately 6 in. from the center of the chamber, that we used in this program. A 6-in.-to-2.75-in. reducing nipple, an X-Y-Z precision manipulator stage, and a push-pull linear motion feedthrough were obtained commercially for attachment to the 6-in. port. The linear motion feedthrough is the keystone for the *in-situ* test fixture in all three of the modes used so far. This feedthrough was modified by (1) welding a 1-in.-O.D., 3/4-in.-I.D. aluminum tube to the inside of the 2.75-in.-diameter flange to provide rigid support for a platform onto which the NTO specimen is positioned, (2) connecting a specimen loading device to the inside end of the linear motion feedthrough shaft, and (3) extending the outside end of the shaft to allow for attachment of a strong coil spring around the shaft to provide an accelerating force to it.

In all modes of operation of the fixture shown in Figure 1, the pellet is stationary and the impacting force is delivered from left to right by expansion of the coil spring. A brass bushing, inside the support tube and surrounding the connecting rod between the shaft and the specimen loading device, adds stability and precision to the loading device.

The position of the specimen with respect to the mass spectrometer cone is controlled by the X-Y-Z stage, while movement of the feedthrough shaft applies the dynamic load to the specimen. The X-Y-Z stage remains attached to the high-vacuum chamber during a test series, but the heavily-modified linear motion feedthrough and specimen platform is unbolted and removed for each test to allow insertion of the NTO specimens.

---

\*More precisely, some of the kinetic energy of the impactor goes to the fracturing process in the target, and some goes to lateral acceleration of the fractured fragments.

In the first Annual Report, we detailed the procedures for the first series of *in-situ* dynamic shear tests on NTO. For the microsecond-delay simple shear and compressive impact tests, we used the same basic fixture and procedures, but with some modifications to allow us to make SALI measurements much sooner after crack completion. Beyond redesign of the subcomponents to hold and shear the pellet differently, the major change that resulted from moving the time scale down by as much as two orders of magnitude was that the distances over which movement must be accurately monitored also decrease by this same factor. The individual modifications of the main test fixture to allow it to perform each of the three categories of *in-situ* fracture experiments are described in the following sections.

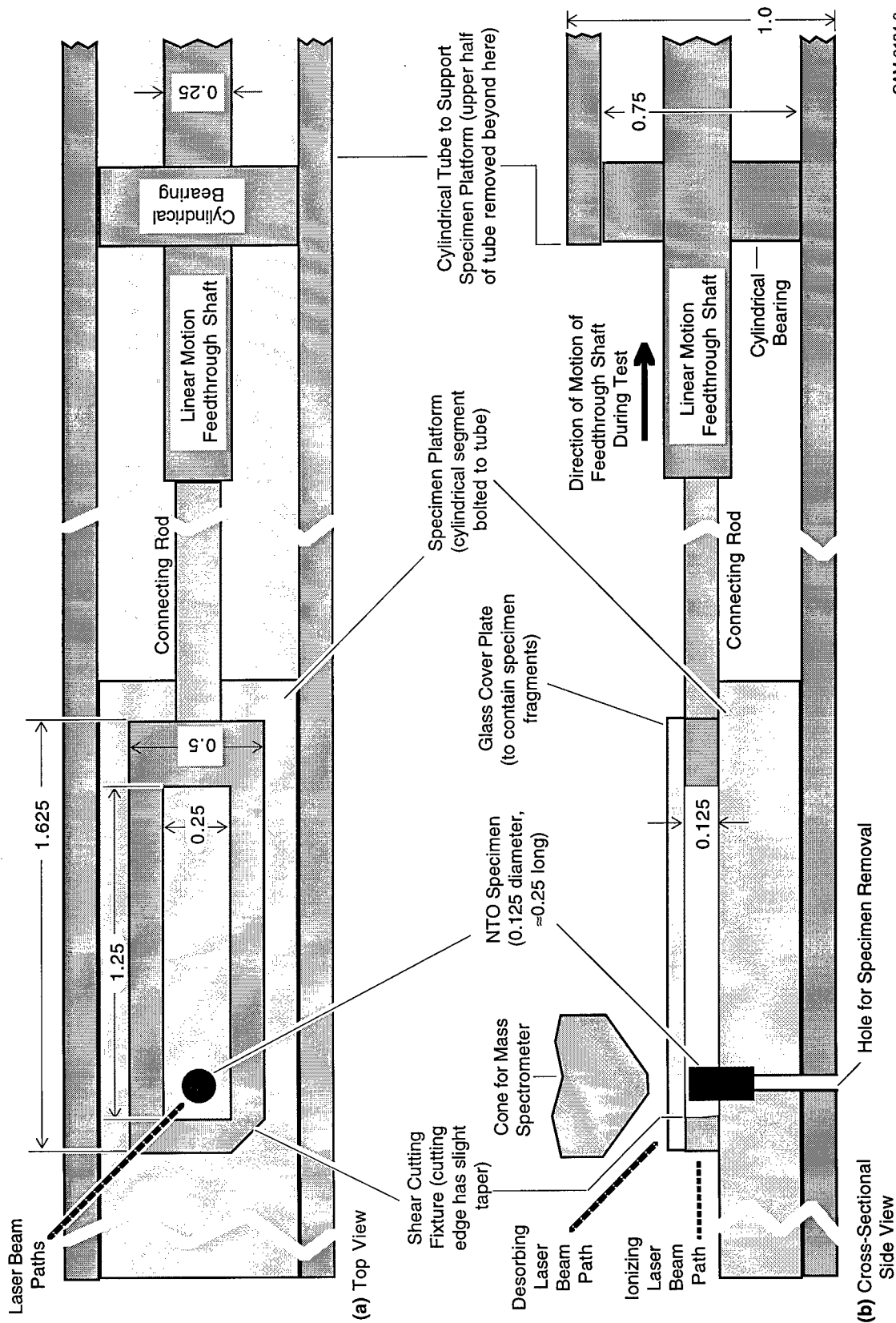
### **Fixture for *In-Situ* Simple-Shear Tests with Millisecond Delay Times**

The details of the pellet fracture region for shear tests with millisecond delay times are shown in Figure 2. As stated above, and described in detail in Appendices A and C, the pellet is held vertically, immediately below the mass spectrometer sampling cone. When the pellet is sheared, the new fracture surface is 90° to the flight axis of the mass spectrometer, optimally arranged for detection of materials emanating from the surface.

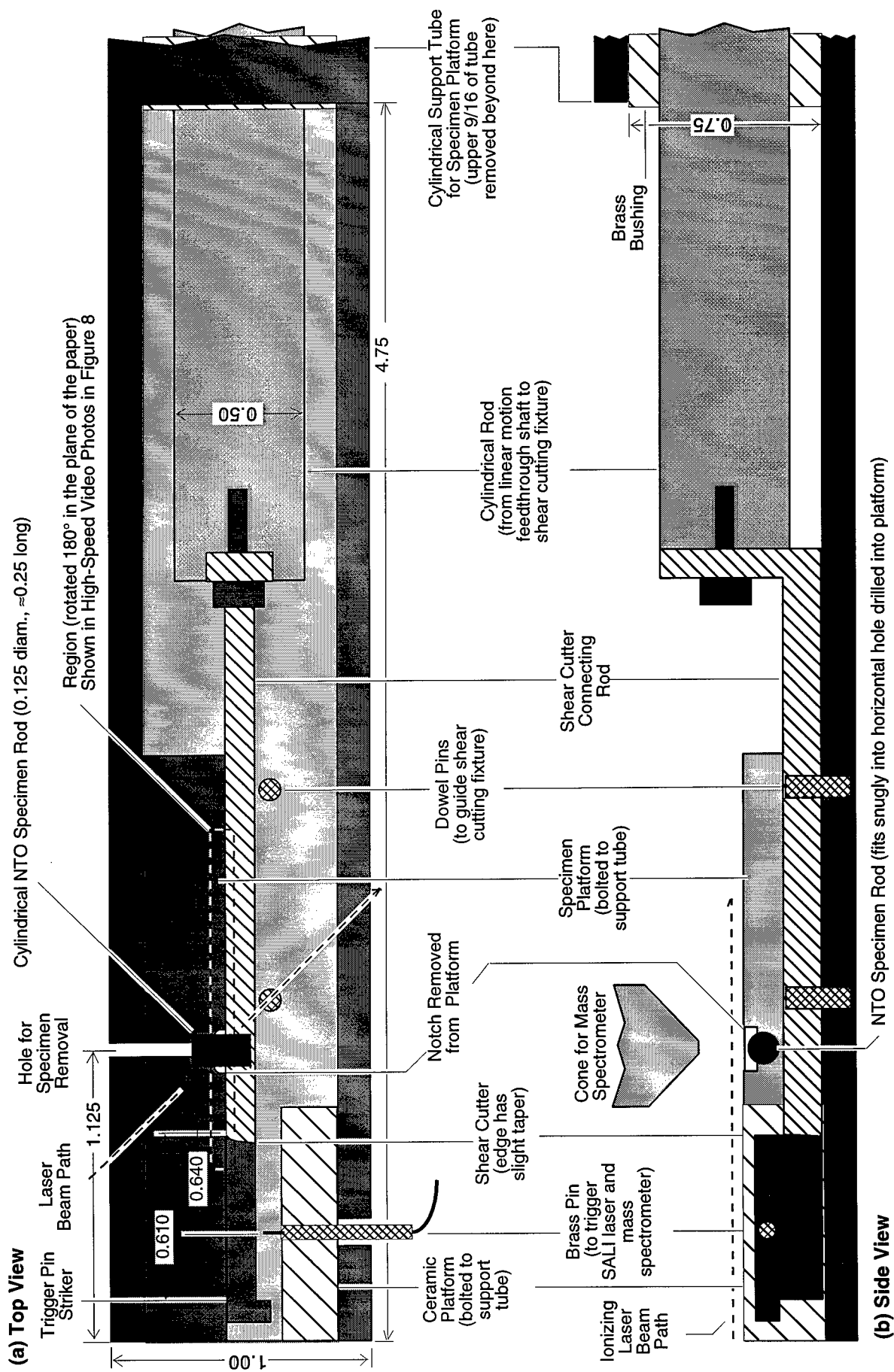
### **Fixture for *In-Situ* Simple-Shear Tests with Microsecond Delay Times**

Figure 3 shows details of the specimen loading geometry as modified to allow a 10- to 100-fold shortening of the delay time. The aluminum specimen platform, a cylindrical segment, is bolted to the bottom of the support tube. The top of the platform lies  $\approx 1.5$  mm below the axis of the feedthrough shaft and support tube and  $\approx 1$  mm below the path of the ionizing laser. The NTO specimen, a cylinder 0.125 in. (3.2 mm) in diameter by approximately 0.25 in. long (6.4 mm), is inserted (with its axis horizontal) into a 0.125-in.-deep (3.2 mm) hole in the side of the specimen platform, with its midpoint directly below the ionizing laser beam path and the mass spectrometer cone. Approximately half of the specimen thus protrudes from the hole; a rectangular notch  $\approx 0.05$  in. high (1.3 mm) and  $\approx 0.04$  in. deep (1.0 mm) cut out of the upper edge of the platform increases the length of the upper third of the specimen that protrudes from the hole, in an attempt to make the shear crack more exposed to the laser and mass spectrometer.

On the other side of the support tube from the specimen platform is bolted an insulating machinable ceramic (Micor) block into which is inserted a brass rod with a 0.010-in.-diameter brass whisker that acts as a trigger pin. The front edge of the pin is located 0.640 in. (16.26 mm) from the front edge of the NTO specimen. The rod is electrically isolated from the rest of the



CAM-6134-6



CAM-6134-20

Figure 3. Detail of SALL *in situ* test fixtures for simple-shear tests with microsecond delay times.  
All dimensions in inches.

support tube and is attached to a lead that travels through an electrical feedthrough in the SALI chamber out to the trigger circuitry box.

The steel shear cutting fixture is attached to a guide bar, which in turn is bolted to the linear motion feedthrough shaft through the connecting rod. The guide bar travels between the specimen platform and a pair of steel dowel pins protruding from the bottom of the support tube. On one end of the cutting fixture is the cutting edge (slightly tapered to minimize any tensile component), which impacts the specimen near its axial midpoint. At the other end, located 0.610 in. (15.49 mm) along the direction of motion from the cutting edge, is the protruding shoulder, which strikes the trigger pin.

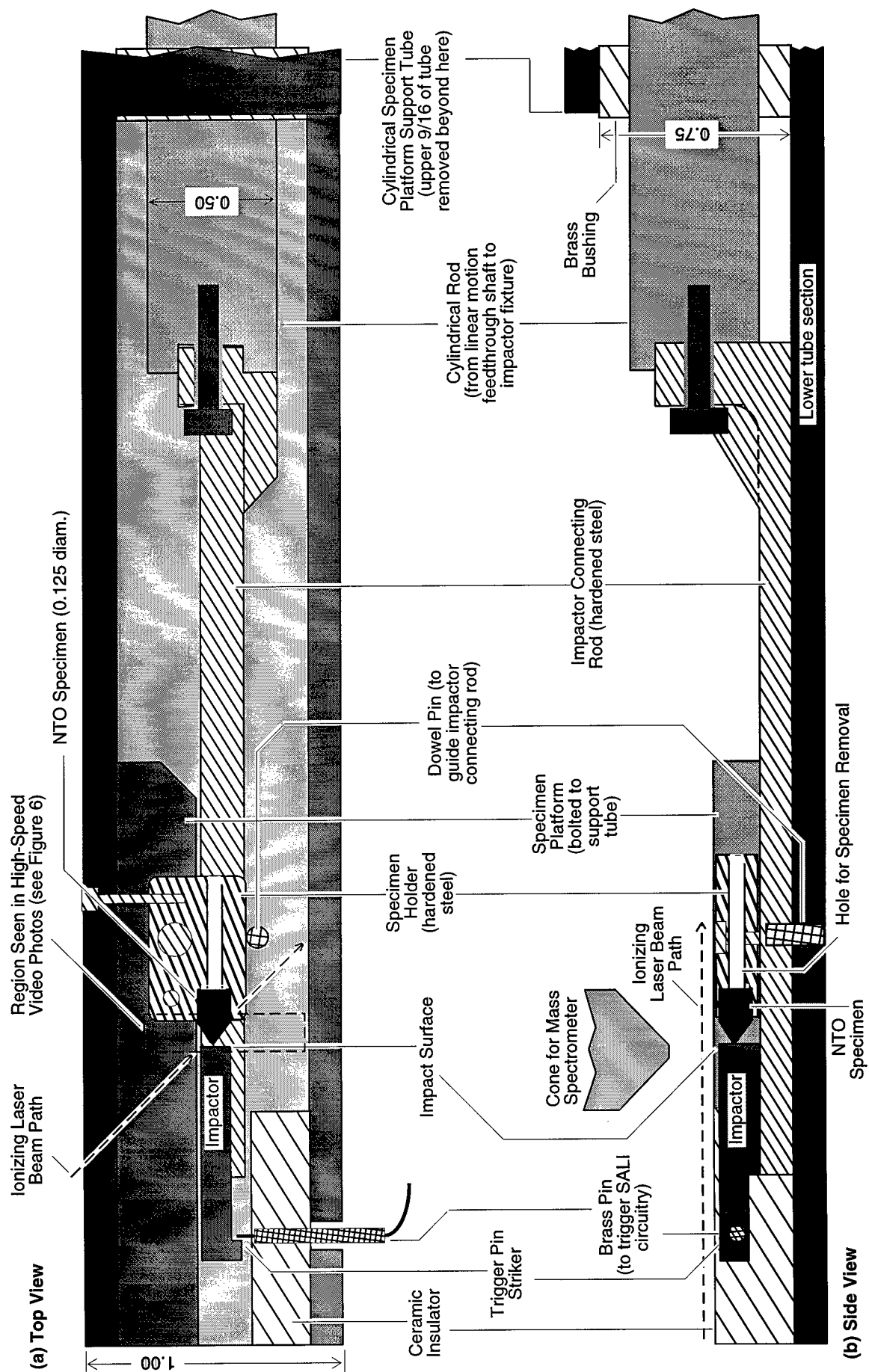
### **Fixture for *In-Situ* Compressive Impact Tests**

Details of the specimen loading geometry for the *in-situ* compressive tests are shown in Figure 4. The aluminum specimen platform (a cylindrical quarter-segment) is bolted to the inside of the support tube, and a hardened steel specimen holder is attached to the platform. The conical-tipped, cylindrical NTO specimen is inserted (with its axis horizontal and parallel to the axis of the feedthrough shaft) into a 0.125 -in.-diameter (3.2 mm) by 0.125 -in.-deep (3.2 mm) hole in the side of the specimen platform. Approximately half of the length of the specimen protrudes from the hole, including all the conical tip and a small portion of the cylindrical segment. The conical tip section is centered directly beneath the ionizing laser beam path; the apex of the cone lies  $\approx 2.5$  mm below the beam path.

The same Micor ceramic block used for the shear tests was used here to hold the brass trigger pin that closes a connection to the ionizing laser trigger circuitry. The impactor is now attached to a hardened steel connecting bar, which in turn is bolted to the linear motion feedthrough shaft through the connecting rod. The hardened steel material and the reinforcements near the bolt end became necessary in the compressive-impact mode to eliminate bending of the connecting bar during the rapid deceleration. Such rapid deceleration was not encountered in the earlier shear-test modes, where the drive spring, once it passed its equilibrium point, simply slowed the shaft in a more gradual fashion.

### **NTO Sample Preparation**

In the first Annual Report, we described the fine-grained (F.G.) NTO powder used in this program, and the fixture and technique used (Aubert, 1993) to warm-press the cylindrical NTO specimen for the first series of *in-situ* dynamic shear tests (see also Appendix A). Identical, or very similar, pressed pellets were used in all three variations of the *in-situ* testing procedure. For



CAM-6134-28

Figure 4. Detail of SALI *in-situ* test fixture for compressive impact tests. All dimensions in inches.



the simple-shear tests with milliseconds delays and for the reoriented shear tests with microsecond delays, we used exactly the same pellets, pressed to a diameter of 0.125 in. (3.2 mm) and a length of  $\approx 0.25$  in. (6.4 mm), using a peak specimen pressure of  $\approx 19$  ksi. In the final set of pellets pressed for shear tests, the density of the specimens ranged only from 1.871 to 1.897 g/cm<sup>3</sup>, a variation of less than 1.5%, corresponding to approximately 97% to 98% of the theoretical maximum density (TMD) of 1.93 g/cm<sup>3</sup>.

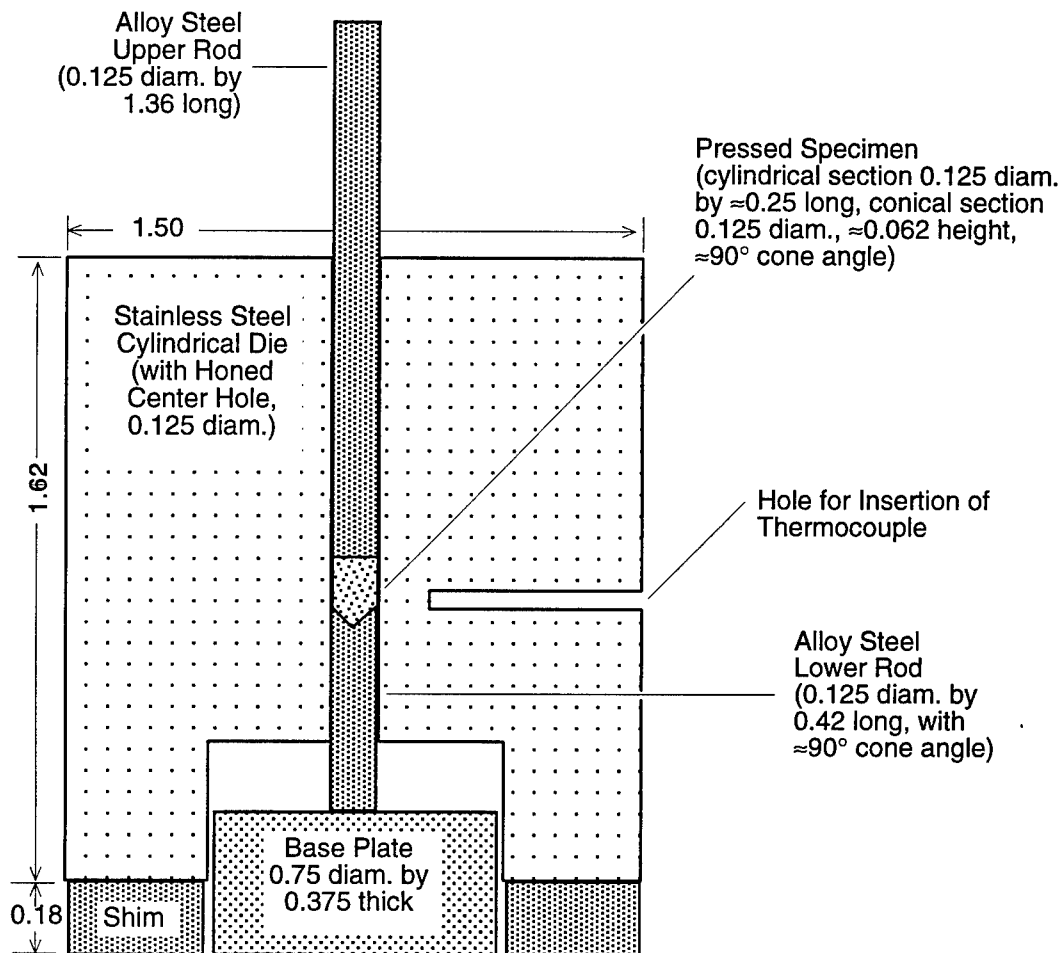
For the *in-situ* compressive tests, we modified the pressing fixture (as shown in Figure 5) to produce specimens with one roughly conical tip (the cone angle is  $\approx 90^\circ$ ; microphotographs, like the one shown in Figure 6(b), reveal a rounded apex with a radius of curvature of about 0.025-in.). The warm-pressing recipe procedure itself was not changed from that used for the simple cylindrical pellets. We used a temperature of 105°C and pressure of 19 ksi. The densities of these pellets are virtually identical to those prepared earlier for the shear tests: ten pressed specimens had densities of  $1.880 \pm 0.013$  g/cm<sup>3</sup>, which is 97% to 98% of the TMD of 1.93 g/cm<sup>3</sup>. The specimens had a diameter of 0.125-in. (3.2 mm), a conical tip length (distance from the cone apex to the closer end of the cylindrical section) of 0.0536 in. (1.36 mm), and a total length from 0.167 in. (4.24 mm) to 0.203 in. (5.16 mm).

### Diagnostic Tests for Pellet-Fracture Fixtures

Before each of the categories of *in-situ* NTO testing, we performed several diagnostic tests to assess the functioning of the fixtures themselves. We needed to determine accurately the relevant distances and velocities, so we could calculate the time interval between the shear crack formation or compressive impact and the SALI measurements. We also wanted to examine the motion of the sheared sections of the specimens to better understand the shearing mechanics. In the compressive impact tests, we also wanted to examine the motion of impactor as it fractured the conical end of the specimen and came to a complete stop.

**Simple-Shear Tests.** For the simple-shear tests with millisecond delay times, timing is simple because the sum of all electronic and inadvertent mechanical delays is well under a millisecond. For the modified shear with  $\sim 100$   $\mu$ s delay times, the timing became more critical, and the following approach was used.

First, we positioned the linear motion feedthrough device on a machinist's mill, and while moving the shaft, very accurately measured the distance traveled after the shoulder strikes the trigger pin whisker, before the edge of the shear cutter reaches the specimen. The result was  $0.0302 \pm 0.0002$  in. ( $0.767 \pm 0.005$  mm). We then measured the additional distance that the shear cutter needed to travel into the NTO specimen after impact before the specimen sheared. This test



CAM-6134-26

Figure 5. Cross-sectional view of NTO pressing fixture with conical die insert.

Electrical heating tape is wrapped around circumference of die.  
All dimensions in inches.

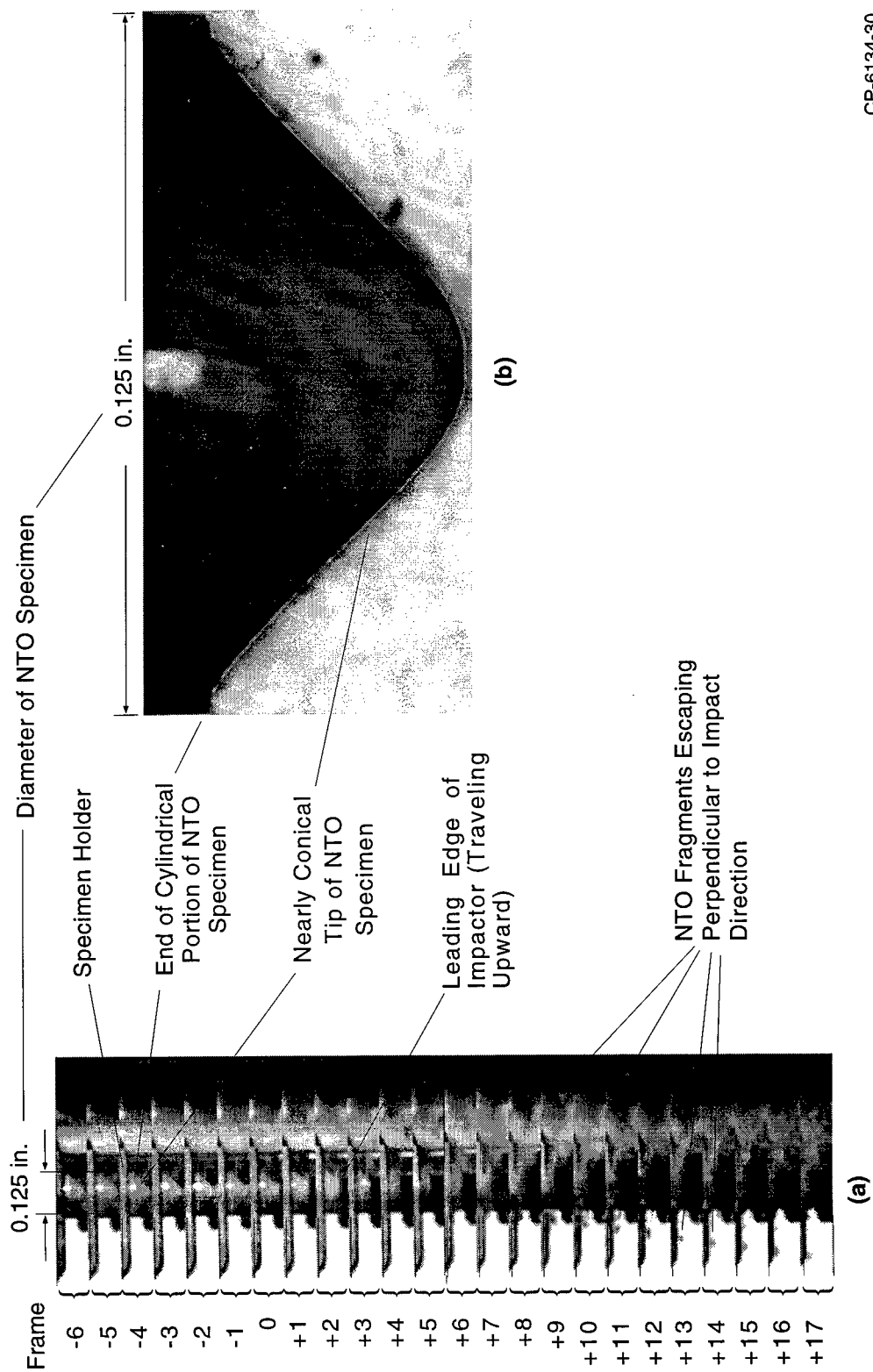


Figure 6. High-speed video images of NTO SALI impact test and microphotograph of conical NTO specimen tip. Successive frames are 83  $\mu$ s apart; impact (at  $2.37 \pm 0.05$  m/s) occurs approximately at Frame 0.

CP-6134-30

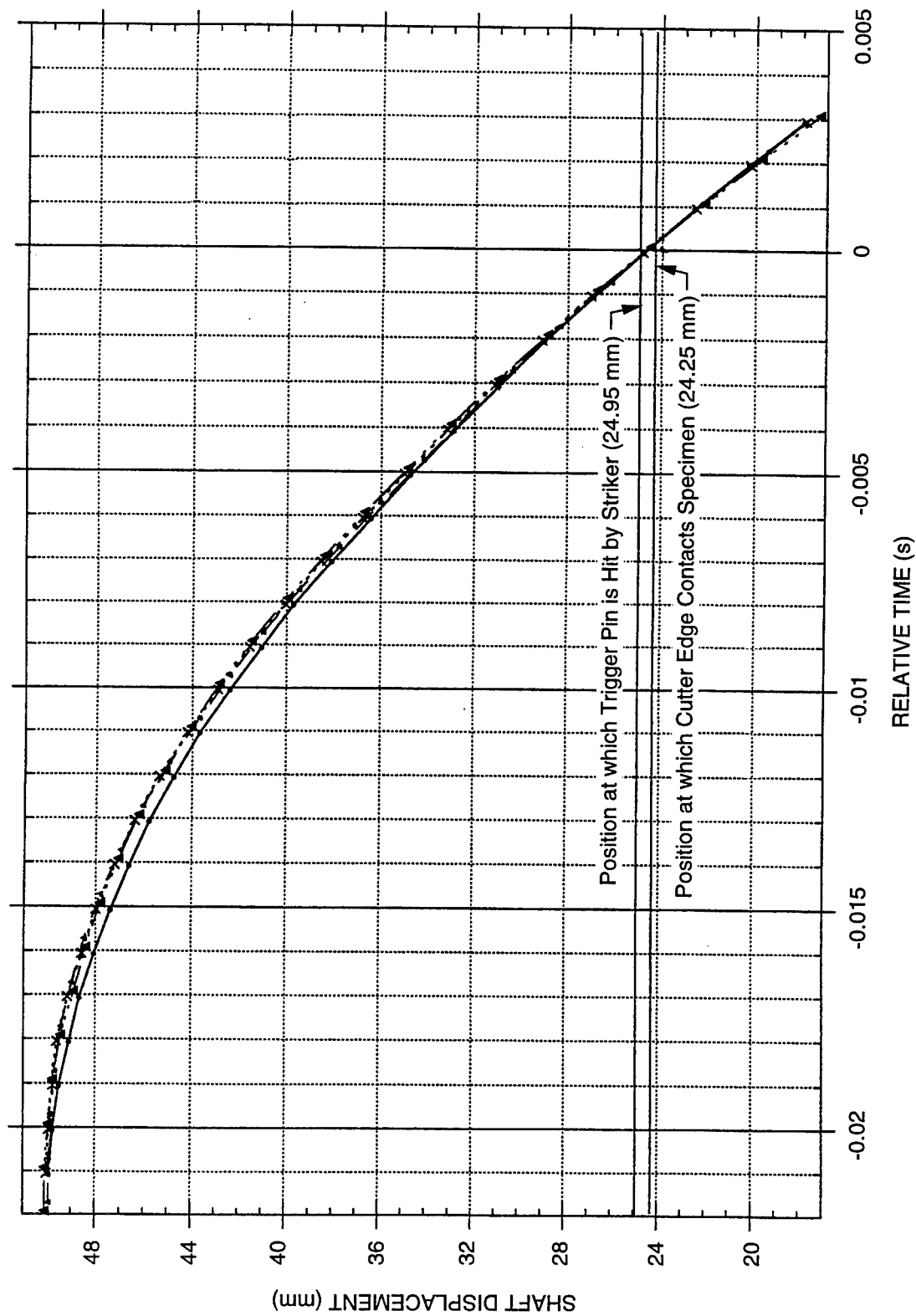
was performed at the very slow rate of less than 0.0002 in./s (0.005 mm/s), and the result was brittle shear crack failure at  $0.007 \pm 0.001$  in. ( $0.175 \pm 0.025$  mm). The cutter edge appeared at first to penetrate the specimen without any observable cracking, and then at a depth that ranged between 0.0060 and 0.0078 in. (0.15 and 0.20 mm) over several tests, a shear crack began and traveled all the way through the specimen at a speed faster than the eye could follow, splitting the specimen in two.\* The distance of penetration of the cutter before specimen shearing may be a function of cutter velocity (at very high velocities, there may be more or less penetration, depending on the mechanism involved). However, we do not expect the penetration distance before fracture to change significantly at the rates for the *in-situ* shear test (2 m/s), because that is still very slow compared with typical crack propagation velocities in brittle materials.

Next, we used a high-speed (up to 12,000 frames per second) videocamera to record the displacement history of the linear motion feedthrough shaft in actual operation, so we could determine the velocity of the cutting edge as it shears through the specimen. Because we wanted to duplicate the exact conditions of the shear tests, the device was first bolted in place on the X-Y-Z stage, and a vacuum was pulled in the SALI chamber (the pressure in the chamber affects the motion of the spring-like welded bellows seal attached to the feedthrough shaft). The shaft motion was then locked in its maximum inward position, just beyond the 50-mm mark, and then released, with the videocamera recording the motion of the shaft marker on the stationary etched grid (see Figure 1). The results of four typical tests are shown in Figure 7, with the time for all the curves shifted so that zero time occurs in the vicinity of the trigger pin closure (near the 25-mm mark). The displacement histories were quite repeatable; the velocity of the cutter as it reaches the position of specimen impact (near the 24-mm mark) was  $2.25 \pm 0.05$  mm/s.

For the final diagnostic test of the shear fixture, we set up the linear motion feedthrough device outside the SALI chamber (so that a closeup lens could be readily used to view the pellet itself), repositioned the spring stop to attain the same shaft velocity (2.25 m/s) at specimen impact that had been obtained with the fixture inside the vacuum chamber (the velocity is faster without the vacuum retarding the motion of the shaft and bellows), and focused the high-speed videocamera on the NTO specimen as it was being contacted and sheared. Typical results are seen in Figure 8(a), which shows 24 frames (in 2 groups of 12 frames) taken at 12,000 frames per second (successive frames are thus 83.3  $\mu$ s apart).

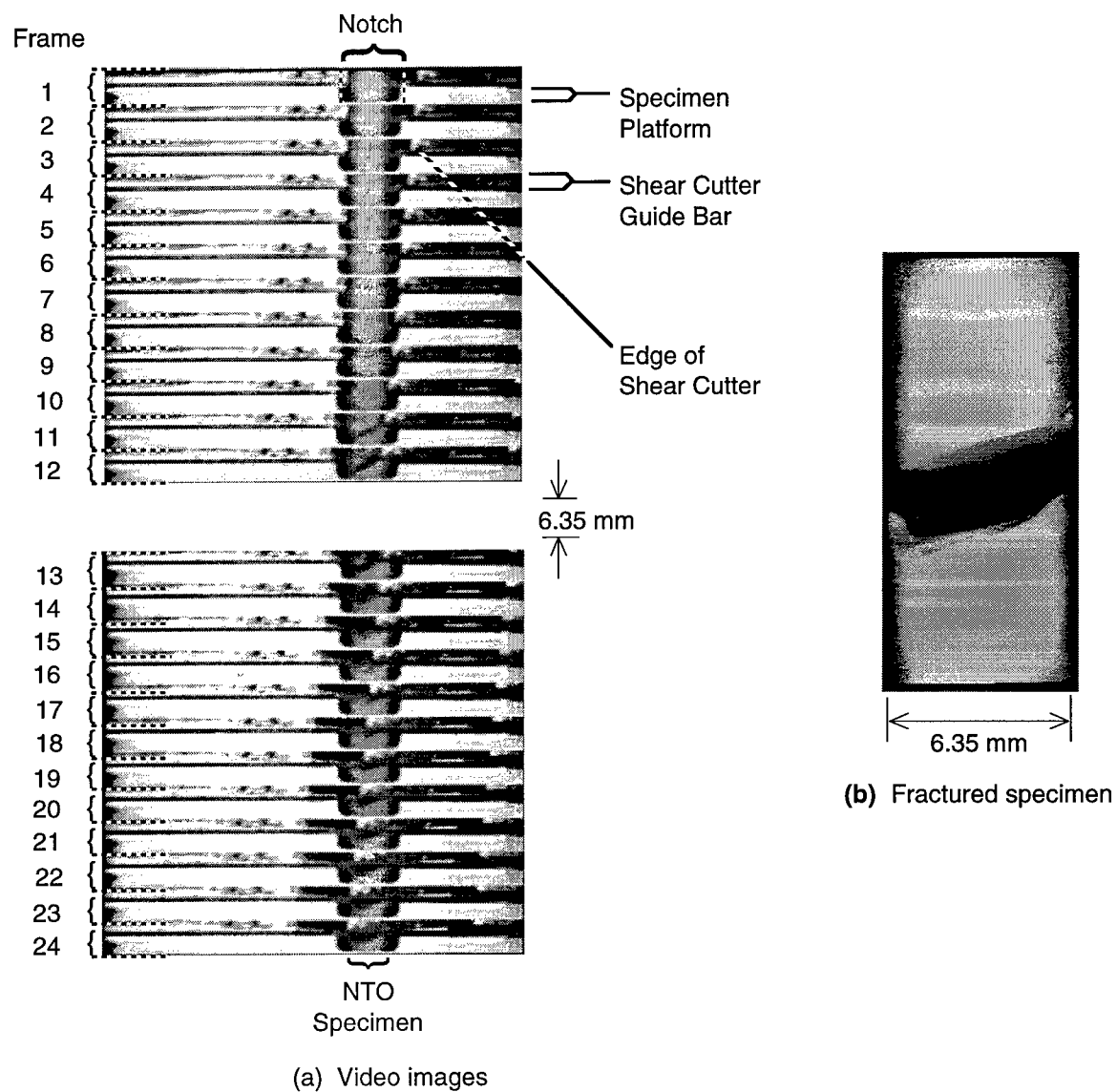
---

\*This brittle shear crack was in marked contrast to the case of an acrylic specimen, for a which a small crack was observed to form in the vicinity of the shear cutter edge at a penetration depth of  $\approx 0.018$  in. (0.45 mm) and then, without any further motion of the cutter, slowly grew across the specimen over tens of seconds until it reached the far edge.



CAM-6134-21

Figure 7. Displacement histories of spring-driven linear-motion feedthrough shaft for four velocity tests of shear fixture.



CPM-6134-22

Figure 8. High-speed video images of NTO dynamic shear test and photograph of fractured specimen. Frames are 83.3  $\mu$ s apart.

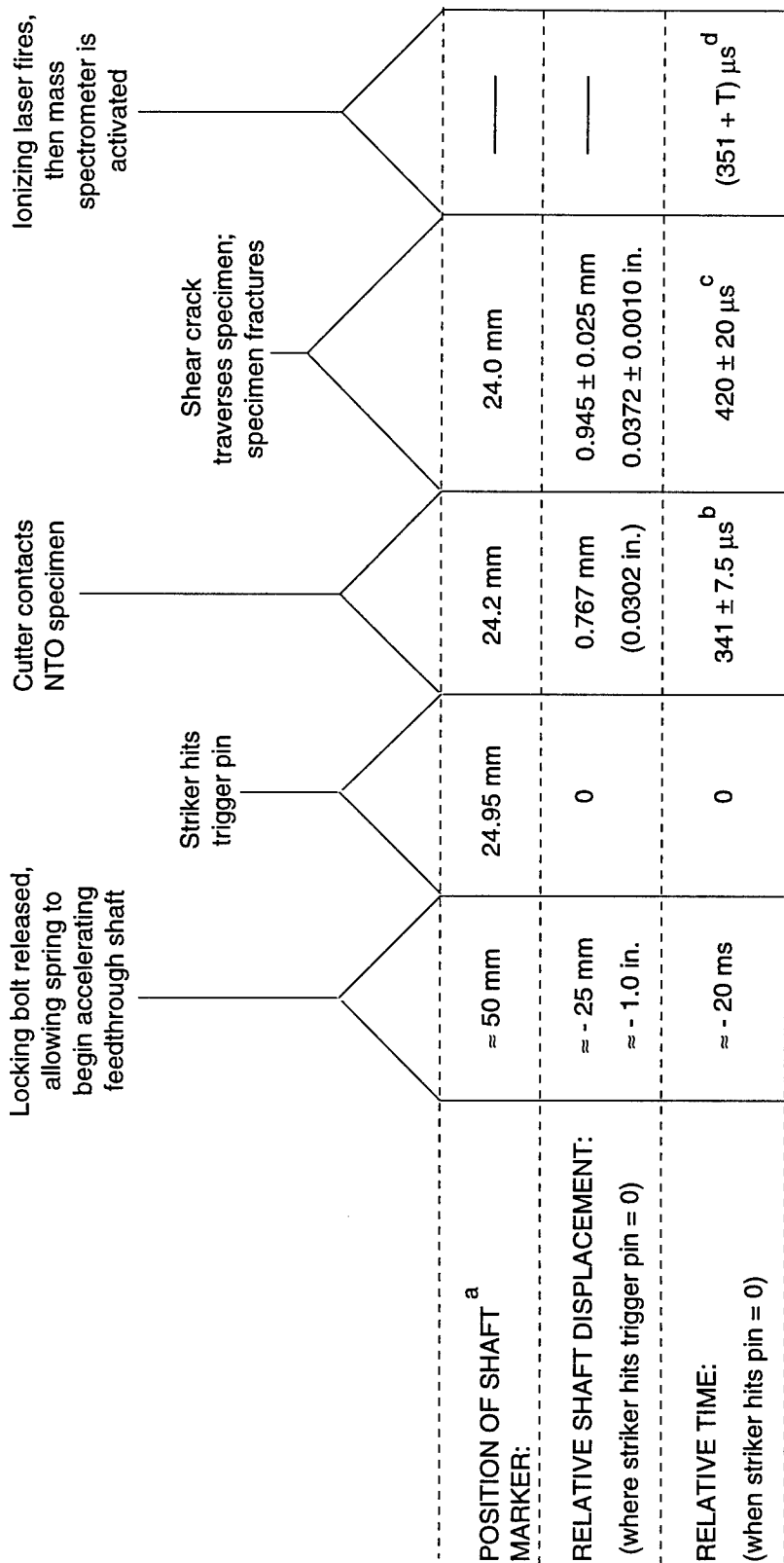
The region in each of the long and narrow frames is the region within the dashed rectangle in Figure 3(a), but is rotated 180° in the plane of the paper. The whitish region on both the left and right sides of each frame is the top of the specimen platform on either side of the bowl-shaped notch, and the gray region near the center of each frame is the mid-axial region of the NTO specimen protruding from the notch. The thin gray band moving from right to left across the upper portion of each frame is the shear cutter guide bar, moving at roughly 2.4 mm/s. The shear cutter edge is the white, roughly triangular shape that appears to hang from the specimen platform and contacts the NTO specimen at about frame 10.

By frame 11, less than 83  $\mu$ s and 0.008 in. (0.2 mm) of cutter travel after the first contact, the crack appears to have grown all (or very nearly all) the way across the specimen. This gives us further evidence that the  $0.007 \pm 0.001$  in. ( $0.175 \pm 0.025$  mm) value we measured quasi-statically for the cutter penetration before shear cracking is a good approximation to the value at the actual *in-situ* test velocities. By frame 12, less than 166  $\mu$ s after first contact, the NTO has clearly separated into two pieces, and the sheared piece is rotating up and to the left, completely disappearing from view by frame 16.

The shear crack does not propagate exactly transversely across the specimen, but as shown in Figure 8(a), angles downward into the notch at  $\approx 15^\circ$  to the transverse direction. Then as the crack nears the back surface, it changes direction and cuts sharply back towards the specimen midplane. Figure 8(b), a photograph of the two halves of a sheared NTO pellet, shows the typical shape of the shear crack. This behavior has been observed to be quite repeatable, based on both the high-speed videocamera images and examination of the recovered specimens. Kalthoff and Winkler (1988) showed that angled shear cracks are a natural result of the stress field in the material ahead of a sharp shear cutter. The presence of the notch may also affect the shape of the sheared surface.

Figure 9 shows a timeline representation of these events for simple shear with microsecond delay times. The laser fires at 351  $\mu$ s (the built-in laser firing delay) + T (the additional time set on the delay generator), whereas the specimen shears at  $420 \pm 20$   $\mu$ s. So the time between specimen shearing and SALI measurement is  $T - 69 \pm 20$   $\mu$ s. In this series of tests, T spanned a range from 100 to 900  $\mu$ s, which means that our measurements nominally spanned a range from 31 to  $831 \pm 20$   $\mu$ s after completion of the shear crack.

**Compressive Impact Tests.** As with the shear tests, we again used a high-speed ( $\leq 12,000$  frames per second) videocamera to record the displacement history of the linear motion feedthrough shaft, so that we could determine the velocity of the impactor as it contacts the specimen. To duplicate exactly the velocity conditions of the *in-situ* impact tests, the device was



<sup>a</sup> This is the location of the linear motion feedthrough shaft marker, as read on the etched grid (see Figure 1).

<sup>b</sup> Assuming shaft velocity in region from trigger pin hit to specimen contact is  $2.25 \pm 0.05$  m/s.

<sup>c</sup> ± 9 μs uncertainty is from 0.05 m/s uncertainty in the velocity, ± 11 μs is from 0.025 mm uncertainty in the shaft position at fracture.

<sup>d</sup> 351 μs is the built-in delay between trigger signal and the laser firing; T is the additional time set on the delay generator.

Figure 9. Timeline for events during *in-situ* dynamic shear test of NTO.

CAM-6134-23



bolted in place on the X-Y-Z stage, and a vacuum was pulled in the SALI chamber. The shaft motion was then locked in its maximum inward position, just beyond the 50-mm mark, and then released, with the videocamera recording the motion of the shaft marker on the stationary etched grid (see Figure 1). The results of four typical tests are shown in Figure 10, with the time for all the curves shifted so that zero time occurs in the vicinity of impact. As with the shear tests, the displacement histories were quite repeatable; the velocity of the impactor as it reaches the position of specimen impact was determined to be  $2.37 \pm 0.05$  mm/s.

Next, we set up the linear motion feedthrough device outside the SALI chamber (so that a close-up lens could again be used to observe the specimen), repositioned the spring stop to attain the same shaft velocity (2.37 m/s) at specimen impact that had been obtained with the fixture inside the vacuum chamber, and focused the high-speed videocamera upon the conical end of the NTO specimen as it was being impacted and crushed. Typical results are seen in Figure 6(a) above, which shows 24 frames taken at 12,000 frames per second (successive frames are thus 83.3  $\mu$ s apart). The region in each of the long and narrow frames is the region within the dashed rectangle in Figure 4(a), but rotated 90° counter-clockwise in the plane of the paper. The long thin gray region on the top of each frame is the edge of the specimen holder. The end of the cylindrical portion and all of the conical-tipped portion of the NTO specimen can be seen protruding from the holder [a magnified view of the protruding region, taken through a microscope, is shown in Figure 6(b)].

The black rectangle protruding from the bottom beginning at frame 0 and traveling upward is the impactor. Impact occurs approximately at frame 0, and the impactor motion appears to stop approximately at frame 10, at which point essentially the entire conical sections of the specimen has been crushed. Due to the presence of NTO fragments traveling outward in the region between the impactor and the specimen holder, the impactor stops before contacting the specimen holder, so all the kinetic energy of the impactor fixture (including the connecting rod, feedthrough shaft, and so on) is absorbed by the specimen and its fragments. (Because the impactor fixture has a mass of  $\approx 460$  g, roughly 1.3 J is absorbed in crushing the conical tip of the specimen. We believe this is several orders of magnitude more energy than is absorbed during an *in-situ* shear test.) NTO fragments can be seen in Figure 6(a) emerging at right angles to the impact direction, traveling from 4 to 9 m/s.

### ***In-Situ* Fracture Procedures**

The general procedure for the modified *in-situ* pellet fracture experiments, each of which required 1 to 2 hours, was as follows. Before inserting the motion feedthrough into the SALI chamber, we (1) lock the shaft at its most inward possible position, just beyond the 50-mm mark

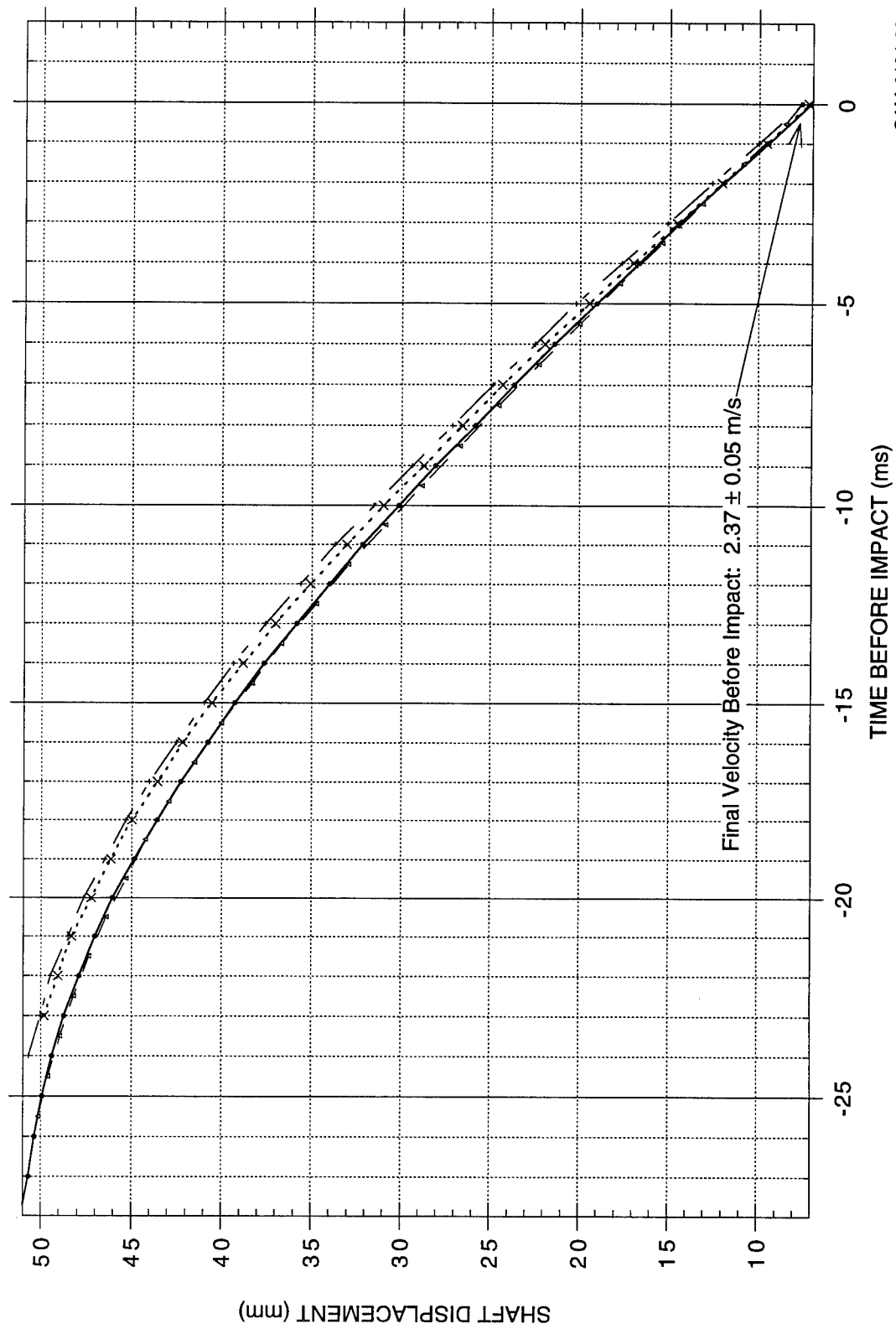


Figure 10. Displacement histories of spring-driven linear motion feedthrough shaft in four SAI dynamic compression tests.

(the spring is thus at its maximum compression), (2) insert an NTO specimen into the platform hole, and (3) position a trigger pin in the Micor block and attach the lead to the back of the pin. We then bolt the shaft onto the X-Y-Z stage, manipulate the stage until the specimen is positioned properly beneath the mass spectrometer cone, pump the chamber down to a high vacuum, and attach the lead from the trigger pin to the trigger circuit.

To begin a test, the thumbscrew on the locking shaft bolt is quickly turned, freeing the shaft to accelerate in the outward direction. After 1.0 or 1.6 in. (25 mm or 40.5 mm) of travel (for shear tests and compressive impact tests, respectively), the pin striker hits the trigger pin, sending a signal to activate a delay generator. After further shaft travel, depending on the specimen length and test type, the shear cutter or impactor strikes the NTO pellet, at which time the impactor has reached a velocity of  $2.25 \pm 0.05$  m/s or  $2.37 \pm 0.05$  m/s. The delay generator is set to trigger the SALI electronics (ionizing laser and mass spectrometer circuitry) at the desired delay after contact. For the shear tests, these delays are keyed to the time the sheared section flies away from the confined portion of the pellet. For the compressive impact tests, they are keyed to the time the impactor has traveled approximately half way into the conical section (i.e., about half of the ultimate travel) and has produced a significant volume of fractured NTO.

## TEST RESULTS

This section describes in detail only those results not fully described in the manuscripts in Appendices A, B, and C. Those earlier results, briefly recounted in the Executive Summary, include the generation of data on the intermediates produced in slow-thermal-, laser-desorption-, and shear-induced decomposition and the use of those data to arrive at a surprisingly satisfactory decomposition rationale that reconciles a substantial portion of earlier, and apparently disparate, data on NTO decomposition. We then constructed a hypothesis about the stable intermediate that may constitute the stabilizing bottleneck that makes NTO a quite insensitive explosive.

The results described in this section include (1) use of the modified *in-situ* shear device to move real-time measurements from the millisecond to the microsecond time-scale, (2) use of the compressive-impact modification to obtain dynamic fracture data from an impact in which the NTO pellet is constrained to absorb much more mechanical energy, and (3) post-fracture LDMS examination of NTO samples that have been subcritically impacted in an external test device and then transferred to the SALI chamber.

## Shear-Induced NTO Decomposition on the 100- $\mu$ s Time Scale

As indicated under Test Procedure Rationale, we wished to examine fragments emitted from the fracture surfaces within as short a delay time as possible after the shearing took place. Delays as short as only a few microseconds are attainable, but the shortest delay in the experiments described here was of the order of 50  $\mu$ s. Because practical limits on spring-applied force prevented the cutter from traveling fast enough to clear the specimen face in microseconds, rather than milliseconds, we needed to view the shear pellet from the long cylindrical side, at an angle far from normal to the crack surface. It was not initially obvious whether, in comparison with our previous measurements on the millisecond time scale, the net result here would be higher signal intensity because of much earlier observation or lower intensity because the viewing angle approaches an unfavorable 90° from normal.

Shear-induced decomposition mass spectra of NTO were obtained with nominal delays (from the time of fracture completion) ranging from 30 to 830  $\mu$ s. These spectra varied widely, from essentially noise only to a signal/noise ratio of 200/1 for the peak at  $m/z$  99. In the latter case, there was a five-fold increase from the best single-shot signal/noise ratio we had observed with millisecond-time-scale viewing normal to the fracture surface and a similar increase in the intensity ratio for  $m/z$  99 and the ubiquitous  $\text{NH}_3$  peak at  $m/z$  17. Thus, in terms of signal strength, we benefited more from going to shorter delays times than we were hurt by poor viewing angle.

In the "worst" cases, however, we saw no enhanced intensity at  $m/z$  99 whatsoever. Our attempts to reliably map the time dependence of the shear fragments were not successful, with the strongest signals appearing at a nominal 30 and 630  $\mu$ s after crack completion, but with some much lower intensities at intermediate delay times. The uncertainties in velocity, position, and time outlined in Figure 9 indicate that the nominal time of fracture completion is accurate within  $\pm 20$   $\mu$ s. The high speed video observations (an example is shown in Figure 8) indicate that pellet fracture *and* separation are reproducible, at least on the resolution scale of the video ( $\sim 100$   $\mu$ m).

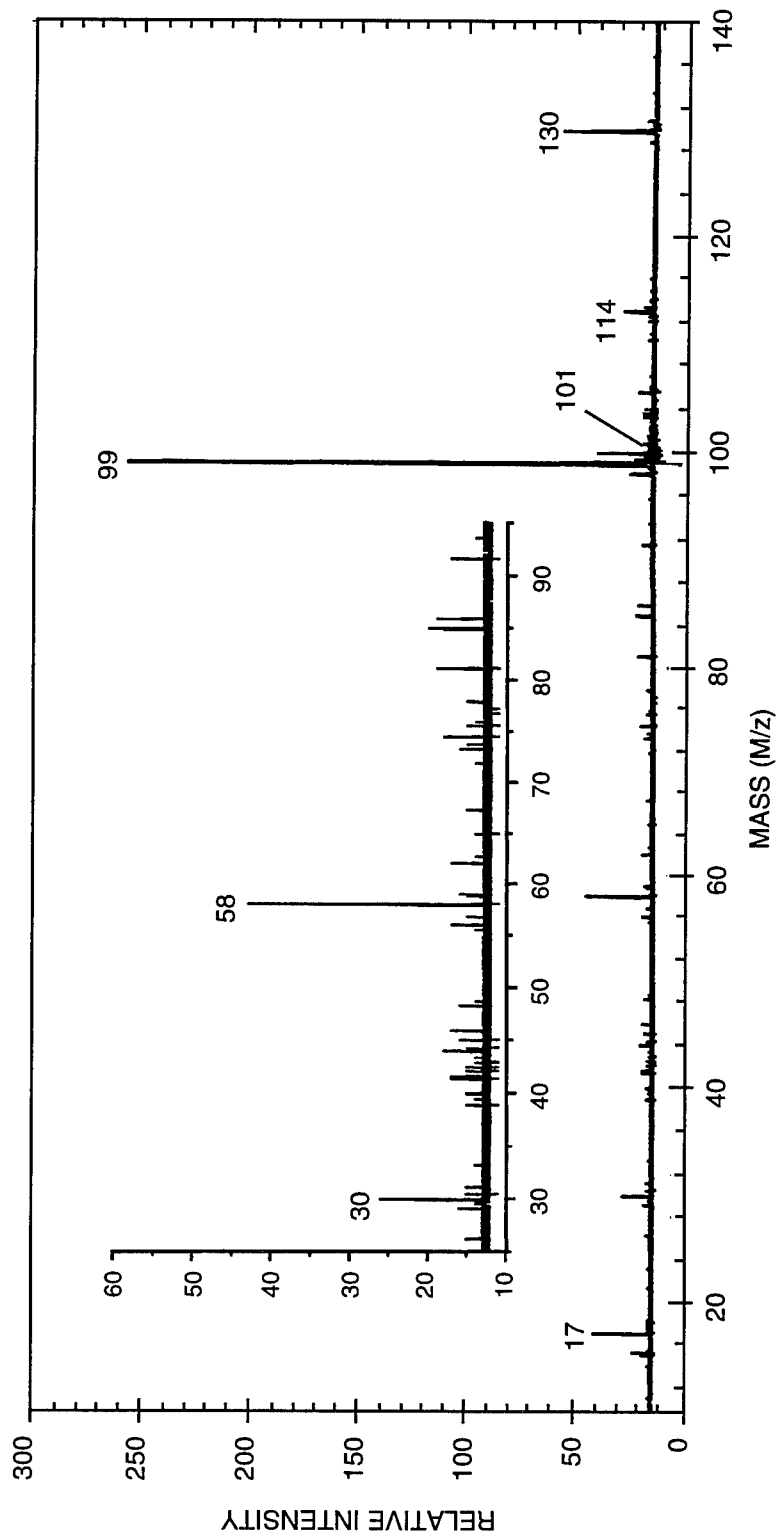
Some small shifts in the lateral positioning of the pellet, relative to the ionizing laser, may be responsible for the variability in fragment emission. However, another possible source is variable rotation of the separating pellet half not only in the plane of the paper, as seen in Figure 8, but also in another plane. Rotation in another plane would change the deviation of the viewing angle from 90° off-normal. If the emission of fragments were to follow, for instance, a  $\cos^2$  distribution, such variability could cause large changes in the signal intensity. Thus, the variability we observed could have little to do with timing uncertainty, but reflect instead varying degrees of rotation to turn a sheared face more toward the mass spectrometer.

Notwithstanding the uncertainties in the time dependence of the emission of the shear-induced fragments (as illustrated in the list of pellet fracture tests given in Table 1), these results show that very strong signals can be observed, on a single-shot basis, even when observing almost 90° off-normal to the nominal plane of the fracture surface(s). The most intense single-shot spectrum we obtained is shown in Figure 11. In contrast to the averaged spectrum acquired from 100 shots of the ionizing laser 50 to 60 s after shear (fracture face perpendicular to the mass spectrometer flight axis, Figure 10, Appendix A), the intensity of  $m/z$  99 is now much greater than that of  $m/z$  17 for background  $\text{NH}_3$ . Also,  $m/z$  58, which is barely seen in the millisecond delay spectra, now clearly rises out of the background and is more intense than  $m/z$  17. Mass 58 also has virtually zero intensity in the thermal desorption spectra shown in Appendix A. However, reexamination of the laser-desorption spectra of subcritically impacted NTO (Figure 13, Appendix A) in the light of the obvious  $m/z$  58 peak in Figure 11 shows a small but significant intensity for this ion. This appearance of  $m/z$  58 in both circumstances not only shows that the small intensity in the previously impacted sample was a true remnant of differing branching ratios that pertain under conditions of mechanical stress, but also illustrates how the *in-situ*, real-time measurements are much more sensitive indicator of such changes, really are clearly present as a remnant of the subcritical impact.

Table 1. Summary Of Test Results For Shear Of NTO Pellets  
With Microsecond Delay Times

Sample No.	Electronic Delay, $\mu\text{s}$	Nominal Delay, <sup>a</sup> $\mu\text{s}$	Relative $m/z$ 99 Intensity
16	100	31	Present
21	100	31	Very strong
22	150	81	Absent
23	150	81	Absent
28	500	431	Absent
29	500	431	Absent
30	450	481	Present
31	700	631	Very strong
32	900	831	At noise level
33	600	531	At noise level
34	600	531	Present
35	750	481	Absent
36	200	131	Absent
37	700	631	Absent

<sup>a</sup>Nominal delay after completion of the crack, as determined by cutter position at time of crack completion during "static" (i.e., slow speed) measurements.



CAM-6124-24

Figure 11. Single-shot SALI spectrum of shear-induced fragment emission of NTO, with nominal 30- $\mu$ s delay after crack completion.

## Compressive-Impact-Induced NTO Decomposition

The shear *in-situ* tests involved relatively little energy being absorbed by the NTO specimen. To substantially increase the energy absorbed by the specimen in the fracturing process (although still remaining well below the threshold of initiation for NTO), we modified the test fixture to impact the NTO specimen in a compressive (or crushing) mode with the impactor coming to a complete stop during fracturing of the specimen, thereby imparting all its kinetic energy to the fracturing process.\* This modification provided for end-on impact of a blunt steel segment on conically ended cylindrical NTO specimens. We decided on a conical shape for target end of the impacted specimen, expecting that this would cause more surface fragmentation than impact on a flat-ended specimen and would also provide an impacted surface that was not originally 90° from normal to the mass spectrometer axis.

Compressive-impact-induced decomposition mass spectra of NTO were obtained with a 300- $\mu$ s delay after initial contact with the conical tip. At this point, the impactor has traveled roughly halfway into the conical section and produced a significant volume of fractured NTO. As with the 100- $\mu$ s delay shear spectra, these impact-induced spectra varied widely, from essentially noise only to a signal/noise ratio of 200/1 for the peak at  $m/z$  99. Figure 12 shows the most intense of these spectra. The total number of counts at  $m/z$  99 is about 200, quite similar to the results in Figure 11 for the 100- $\mu$ s delay shear-induced spectra. Also similar is that the only significant secondary peaks are  $m/z$  58, 30, and 17. Figure 13 is the sum of four compressive impact spectra, all taken 300  $\mu$ s after initial contact of the impactor with the conical tip. Two other spectra taken at the same delay showed no appreciable intensity at  $m/z$  99 or any other mass.\*\*

The most striking difference in these compressive-impact-induced spectra from the shear-induced spectra taken earlier is that the molecular ion,  $m/z$  130, is now *completely* absent. The absence of  $m/z$  130 cannot simply be accounted for by an uncontrolled lowering of chamber temperature and therefore a lowering of a peak due to thermal desorption: the chamber temperature is not specifically controlled, but it does not differ appreciably from the room temperature, which is always  $24 \pm 2^\circ\text{C}$ . However, the absence of any intensity at  $m/z$  130 may reflect the fact that, for species to be emitted in the compressive impact mode, they effectively need to squeeze out from the cracks in a "pile of rubble." Under these conditions, any NTO molecules that are "bumped" off the surface by movement stemming from the fracture process will have a high probability of

---

\*More precisely, some of the kinetic energy of the impactor goes to the fracturing process in the target, and some goes to lateral acceleration of the fractured fragments.

\*\*Other than chamber background at  $m/z$  17 and anthracene mass marker at  $m/z$  178.

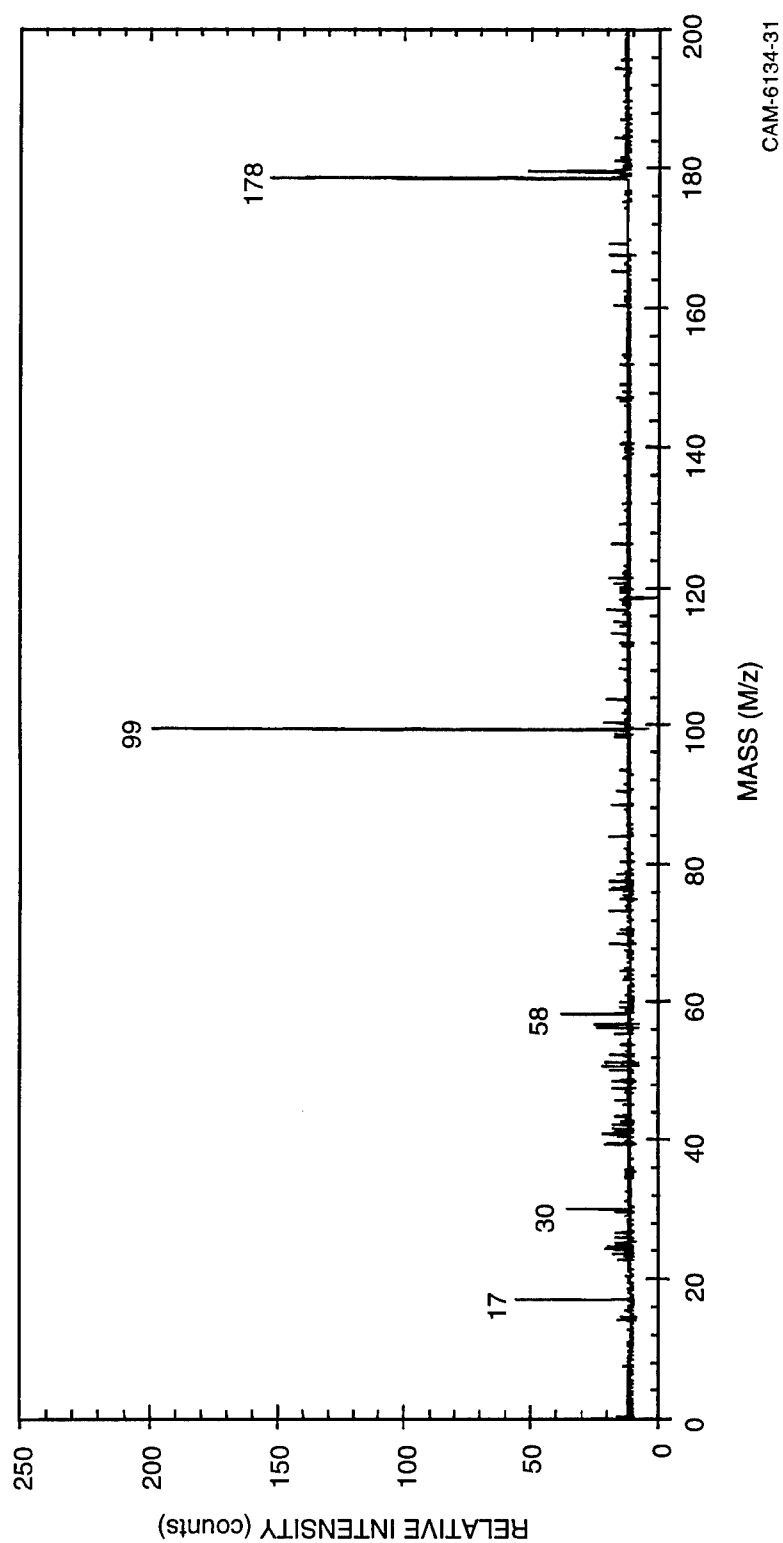


Figure 12. Single-shot SALI spectrum of compressive-impact-induced fragment emission of NTO, with nominal 300- $\mu$ s delay after initial impact.



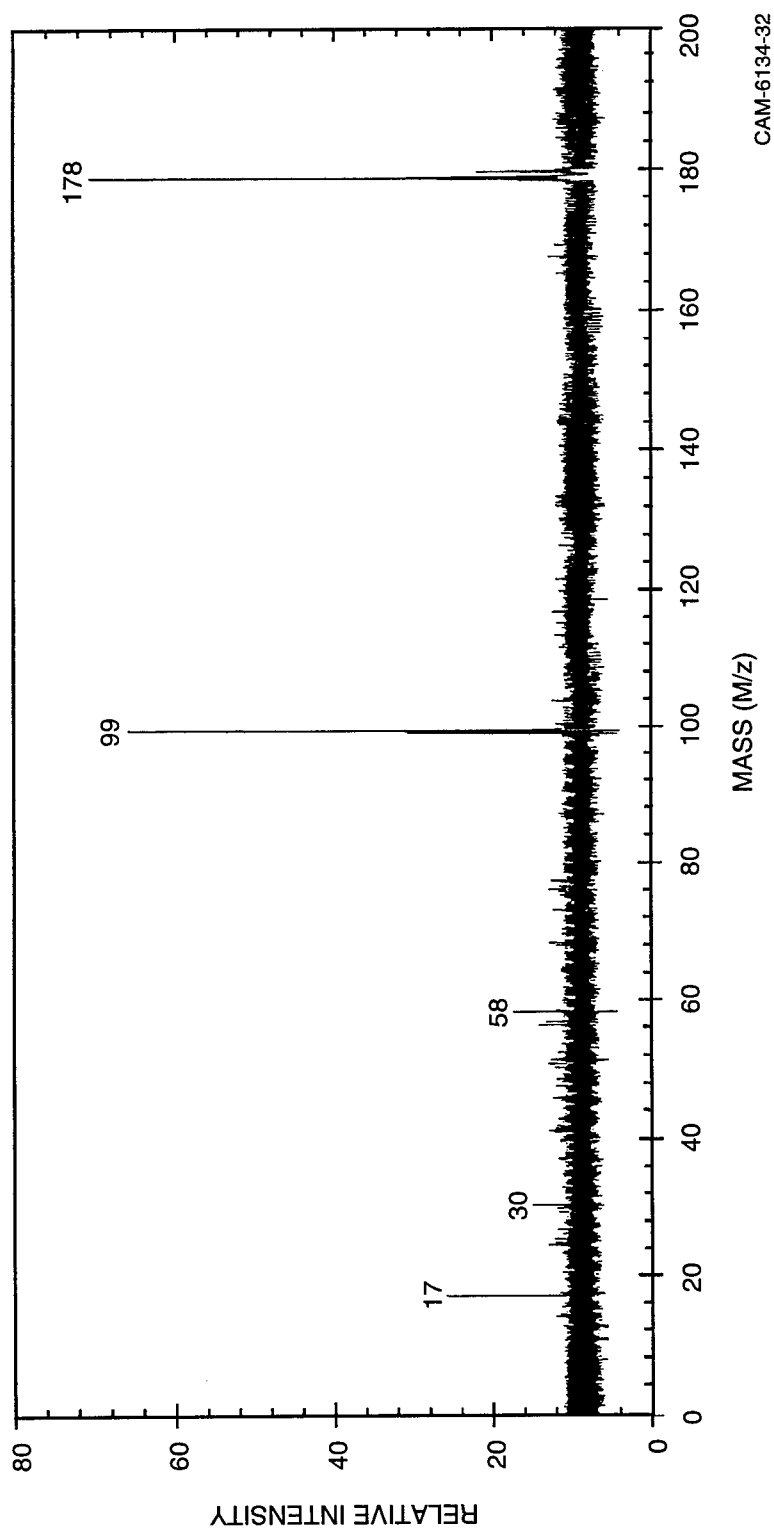


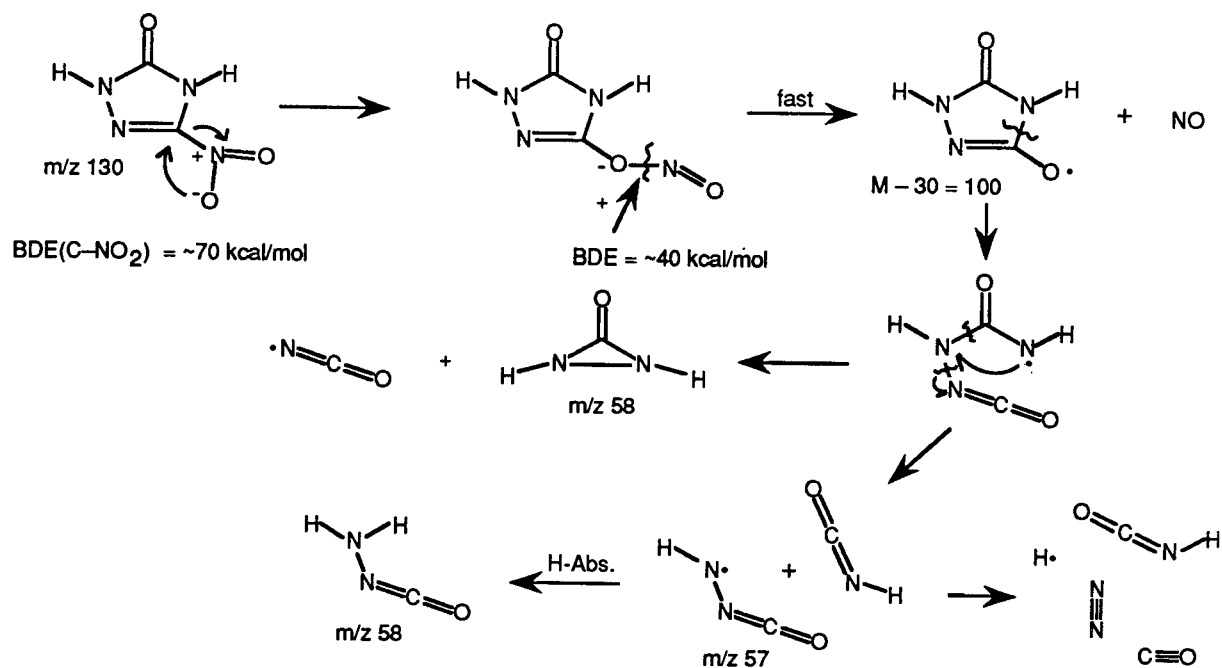
Figure 13. Four-test average spectrum of compressive-impact-induced fragment emission of NTO.

encountering another NTO surface and being readsorbed or condensed. In contrast, the simple-shear experiments, in generating a "clean" fracture surface, provide for little opportunity to readsorb NTO that has been bumped off the surface by a migrating shear band (see discussion below under General Mechanisms of Stress-Induced Chemical Reaction). This explanation would of course require that the lower molecular weight and lower polarity of the mass 99 species be sufficient to make its readsorption substantially less effective.

The mass 58 fragment likely has the composition  $\text{CH}_2\text{N}_2\text{O}$ . The probable origin of this species can be seen as a variation of the reaction schemes discussed in detail in Appendix A and summarized in Scheme 1. Scheme 2 shows how  $m/z$  58 could arise from the alkoxy radical initially generated by nitro-nitrite rearrangement and  $\text{O}-\text{NO}$  scission. As shown in Scheme 2, there are two obvious possibilities for mass 58, starting with ring-opening C-N  $\beta$ -scission of the mass 100 alkoxy radical species. The first  $\beta$ -scission would give a mass 100 species having  $-\text{N}=\text{C}=\text{O}$  connected to the mass 58 fragment  $-\text{NH}(\text{C}=\text{O})\text{NH}\cdot$ . This species in turn could undergo either a quasi  $\beta$ -scission process to form  $\cdot\text{N}=\text{C}=\text{O}$  and the three-membered mass 58 three-membered ring ( $-\text{NH}(\text{C}=\text{O})\text{NH}-$ ) directly, or it could undergo a simple  $\beta$ -scission to eliminate the mass 57 radical shown in Scheme 2.

The latter scission seems much more likely and could produce a mass 58 species if, under the high concentration, relatively low-temperature shear conditions, this radical could pick up a hydrogen in competition with its facile further  $\beta$ -scission to  $\text{CO}$ ,  $\text{N}_2$ , and  $\text{H}\cdot$ . It must be remembered that the apparently dominant  $m/z$  58 we see could in fact represent only, say, 20% of the fragments of the ring-opened mass 100 intermediate. Because the ionization potentials of  $\text{CO}$  and  $\text{N}_2$  are 14.0 and 15.6 eV, respectively, neither of these would be photoionized by the 10.5-eV ionizing laser.  $^{15}\text{N}$  labeling could be used to distinguish between these particular alternatives.

Although it is not yet clear which of these alternatives accounts for  $m/z$  58, and what is the precise explanation for the shift in branching as the delay time is shortened to the 100- $\mu\text{s}$  range, it is clear that shifts in reaction conditions change the relative opportunities for unimolecular reactions and bimolecular hydrogen-transfer reactions, and the results of these shifts can be seen in comparing thermal decomposition mass spectra with various fracture-induced spectra. Thus, although the story is still far from complete, once again the ability to characterize stress-induced chemical changes in real-time measurements has provided interesting clues to the behavior of energetic materials—clues that have been inaccessible by other means.



**Scheme 2. Possible route to m/z 58 during mechanical-stress-induced decomposition.**

## Post-Examination of Subcritically Shocked NTO

For comparison with our real-time stress-induced measurements as well as with the recent work of Beard and Sharma (1993), we prepared samples by subjecting them to near-threshold impacts in a standard drop-hammer test apparatus and then analyzed them under laser-desorption conditions. These results are described in Appendix A, but in brief are as follows.

Consistent with the above results on shear- and compression-impact-induced decomposition, laser-desorption spectra of the previously impacted samples (examined about 1 hr after impact and handling in air), now show small peaks at  $m/z$  99 and 58, where previously there were none visible in the laser-desorption spectra. The  $m/z$  99 intensity is about 2% of the  $m/z$  130 intensity in the impacted NTO, compared with 1.3% in the post-examination of the sheared pellet, essentially zero ( $<0.05\%$ ) for a fresh pellet and contrasted with  $\sim 500\%$  of  $m/z$  130 in the real-time shear-induced spectra themselves. Thus, the appearance of a new peak at  $m/z$  99 is common to the very modest stress caused during simple shear and to the much larger stresses resulting during marginally subcritical impact. That  $m/z$  99 is stable enough for some of it to survive roughly an hour during transfer to the SALI apparatus and pumpdown is certainly consistent with our

suggestion that its stability as a closed-shell species may represent a bottleneck in the NTO initiation sequence.

## **General Mechanisms of Stress-Induced Chemical Reaction**

Appendices A and B discuss the chemical sequences in NTO decomposition that are indicated by the present work. In this section, we focus on the general process by which deposited mechanical energy generates and liberates to the gas phase the chemical decomposition products. Given that 3000  $\mu$ s (our original minimum delay time) is several thousand times the period required for thermal fragments emitted from the fracture surface to travel to the mass spectrometer ionizing region, one might be surprised that we were able to detect fracture-induced fragments with the relatively high single-shot signal/noise ratios (up to 40/1) as reported in the initial series of fracture-induced measurements. That is, any fragments generated and emitted from the fracture surface at the time of the crack would, in 3 ms, have traveled far beyond the mass spectrometer sampling region.

The long delay times we observe for the shear-induced spectra mean that fragments are not merely liberated in the initial crack event but for some reason are slowly emitted for a relatively long time after that event. Dickinson and coworkers (1984, 1991) discussed several mechanisms by which neutral species, charged particles, and photons are evolved in "fracto-emission" processes. They suggested that long-lived emission can result from the time required for deeply buried shear bands to migrate to the surface. With this general suggestion in mind, it is useful to consider what we observed when the delay time for observation was moved from milliseconds/seconds to microseconds.

First, we were unable to formulate any expectation about what would be seen with a delay of only a few hundred microseconds after the shear event, but under circumstances where a much less favorable observation angle (almost 90° off-normal) was dictated. Nor could we predict what would be seen with a much more energetic compression event, but one in which most of the new surfaces generated in the crushing are buried in the rubble pile, with little line-of-sight access to the ionization and extraction region.

Dickinson et al. (1984) had earlier reported that electronic emission from RDX samples was much stronger under compressive impact conditions, but we had no real basis for extrapolation from their conditions or from electronic emission to evolution of neutral fragments. We now know we can see signals with five-fold (but apparently not orders of magnitude) higher intensities are seen at delay times of around 100  $\mu$ s, compared with those we saw with delays of 3 to 10,000 ms. The decay time constant, which we first determined by fitting the data from 100

milliseconds to 90s to a simple exponential, was about 10 s. This long time constant does in fact appear consistent with spectra that are only five times more intense at much shorter delay times ( $\sim 100\ \mu\text{s}$ ). However, short delay-time spectra that are not greatly more intense than those observed at long reaction times are intuitively surprising when considered from the following point of view.

Given that the appearance of the new fracture surface is rather monolithic, as if failure had taken place primarily along a single "plane," it seems surprising that more total emission (implying more deposited energy in total) could originate from many smaller, buried shear bands than from the one large fracture that ultimately causes failure.\* Of course, nothing requires a single time constant to cover emission over the entire microsecond to second time scale. We can only reiterate that, thus far, our measurements of shear-induced emission and of compressive impact emission (each with  $\sim 100\text{-}\mu\text{s}$  delay) give spectra only about five times more intense than those obtained with millisecond delay times and, therefore, provide no suggestion of initial emission intensities that are many orders of magnitude higher.

One might ask if long decay times arise from the fact that long times are required for thermally produced decomposition products to be chemically generated. However, any heat generated locally in the shear process will dissipate extremely rapidly. For example, for a  $1\text{-}\mu\text{m}$  hot spot, the time constant for conductive accommodation to the bulk temperature will be  $\sim 10\ \mu\text{s}$ ). Therefore, thermally driven chemistry cannot continue for very long. Similarly, simple vaporization of fragments like  $m/z\ 99$  from the fracture surfaces should be relatively fast. Taking the cyclic imide succinimide as a model that should have vapor pressure not greatly different from the triazodiketone  $m/z\ 99$ , we estimate that the rate of vaporization of pure  $m/z\ 99$  from a fracture surface at  $20^\circ\text{C}$  would be fast enough to remove one full monolayer in about 2 ms. Although this time is a lower limit, because  $m/z\ 99$  would actually be desorbing from the more polar NTO surface, we would *not* expect chemisorption of the triazodiketone on NTO to increase the desorption time by three orders of magnitude.\*\* Thus, it appears that slow decay of the intensity of  $m/z\ 99$  must involve something more than simple slow desorption of decomposition fragments from the fracture surface.

---

\*If we compare total emission in a presumed initial "burst" at, say  $0\text{-}100\ \mu\text{s}$  from the instant of completion of the main fracture, with a lower emission intensity over the period of  $100\ \mu\text{s}$  to  $10\ \text{s}$ , the "initial" intensity would have to be higher by a factor of  $10\ \text{s}/100 \times 10^{-6}\ \text{s} = 10^5$  for the total species emitted initially to exceed the total of those emitted over the  $100\text{-}\mu\text{s}$  to  $10\text{-s}$  time period.

\*\*The published "vacuum stability" of NTO (Aubert, 1993) corresponds to a vaporization time of about 30 ms per monolayer at  $100^\circ\text{C}$  even for NTO itself.

Returning to the suggestion that the decomposition products may be generated within shear bands that are not exactly at the surface, we can readily estimate the diffusion time for such products. Assuming that the depth of such shear bands is typically a maximum of 10  $\mu\text{m}$  (Mohan et al., 1988), a diffusion coefficient typical of organic solute diffusion in solid polymers  $2 \times 10 \text{ cm}^2/\text{s}$  (Cussler, 1984), would lead to a characteristic diffusion time of about 2 s, and a diffusion depth of 1  $\mu\text{m}$  would lead to a diffusion time of about 0.02 s. Thus, material rising from  $\sim 10\text{-}\mu\text{m}$  depths within the fracture surface could possibly account for the long delay times observed here.

The specific observations of Dickinson et al. (1984) on fracto-emission of RDX crystals seem very relevant to our results showing quite long-lived emissions of fractured NTO. These authors note that, when the single-crystal three-point bend fracture surfaces are smooth, the emission tends to be low level and short lived (decay time constant  $\sim 20 \text{ ms}$ ), but when the fracture surfaces are rougher, even with the same three-point bend procedure, the emission tends to be substantially more intense and to have a much longer decay time ( $\sim 300 \text{ s}$ ). Similarly, the compressive failure of RDX produced more intense, long-lasting emission. A three-point bend that produces a quickly growing crack under pure tensile stress may generate electrons and other decomposition fragments, as Dickinson proposes, via a gaseous electric discharge driven by rapid charge separation on the two parting surfaces. However, when the stress is more complex (e.g., containing a significant shear or compression component), fracture may involve production of shear bands that do not lie exactly at the surface, and, therefore, whose decomposition products require time to diffuse to the surface.

An alternative explanation for the long decay times is that mechanical energy not released in the initial crack formation is stored as strain that is released bit by bit as time goes on. Each release of strain could generate local hot spots and cause additional chemical reaction. However, this latter variation seems less likely because we expect these later releases would have to involve much less energy than the original crack propagation and would lead to a more pronounced decrease in emission intensity with time.

We have not in this work made observations within the flight time ( $\sim 1 \mu\text{s}$ ) of the initial crack growth event (which would have provided a direct assessment of intensity decline from the very beginning). The present experimental arrangement allows *in principle* for such measurements, but because the repetition rate of the ionizing laser is 10 Hz, all time dependence to be mapped out on a finer than 100-ms time scale requires an entire series of experiments, each with a new pellet introduced separately into the vacuum chamber. Such an approach is time consuming

when the time grid is 100  $\mu$ s; it becomes impractical when the time grid is 10  $\mu$ s or less. The 100- $\mu$ s time scale shear tests themselves were already beyond the originally planned scope of work.

At this point, we believe that the most useful application of the techniques developed in this project involves use at the millisecond time scale (and selectively at the 100- $\mu$ s scale) to study the effects of chemical variations in the material to be fragmented, in order to test the chemical explanations we have put forward for the sequence of products and for the origin of NTO's insensitivity. The useful variations would include (1) isotopic substitution to confirm structures of speculatively identified intermediates, (2) additives that would influence competitive reactions and change branching ratios, (3) other explosive materials, alone and in combination with NTO, and (4) compositions that include either the NTO intermediates indentified here or sources of those intermediates other than NTO.

## CONCLUSIONS

Results obtained from slow- and rapid-heating laser-desorption mass spectrometry and from fracture-induced fragment emission under simple-shear and compressive impact conditions have allowed us to suggest (1) an NTO decomposition sequence that reconciles previously disparate literature data on NTO and (2) that the origin of the marked initiation insensitivity of NTO may be the stability of the closed-shell intermediate species  $m/z$  99. The results also suggest that increased tendency to form this stable intermediate in bimolecular hydrogen-transfer processes under condensed phase (i.e., high concentration), low-temperature (i.e., marginal) conditions shifts the branching ratio in decomposition toward a relative dead end.

Real-time measurements of shear-induced NTO fragments were performed by means of a spring-driven shearing device installed in a SALI chamber directly beneath the mass spectrometer sampling region. The shear-induced spectra are dominated by a peak at  $m/z$  99, which is not seen in the thermal or laser desorption spectra. This peak is assigned to the closed-shell triaza-diketone produced by a nitro-nitrite rearrangement, followed by NO loss and then by rapid *bimolecular* H-atom removal. The stability of the cyclic diketone intermediate thus generated could help to explain the shock insensitivity of NTO. Laser-desorption spectra were also obtained both on fresh NTO samples and on samples recovered from marginally subcritical drop-weight impact tests. Comparisons of spectra obtained with and without laser desorption and as a function of temperature indicate that the sequences of fragment ions observed under laser desorption conditions are the result of thermal decomposition, not ion-fragmentation.

Laser-desorption spectra of NTO powder and pellets give thermally generated fragments dominated by M-16, M-30, M-45, M-46, and M-59 (giving ions at  $m/z$  114, 100, 85, 84, and 71, respectively). This series suggests several decomposition pathways, dominated by the same nitro-nitrate rearrangement and NO loss. This sequence indicates that thermal decomposition, either in the heated surface layers or in the laser plume, proceeds largely by the same nitro-nitrate rearrangement and NO loss as the shear-induced decomposition, but then branches to ring opening adjacent to the carbonyl group, followed by additional  $\beta$ -scission and oxygen-transfer reactions. This sequence satisfactorily explains the "initial" formation of CO<sub>2</sub> previously reported (Botcher, 1996), as well as the results of nitrogen double-labeling experiments (Oxley, 1997), and also the fact that neither NO<sub>2</sub> nor HONO has been seen as a significant initial product (Williams, 1994). Furthermore, the suggested ring-opening sequence is arguably consistent with reported deuterium isotope effects (Oxley, 1995) that can be categorized as "diluted" primary isotope effects. However, under the



lower-density, but higher temperature, thermal or laser-desorption conditions, subsequent bimolecular H-atom removal to produce the closed-shell diketone is evidently slower than unimolecular ring-opening adjacent to the carbonyl group.

While quite plausible, our suggestion that the closed-shell species  $m/z$  99 could contribute to initiation insensitivity by inhibiting further reaction under high-concentration (i.e., condensed-phase), low-temperature (i.e., thermally marginal) conditions needs to be tested against other possibilities. The high molecular-weight polymer previously reported (Williams, 1995) at 10%-30% yield under various slow decomposition conditions also represents a dead-end; its structure and the factors affecting its formation need to be further considered. However, even at this early stage, single-photon ionization MS measurements and the capability for performing *in-situ* shear and impact experiments have provided us a new window on NTO decomposition chemistry, allowing observation of intermediate molecular weight species not previously detected and aiding in the connection of these intermediate species in chemically rational decomposition pathways.

## REFERENCES

- Aubert, S. "Characterization of the Hydrodynamic Performance Properties for NTO and TNTO Composite Explosives," Final Report WL-TR-94-7037 for Wright Laboratory, Armament Directorate, May 1994.
- Aubert, S.; Corley, J. D.; Glenn, J. G., "Development of TNTO Composite Explosives," Final Report WL-TR-92-7073 for Wright Laboratory, Armament Directorate, June 1993.
- Beard, B. C.; Sharma, J., *J. Energetic Materials* **11**, 325 (1993).
- Becker, C. H.; Gillen, K. T., *Anal. Chem.* **56**, 1671 (1984).
- Botcher, T. R.; Beardall, D. J.; Wright, C. A., "Thermal Decomposition Mechanism of NTO," *J. Phys. Chem.* **100**, 8802 (1996).
- Chapman, L. B. In *Proceedings of the Ninth Symposium (International) on Detonation*; The Combustion Institute: Portland, Oregon, 1989; p. 1001.
- Cussler, E. L., *Diffusion: Mass Transfer in Fluid Systems*, Cambridge University Press, 1984, p. 130.
- Dickenson, J. T.; Jensen, L. C.; Langford, S. C., *Phys. Rev. Lett.* **66**, 2120 (1991).
- Dickenson, J. T.; Miles, M. H.; Elban, W. L.; Rosemeier, R. G.; *J. Appl. Phys.* **55**, 3994 (1984).
- Kalthoff, J. F.; Winkler, S., "Failure Mode Transition at High Rates of Shear Loading," in *Impact Loading and Dynamic Behaviour of Materials*, Chiem, C. Y.; Kuncze, H.-D.; Meyer, L. W., Eds.; DGM Informationsgesellschaft: Germany, 1988; pp. 185-195.
- Lee, K.-Y.; Coburn, M. D. *J. Energ. Mater.* **5**, 27 (1987).
- Mohan, V. K.; Bhasu, V.C.J.; Field, J. E., *Proceedings of the Ninth Symposium (International) on Detonation*, 1988, pp. 557-564.
- Oxley, J.; Smith, J. L.; Yeager, K. E.; Rogers, E.; Dong, X. X., "NTO Decomposition Products Tracked With  $^{15}\text{N}$  Labels," *J. Phys. Chem. A* **101**, 3531 (1997).
- Oxley, J.; Smith, J. L.; Zhou, Z.-L.; McKenney, R. L., *J. Phys. Chem.* **99**, 10383 (1995).
- Pallix, J. B.; Schule, U.; Becker, C. H.; Huestis, D. L., *Anal. Chem.* **61**, 805 (1989).
- Williams, G. K.; Palopoli, S. F.; Brill, T. B., *Combustion and Flame* **99**, 197 (1994).

## **APPENDIX A**

### **FRACTURE-INDUCED AND THERMAL DECOMPOSITION OF NTO USING LASER IONIZATION MASS SPECTROMETRY**

**In Press, Combustion and Flame August 1997**

# FRACTURE-INDUCED AND THERMAL DECOMPOSITION OF NTO USING LASER IONIZATION MASS SPECTROMETRY

D. F. McMillen\*, D. C. Erlich, C. He, C. H. Becker, and D. A. Shockey  
Molecular Physics and Poulter Laboratories  
SRI International, Menlo Park, CA

## ABSTRACT

A surface analysis by laser ionization (SALI) apparatus has been used to obtain, for the first time, real-time photoionization mass spectra of the shear-induced molecular-fragment emission from an explosive. NTO (5-nitro-1,2,4-triazol-3-one) was chosen for these experiments because of its potential utility as a reasonably energetic, but very insensitive, explosive. Using vacuum ultraviolet single photon ionization, the shear-induced NTO spectra were obtained with a spring-driven shearing device installed in a SALI chamber directly beneath the mass spectrometer sampling region. For comparison, we also obtained spectra under either slow-heating or rapid pulsed-laser heating conditions.

The shear-induced spectra are dominated by a peak at  $m/z$  99, which is not seen in the thermal- or laser desorption spectra. This peak is assigned to the closed-shell triaza-diketone produced by a nitro-nitrite rearrangement, followed by NO loss and then by rapid *bimolecular* H-atom removal. The stability of the cyclic diketone intermediate thus generated could help to explain the shock insensitivity of NTO. Laser-desorption spectra were also obtained both on fresh NTO samples and on samples that have been recovered from marginally sub-critical drop-weight impact tests. Comparison of spectra obtained with and without laser desorption, and as a function of temperature, demonstrate that the sequences of fragment ions observed under laser desorption conditions are the result of thermal decomposition, not of ion-fragmentation.

The sequence of thermally generated fragments is dominated by M-16, M-30, M-45, M-46, and M-59. This series suggests several decomposition pathways, dominated by the same nitro-nitrate rearrangement and NO loss as the shear-induced decomposition. However, under the lower-density, but higher temperature, thermal or laser-desorption conditions, subsequent bimolecular H-atom removal to produce the closed-shell diketone is evidently slower than unimolecular ring-opening adjacent to the carbonyl group. We show how this sequence satisfactorily explains (1) the "initial" formation of CO<sub>2</sub> that has been previously reported, (2) the results of nitrogen double-labeling experiments, and (3) the fact that neither NO<sub>2</sub> nor HONO have been seen as substantial initial products of NTO decomposition.

## LIST OF FIGURES

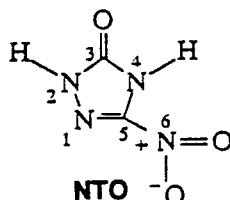
- Figure 1. Temperature-programmed thermal desorption SALI spectrum of NTO crystals at 118°C.
- Figure 2. Schematic view of *in situ* test fixture on SALI apparatus, for use in dynamic simple shear and three-point bend tests.
- Figure 3. Detail of SALI *in situ* test fixture for simple shear testing.
- Figure 4. SEM views of fine-grained NTO.
- Figure 5. SEM view of various regions of the fracture surfaces from *in situ* simple shear tests on NTO pellet.
- Figure 6. SALI spectra of NTO crystals during slow heating in copper grid.  
a. 50°C, no desorption laser.  
b. 50°C, desorption laser on.
- Figure 7. SALI spectra of NTO crystals during slow heating in copper grid.  
a. 200°C, no desorption laser.  
b. 200°C, desorption laser on.
- Figure 8. Laser-desorption SALI spectra of NTO.  
a. crystals pressed into indium foil;  
b. surface of pressed pellet.
- Figure 9. Single-shot SALI spectra of shear-induced fragment emission taken 3.3 and 203 ms after shear.
- Figure 10. 100-shot average SALI spectra of shear-induced fragment emission accumulated between 50 and 60 s after shear.
- Figure 11. Decay of  $m/z$  99 intensity following simple-shear test.
- Figure 12. Comparison of laser-desorption SALI spectra taken before and after shear test.
- Figure 13. Laser-desorption SALI spectrum of NTO recovered from a sub-critical impact test.

## LIST OF REACTION SCHEMES

- Scheme 1. Proposed NTO decomposition sequence following a nitro-nitrite rearrangement.
- Scheme 2. Nitroso compound formation from NTO and possible subsequent reactions.
- Scheme 3. NTO decomposition by nitro-nitrite rearrangement, O–N bond cleavage, and NO recombination on nitrogen.
- Scheme 4. Intermolecular oxidation by NTO of the ring-opened acyl radical intermediate to produce CO<sub>2</sub>.
- Scheme 5. Required products for unimolecular- and H-transfer-promoted bimolecular elimination of HONO.
- Scheme 6. Stoichiometry of possible combined reaction sequences for NTO decomposition.
- Scheme 7. Possible formation of cyclic diketone by acid-promoted nitro-nitrite rearrangement, followed by bimolecular H-atom transfer.

## INTRODUCTION

As an explosive with performance characteristics (i.e., detonation velocities) that approach those of RDX, but which is much more insensitive [1], 5-nitro-1,2,4-triazol-3-one (NTO) provides a new opportunity to address the perennial questions of what sequence of decomposition reactions is responsible for initiation of an explosive event, and why some explosives have bottlenecks that make it much more difficult for decomposition to become self-sustaining. Essentially a nitro olefin, NTO is expected to have a C-NO<sub>2</sub> bond strength about that of TNT. It exhibits detonation pressure and velocity values that exceed those of TNT [2], but its sensitivity is lower. Thus, it appears to fall outside the correlation noted by Nielsen [3] between initiation sensitivity and a function dependent on calculated detonation temperature and X-NO<sub>2</sub> bond strength. In this paper, we report for the first time the use of a highly sensitive mass spectrometric technique for real-time detection of stress-induced decomposition products of NTO. We also examined, for comparison, products from two different modes of heating.



Surface analysis by laser ionization (SALI) is a laser-desorption mass spectrometric technique that, unlike the more commonly used secondary ion mass spectrometry (SIMS) or laser microprobe mass spectrometry, uses a second, shorter wavelength laser pulse to ionize molecules (or thermal fragments) that are desorbed from the surface by a longer wavelength laser. This two-step process provides the capability for high sensitivity detection of a range of products, including high molecular weight, very non-volatile species, under conditions that provide minimal fragmentation either before or after ionization. We have modified the vacuum chamber of SRI's SALI instrument so that it can be used for real-time detection of the products of NTO decomposition that result from shear and tensile failure, as well as for the normal types of slow-heating and laser-heating decomposition measurements.

Since NTO is kinetically very stable relative to the energy stored in its chemical framework, it presents both the advantage of being reluctant to ignite or initiate and the disadvantage of being difficult to bring to a high-order detonation [1]. Thus the failure diameter is rather large (typically ~1 in.), and the puzzling dependence of detonation pressure and velocity on particle size and

density has resulted in detonation pressures that do not increase significantly with density beyond a point: detonation pressures 18% or more below those expected from calculation have been reported at 96% theoretical maximum density [1]. Some of these challenges have been met in the case of NTO itself via a thorough characterization by Aubert and coworkers of the factors affecting initiation and performance of both pure- and composite explosives containing NTO [2,4]. However, not only is the sequence of chemical reactions necessary for a successful initiation event essentially unknown for NTO, but compared to nitro-aromatics and nitramines, relatively little work has been performed even to determine the intermediates generated during slow thermal decomposition.

Recently researchers have variously reported evidence for NTO thermal decomposition by C-NO<sub>2</sub> scission, intermolecular H-atom transfer, intra-molecular oxygen atom transfer, and HONO elimination. Rothgery et al. used differential scanning calorimetry, (DSC), thermogravimetric analysis (TGA), and TGA-MS methods to study the slow thermal decomposition of NTO [5]. These authors reported autocatalytic behavior and the formation of H<sub>2</sub>O, NO, NO<sub>2</sub>, N<sub>2</sub>, and CO<sub>2</sub>, but no identifiable larger fragments. Menapace et al. used ESR to detect radical species and have reported results consistent with the formation of an initial nitroxyl radical intermediate in the condensed phase thermal reaction of NTO [6]. More recently, Williams et al. used rapid-heating FTIR studies to examine the gaseous and condensed-phase products of NTO decomposition [7]. They report IR identification of the fixed-gas species reported by Rothgery et al., along with HCN and HNCO. Oxley et al. have used batch micro-reactor studies and isotopic labeling to follow the decomposition of both neat and solution-phase NTO, and suggest that decomposition can take place either by NO<sub>2</sub> or HONO loss [8]. Botcher et al. report FTIR tracking of IR-laser decomposition of NTO thin films [9]. They observe CO<sub>2</sub> as the dominant and most quickly developing *small molecule* product that can be identified, and interpret their results as indicating *intra*-molecular oxidation of the carbonyl group by the NO<sub>2</sub> group. Finally, and most directly related to the present results, is the work of Beard and Sharma who used X-ray photoelectron spectroscopy (XPS) and chemical ionization mass spectrometry (CIMS) to examine unstressed NTO, as well as NTO damaged by sub-critical drop-weight impact, shock, radiation, and heat [10]. They report mass spectrometric peaks for larger NTO fragments that correspond to loss of O, NO, HONO, and NO<sub>2</sub> minus H. The losses of O and NO were most enhanced in the shock-damaged samples.

The results of these previous studies can be basically summarized as follows. Autocatalytic decomposition becomes significant at about 240°C, typically yielding low molecular-weight gases and a small amount of polymeric material. ESR studies show that nitroxyl radical species are generated in visible concentrations at temperatures 150°C lower, and are enhanced by



mixing of NTO with compounds having C-H bonds weaker than either of the N-H bonds in NTO [6]. However, in these same mixtures, there is no enhancement of gross thermal instability or sensitivity [2], suggesting that the nitroxyl radical is not a limiting intermediate on the main decomposition route. Although unimolecular scission of the C-NO<sub>2</sub> bond and HONO elimination have both been postulated by several groups as the initial decomposition step, and the latter *appears* to be supported by deuterium isotope effects, [8] the pressure-dependent IR studies of Williams et al. do *not* show initial generation of either NO<sub>2</sub> or HONO [7]. Williams et al. do show early generation of CO<sub>2</sub>, but since its level rises, rather than falls, with time, it is not clear that their data support the conclusion of Botcher et al. [9] that CO<sub>2</sub> is formed in an initial reaction. Furthermore, a rate-determining, bimolecular first step between two NTO molecules cannot explain the autocatalytic decomposition behavior reported by several other authors.

Relatively little help in mechanistic understanding has been provided by the ~10% yield of polymeric material that appears as an NTO decomposition residue in either slow or moderately rapid thermal decomposition. This material, being insoluble, cannot be readily characterized, except for measurement of its FTIR spectrum after generation on a hot nichrome ribbon [7] and by elemental analysis [5,8]. The FTIR characterization suggests the residue is not simply a polymer of triazalone, since it contains only traces of this material, and moreover, is not generated by heating triazalone [8]. The polymer formation in the TGA experiments is very curious: there is a precipitous weight loss, which both in the present work and in Reference 5 stops abruptly at  $11 \pm 1$  wt % residue. The abruptness of the shutoff might suggest a stoichiometrically determined residue yield, but in the sealed-tube studies of Oxley et al., the residue was substantially higher (31%) [8]. The empirical formulas of these residues (~C<sub>2</sub>H<sub>3</sub>N<sub>3</sub>O, TGA, ~C<sub>2</sub>H<sub>2</sub>N<sub>2</sub>O sealed-tube) might suggest loss of the NO<sub>2</sub> group as the major change, but the observed 90% weight loss in TGA far exceeds the 35% weight fraction constituted by the NO<sub>2</sub> group in NTO.

In short, the available information on NTO decomposition, even slow thermal decomposition, is not all easily reconciled, providing no clear mechanistic picture. Furthermore, there is even less information that would allow us to relate the slow thermal decomposition to the mechanical-stress initiated sequence of reactions that leads to detonation (or deflagration) of NTO. To help fill this gap, and hopefully to reconcile some of the previously reported results, we have used SALI to make real-time observations of the fragments generated from both mechanical and thermal stresses.

## EXPERIMENTAL PROCEDURES

**SALI Measurements.** Since much less is known about the sequence of chemical intermediates generated during NTO decomposition even than is known for other explosives, we chose to use a detection technique that is essentially "universal" in terms of product sensitivity. Surface analysis by laser ionization (SALI) combines post-ionization of sputtered neutrals by multiphoton ionization (MPI) with time-of-flight (TOF) mass spectrometry [11,12]. The method offers high sensitivity ( $< \text{ppm}$ ) and wide dynamic range ( $\geq 10^5$ ). The SALI method is a three-step process. The surface or material of interest under high vacuum is first irradiated by a pulsed probe beam of photons, ions, or electrons to cause the desorption or sputtering of a small amount of adsorbate or surface material. Second, the neutral material released from the surface is ionized by a high intensity pulsed laser beam (the ionizing beam) passing close to the surface. Third, these ions are accelerated, focused, and then allowed to drift in a field-free region for TOF mass spectral analysis before detection.

An important aspect of the SALI approach is the separation of the desorption step from the ionizing step. The separation permits (1) detection of the overwhelmingly abundant neutral fraction rather than the selectively ionized material generated in an intense laser plume, (2) greater control and flexibility in types and intensities of the probe- and ionizing beams, allowing a relatively gentle, low fluence surface irradiation to minimize surface damage and allow a quantifiable ionization step, and (3) the avoidance of large matrix effects where the ionization probabilities of molecules vary greatly as a function of the chemical environment. This separation of desorption from ionization is in contrast to the related techniques of secondary ion mass spectrometry (SIMS), fast atom bombardment (FAB), and laser microprobe analysis, where the desorption or sputtering process is also responsible for ionization.

In these experiments we used a single-photon ionization (SPI) scheme for the ionization step. The coherent vacuum-ultraviolet (VUV) light generation is based on the 9th harmonic of a 35-psi Nd:YAG laser at 118 nm (10.5 eV). A driving reason for using SPI is its "soft" (i.e., relatively nonfragmenting) ionization. In the experiments on NTO, we specifically tested whether significant photofragmentation is induced by the ionization laser. For example, as shown in Figure 1, the mass spectrum taken of the thermally desorbing gas above NTO crystals at 120°C by SPI at 118 nm gives only a single peak for the molecular ion at 130 amu, indicating complete absence of photo- or ion fragmentation. Another advantage of SPI is that, for molecular systems, photoionization cross sections tend to differ relatively little from one another for molecules having 3 or more heavy atoms.

and ionization potentials of less than about 11.0 eV, typically falling within the range 3-30 Mb [13], and within an even narrower range if they contain  $\pi$ -electrons. Although absolute cross sections are difficult to measure, because essentially all window and lens materials absorb 118-nm radiation, this same "universal overlap" with electronic transitions of most substrate molecules enables 118 nm ionization to provide semi-quantitative molecular abundance measurements between different species, with the requirement for specially prepared standards that is encountered with SIMS. This generalization is borne out by experience derived from use of gas chromatographic photoionization detectors [14].

With the exception of timing and sequence of single- and averaged multiple shot spectra, the procedures used for obtaining SALI spectra are essentially those that have been developed over the last six years in our laboratory using the SRI prototype instrument [11,12]. These include laser-desorption spectra at room temperature and under temperature-programmed heating, as well as spectra with no laser desorption. For the *in-situ* simple shear tests on NTO pellets, no desorption laser is used; the procedures are not standard and required the construction of a special modification to the SALI chamber, which is described below. Mass calibration is achieved by interpolation between the ubiquitous background peak at  $m/z$  17 ( $\text{NH}_3$ ) and a small residual vapor pressure of anthracene ( $m/a$  178) deliberately introduced into the chamber. The uncertainty of interpolation and peak assignment throughout the range is  $< 0.2$  amu.

**Real-Time Detection of Fragments Generated by Simple Shear.** *In situ* testing in the SALI facility required a fixture that would hold a small NTO specimen near the center of the 8-in.-diameter high-vacuum chamber (so that the surface to be examined was within a few mm of the mass spectrometry sampling cone), and could load the specimen along a variety of load paths with a device that could be controlled from outside the chamber (i.e. by means of a high-vacuum motion feedthrough). Furthermore, the geometry of the fixture had to be such that each of the two lasers involved in the SALI technique had a clear path either onto the specimen's surface of interest (in the case of the desorbing laser) or slightly above the surface (in the case of the ionizing laser), either during the loading process (in the case of quasistatic loading) or very shortly afterwards (in the case of dynamic loading).

A schematic diagram of the generalized *in situ* test fixture is shown in Figure 2. The foundation of the fixture is provided by an X-Y-Z precision manipulator stage, and push-pull motion, bellows-sealed feedthrough, which were attached via a reducing nipple to a 6-in. diameter port that is approximately 6 in. from the center of the SALI chamber. The linear motion feedthrough was modified by: 1) welding a 1-in.-O.D. tube to the inside of the 2.75-in.-diam. flange to provide rigid support for a platform into which the NTO specimen is inserted, 2) bolting a specimen loading device to the inside end of the linear motion feedthrough shaft, and 3) extending

the outside end of the shaft to allow for attachment of a spring to provide an accelerating force to the shaft and an opaque plate to provide a means for triggering the SALI electronics.

The position of the specimen with respect to the mass spectrometer cone is controlled by the X-Y-Z stage, while movement of the feedthrough shaft applies the load to the specimen. The X-Y-Z stage positioning controls remain attached to the high-vacuum chamber during the course of a test series, while the heavily-modified linear motion feedthrough (holding the sample platform itself) is unbolted and removed for each test to allow insertion of the NTO specimens. When the linear motion feedthrough and the sample platform are reconnected to the X-Y-Z stage, they return to the originally aligned position within a few thousands of an inch.

Details of the specimen loading geometry for the *in situ* simple shear tests is shown in Figure 3. The NTO specimen, a cylinder 0.125 in. (3.2 mm) in diameter by approximately 0.25 in. (6.4 mm) is inserted into a 0.125 -in.-(2.3 mm)-deep hole in the specimen platform, with the upper half sticking above the surface of the platform. A cutting tool attached to the linear motion feedthrough shaft shears the specimen at the level of the platform, and then continues in the same direction until the tool and the sheared upper half of the specimen are clear of the SALI lasers and the mass spectrometer cone. A thin glass cover plate atop the shear cutting fixture and a thin brass cylindrical sleeve surrounding the support tube and extending out to the platform region (not shown in Figure 3) contain the sheared NTO fragments after the test.

Before the *in-situ* NTO testing began, we used a high-speed videocamera to record the displacement history of the linear motion feedthrough shaft, so that we could determine the velocity of the cutting tool as it shears across the specimen surface, and determine when the cutting tool cleared the laser beam paths, so we could set up the laser-photo diode trigger for the SALI electronics. In the experiments reported here, the velocity of the cutter as it crosses through the specimen diameter was a nearly constant 1.75 m/s. The cutter clears the ionizing laser beam path  $\approx 3$  ms after contacting the specimen, which means that we are able to obtain a mass spectrometer measurement within 3 ms of the specimen shearing.

**Pressing the NTO Specimens for the *In Situ* Tests.** NTO samples were obtained in two different particle sizes: 20  $\mu\text{m}$  and 200  $\mu\text{m}$ . Whereas the coarse-grained NTO consists of roughly cubical crystalline chunks of from  $\approx 50$  to  $\approx 250$   $\mu\text{m}$  on a side, the fine-grained NTO appears to consist of rough spheres, from  $\approx 15$  to  $\approx 25$   $\mu\text{m}$  in diameter. These spheres are in fact bundles of very fine crystals that radiate outward from the center of the sphere, as can be perceived from the scanning electron microscope view shown in Figure 4.

Our goal for pressing the NTO specimens was to attain densities of 1.85 g/cm<sup>3</sup> ( $\approx 96\%$  of the TMD of 1.83 g/cm<sup>3</sup>) or slightly lower, since higher densities are not reported to produce a

higher explosive yield [4]. We used a modification of the procedure described by Aubert [2] for pressing NTO specimens that calls for one cycle at 24,000 to 28,000 psi for 5 minutes at a temperature of 105°C. The fixture we used consists of a stainless steel die, two alloy steel rods, a base plate, and shims that allow us to press the specimen from both sides and thereby minimize density gradients along the specimen. Electrical heating tape is wrapped around the die to allow for warm pressing. A thermocouple inserted in the die to within 0.25 in. of the specimen, recorded the temperature.

We first tried to press cylindrical specimens with an aspect ratio of about 5 [0.080 in. (2 mm) diameter by  $\approx$ 0.375 in. (9.5 mm) long], but found that these specimens could not be easily removed from the press or handled without being damaged. We then switched to a smaller aspect ratio [0.125 in. (3.2 mm) diameter by  $\approx$ 0.25 in. (6.35 mm) long] and were successful in obtaining specimens of good material integrity

## RESULTS

**Physical Appearance of Fracture Surfaces.** The tests described in this paper were all performed on the fine-grained NTO, since pellets of the appropriate mechanical strength are more reliably prepared with this material. SEM views of various regions on the fracture surfaces obtained from simple shear tests on an NTO specimen are shown in Figure 5. The direction of surface fracture can be clearly seen in Figures 5(a) and (b) as traveling from left to right. The surface has a finely grained polycrystalline appearance, except at various regions scattered around the surface, such as that seen in Figure 5(c), where a clear crystalline step structure appears. We presume that this is an example of an area in which large-scale recrystallization has taken place during pressing. Thus this section of the fracture surface may represent an area in which shear forces are more concentrated than in the more finely-grained regions. The electron micrograph in Figure 5(c) reveals none of the ca. 1- $\mu\text{m}$  round cavities such as those identified by Sharma and co-workers as "quenched" hot spots [15]. Some large, irregular, but rounded-edge craters were observed. These depressions appear too deep to be caused by the laser desorption, although they seem to show the very pronounced channeling that is observed for deep holes bored in polymeric materials by IR or visible lasers. Their origin will be explored in later experiments.

### Effect of Sample Temperature and Laser Desorption on NTO

**Fragmentation.** In this study, we obtained mass spectra from NTO under a range of conditions: laser desorption of unheated NTO, laser desorption of NTO heated through its decomposition temperature, thermal desorption near the NTO decomposition temperature, laser photoionization of neutral shear-induced fragments, and laser desorption after shear. As expected, there are major similarities, as well as some differences, between the spectra obtained under these different thermal decomposition conditions. Both the similarities and the differences help us to distinguish between thermal and ionic fragmentation, between thermal decomposition that takes place in the laser plume as opposed to the heated solid, and between the sequence of reactions that results from either laser heating or from bulk heating and the sequence that takes place as a result of mechanical stress.

It is clear from thermal desorption spectra (temperature-programmed heating @ 10°C/min of NTO crystals held in a resistively heated copper mesh) obtained at intermediate temperatures that fragmentation does *not* occur as a result of the ionization process. At 120°C, where the vapor pressure of NTO is appreciable but where thermal decomposition is very slow, the spectrum obtained without laser desorption (Figure 1 above) shows the NTO molecular ion at  $m/z$  130, but no other peaks. Figure 6 shows that at lower temperatures (50°C) there is no significant ion

intensity at *any* mass without the desorption laser, while with the desorption laser on, the dominant molecular ion is accompanied by a number of fragment peaks at 1-30% of the base peak. At temperatures much closer to the ca. 230°C NTO decomposition temperature (e.g., at 200°C), some fragments begin to appear at very low intensities in the thermal desorption spectra (Figure 7a). At this temperature, use of the desorption laser was observed to increase the relative intensity of the fragment peaks at  $m/z$  30, 43, 71, and 114 roughly tenfold (Figure 7b), but their intensities were still only about 1% of the molecular ion, much less than in the 50°C laser-desorption spectra. Clearly, under laser-desorption conditions we see both sublimation and thermal decomposition, and the intensity of the fragment peaks relative to the molecular ion is a function of both sample temperature and the intensity of the desorbing laser. Thus at intermediate temperatures (ca. 120°C), sublimation is the sole process, as one would expect from the results of Williams and Brill [16]. Even at 200°C sample temperature, with or without the desorption laser on, sublimed intact NTO still accounts for >95% of the ion intensity.

Above 240°C, the temperature at which Menapace et al. report 50% to 90% decomposition in 200 minutes [6], we continue to observe the NTO molecular ion, but at much diminished intensity, and the intermediate peaks decline roughly proportionately. Most of the NTO that has not sublimed has decomposed, and the thermal decomposition intermediates that we observe appear to be transient; under these conditions, they do not accumulate to any appreciable extent in the bulk NTO.

Figure 8 shows two laser desorption spectra of NTO, one of loose crystals and one of the surface of a pressed pellet, obtained with nominally identical desorption laser intensities. The relative intensities of the molecular ion and various fragment peaks are similar, but clearly not identical. The relative intensity of fragment peaks is dependent not only on desorption laser intensity, but also on the physical character of the sample and its effect on the plume created by the desorption laser. Thus in this paper we are wary about drawing mechanistic conclusions merely from an observed increase or decrease in the fragment peaks as a whole, and have focused our attention instead on shifts observed *within* the fragment groupings.

**Detection of Shear-Induced Fragments with no Laser Desorption.** Figure 9 shows single-shot spectra recorded 3.3 and 273.3 ms after initial contact of the shear cutting tool. Figure 10 is the sum of 100 ionizing laser shots, recorded in the interval between 50 to 60 seconds after shear. The decay of  $m/z$  99, the dominant peak in these spectra, is plotted in Figure 11. The intensity of this peak fluctuates initially (on the millisecond time scale) after pellet fracture and then decays slowly over the next 100 seconds.

These shear-induced spectra contrast in three ways with laser-desorption spectra obtained without the shear stress. First, the shear-induced fragments are dominated by a single peak, and other intermediates are very low by comparison. Second, this dominant peak occurs at  $m/z$  99, one mass unit *less* than that observed with laser desorption and no stress. Third, those more minor fragment peaks that do occur as a result of shear, differ somewhat from those that appear under laser-desorption conditions. The chemical interpretations of the spectra obtained under these various conditions are considered in the discussion section.

**Laser Desorption After Shear.** Laser desorption spectra obtained before and after shear are in general terms very similar, but some differences do exist. As Figure 12 shows, significant shear-induced signal intensity persists at  $m/z$  99 even seconds after shearing, although this intensity is quite low relative to the signals induced by laser desorption. Thus, whatever chemical intermediates are generated by the cleavage process and remain on the fracture surface are not different enough or present in high enough concentrations (at least on a regionally averaged basis) to be prominent *relative* to the laser-desorption spectrum of the intact NTO itself.

**Laser Desorption after Impact.** For comparison with the real-time shear-induced spectra, we subjected NTO samples to impact in a standard drop-weight impact apparatus at the threshold of detonation (6 kg @ 55 cm), and then examined the NTO recovered from the sub-critically impacted samples. On the gross scale there is little difference between the laser-desorption spectra of these samples and those obtained with fresh samples. The principal difference is a small peak at  $m/z$  99, and a shift of the peak intensities *within* the minor peak groups. The most pronounced case of this shift was with  $m/z$  84. It increases from an intensity generally less than or equal to  $m/z$  85 in fresh NTO, to an intensity two-to-three times that of  $m/z$  85 in the impacted samples. Both of these differences can be seen by comparing Figure 13 with Figure 12. The SALI spectra taken following either shear or subcritical impact show  $m/z$  84 to be substantially larger than  $m/z$  85. The  $m/z$  99 intensity in an NTO sample recovered from subcritical impact is ~1.8% of the  $m/z$  130 intensity. This is intermediate between nothing (< 0.1%) in fresh NTO (e.g., Figures 6-9) and ~1.3% in the post-examination of the sheared pellet (Figure 12b), and ~500% of  $m/z$  130 in the real-time shear-induced spectra (Figure 10, no desorption laser, 50 s after shear).



## DISCUSSION

Both the laser-desorption SALI spectra of unstressed NTO and the fracture-induced spectra obtained in the *in-situ* simple-shear experiments provide us with views of the NTO decomposition sequence that are largely unavailable from literature data. These new observations, when coupled with recent literature data, constitute a new opportunity for developing a more coherent picture of NTO thermal decomposition. Ultimately, they should also provide a good basis for elucidating the factors that determine whether a mechanically induced decomposition sequence proceeds or fails to proceed to macroscopic self-sustaining decomposition. The thermal- and laser desorption spectra are discussed first, since what happens to NTO during the thermal stresses provided either by heating to the point of gross decomposition or by laser desorption constitute the relevant background for considering the shear-induced emissions of NTO under presumably milder thermal stress.

**Thermal- and Laser-Desorption Spectra.** The essential absence of fragments when the desorption laser is off (Figures 1, 6a, and 7a) indicates that the fragmentation in the laser desorption spectra (Figures, 6b, 7b, and 8) is largely thermal decomposition rather than ion fragmentation. The sequence of fragments we observe under the added thermal stress of the desorption laser differs slightly from that reported by Beard and Sharma for heated-source chemical ionization mass spectra of NTO [10]. The sequence we observe represents, in all likelihood, at least two separate degradation pathways. Scheme 1 shows a probable set of reactions beginning with a nitro-nitrite rearrangement of NTO.

The rearrangement that begins Scheme 1 has literature precedent both for C-nitro and N-nitro compounds [17-19], and can conceivably occur in either as a single unimolecular reaction or as a dissociation-recombination sequence. It converts the weakest bond in the original molecule (C-NO<sub>2</sub>) to the still weaker O-NO bond and leads directly to loss of NO and generation of the alkoxy radical at *m/z* 100.\* As seen in Figures 6 and 7, the intensity at *m/z* 100 is quite low. This is presumably because the alkoxy radical can either be scavenged to produce mass 101, or can undergo ring-opening to lead to smaller fragments. The substantial unpaired-electron density on one of the nitrogens  $\alpha$ - to the alkoxy carbon, as well as on the oxygen, makes possible the

---

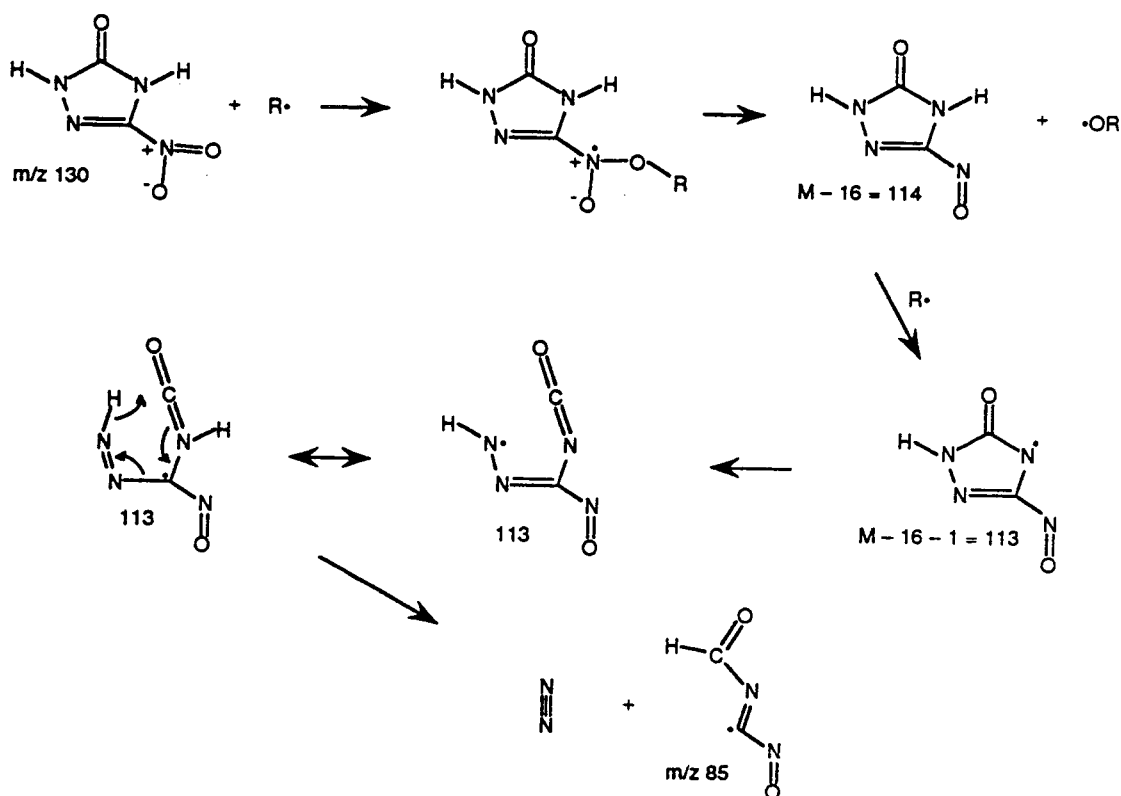
\* Depending on the circumstances, it can be operationally difficult to distinguish a true nitro-nitrite rearrangement from a dissociation-recombination process; for the present discussion, the difference is not critical.



since, for example, the formation of substantial amounts of mono-, di-, and tri-nitroso cyclo-trimethylene amines have been reported for RDX [21]. Such an oxygen loss, which is shown in Scheme 2, necessarily occurs by bimolecular reaction, since heats of formation of other nitro-nitroso compound pairs dictate that the activation energy for simple unimolecular loss of oxygen atom from a nitro group would have to be at least 83 kcal/mol [20]. However, oxygen loss should easily occur via the radical addition–elimination reaction shown in Scheme 2. This radical-oxidation reaction has precedent in the analogous reactions proposed for nitramines by Schroeder [22], and computationally explored by Melius and Binkley [23], and indirectly in the intermolecularly formed nitroxyl radical observed by Menapace et al. [6].

Although  $m/z$  114, as a closed-shell species, should be relatively stable to further reaction (and indeed is typically the largest fragment peak in laser desorption spectra of NTO), it could lose a hydrogen atom by abstraction to form the radical  $m/z$  113. Once  $m/z$  113 is formed, it can ring-open and lose  $N_2$  to give  $m/z$  85, the dominant ion in the last major fragment group to be accounted for. It is interesting that the spectrum obtained from NTO at 200°C with no desorption laser (Figure 7a) shows  $m/z$  85 as the only significant fragment, whereas all spectra obtained under laser-desorption conditions show  $m/z$  114 to be substantially larger than  $m/z$  85. A reasonable rationalization here is that when the nitroso-triazalone intermediate (114) is not driven off rapidly in a desorption laser plume, but remains longer in the slowly heated NTO, it has more opportunity to lose a hydrogen and then ring-open to mass 85 and a nitrogen molecule.

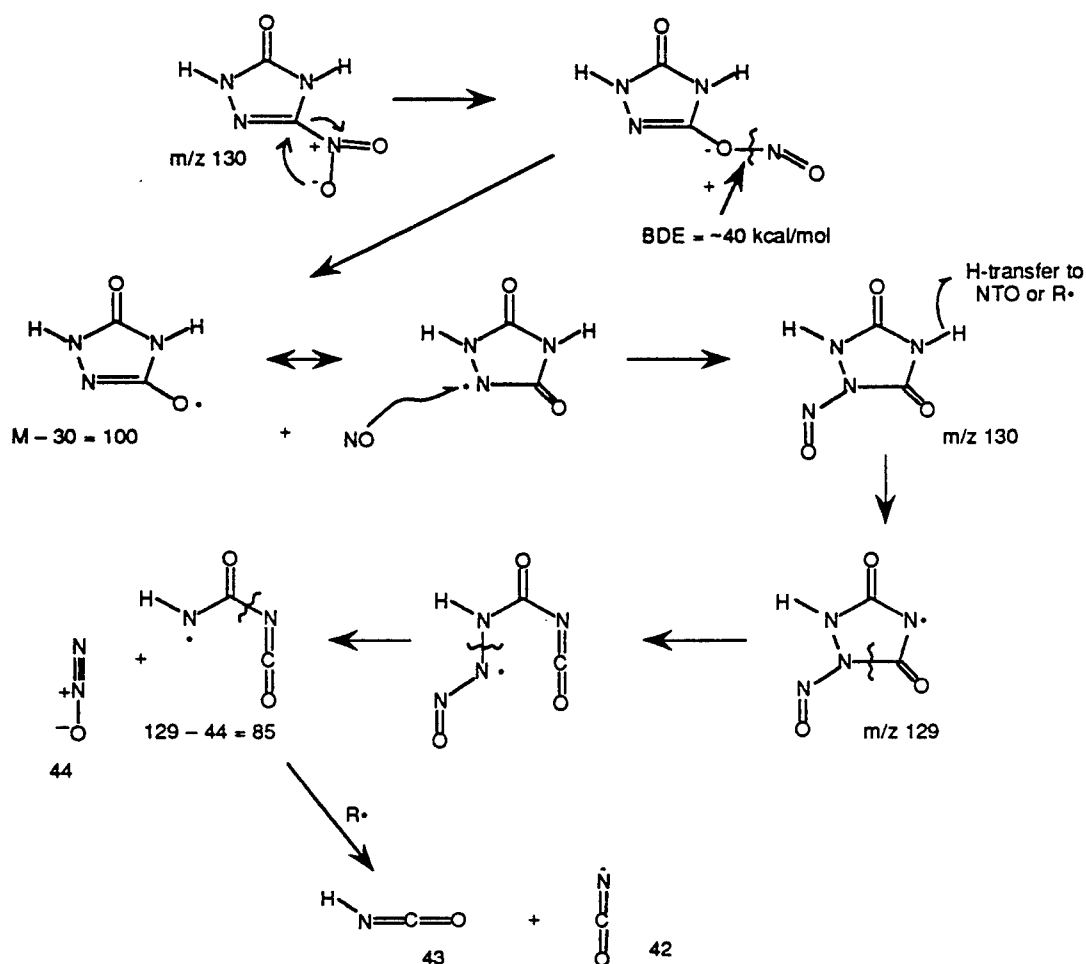
An alternative route to a  $m/z$  85 product is suggested by considering another sequence of reactions that can result from a dissociation–recombination of the nitrite rearrangement product. After O–NO scission, NO recombination on the adjacent nitrogen generates the N-nitroso compound ( $m/z$  130). A hydrogen abstraction from this N-nitroso intermediate could lead to the ring-opened  $m/z$  129 shown in Scheme 3, which in turn could lose  $N_2O$  to give  $m/z$  85 (having the same molecular formula, but actually a different structure than the  $m/z$  85 shown in Scheme 2). This pathway to  $m/z$  85 results in formation of  $N_2O$ , which cannot be generated in Schemes 1 or 2, because no N–N connection was made there. Although we obtained no direct information about  $N_2O$  because the 10.5-eV photoionization used in these SALI experiments will not ionize either it or  $CO_2$  (with IPs of 12.9 eV and 13.8 eV, respectively), Williams et al. did report  $N_2O$  (as determined by FTIR) to be a significant low molecular-weight product of NTO decomposition [7]. (The small  $m/z$  44 we observe could be  $H_2NCO$ ,  $C_3H_8$ , or possibly  $N_2O$  as an ion-fragment of a larger species.)



Scheme 2. Nitroso compound formation from NTO and possible subsequent reactions.

A third alternative for m/z 84/85 generation could be C-NO<sub>2</sub> scission, which would give m/z 84 directly. Figure 6(b) does show some intensity at m/z 84; however, the most plausible ring-opening sequences following NO<sub>2</sub> loss would lead to m/z 56 and/or 41, at which only minuscule intensities appear.

Schemes 1, 2, and 3 together account satisfactorily for the thermally generated sequence of fragments observed during laser desorption of NTO, except for the set of still more minor peaks grouped around m/z 55. Although the set of decomposition pathways suggested by the mass-spectral data is evidently purely thermal (i.e., precedes photoionization), it is not necessarily identical either to that which occurs under other thermal decomposition conditions, or during the initiation process. Nevertheless, we find that the present results, when viewed against the background of previous NTO studies, enable us to come to a more integrated picture of what happens during decomposition, and to arrive perhaps at some beginning insights regarding NTO initiation.

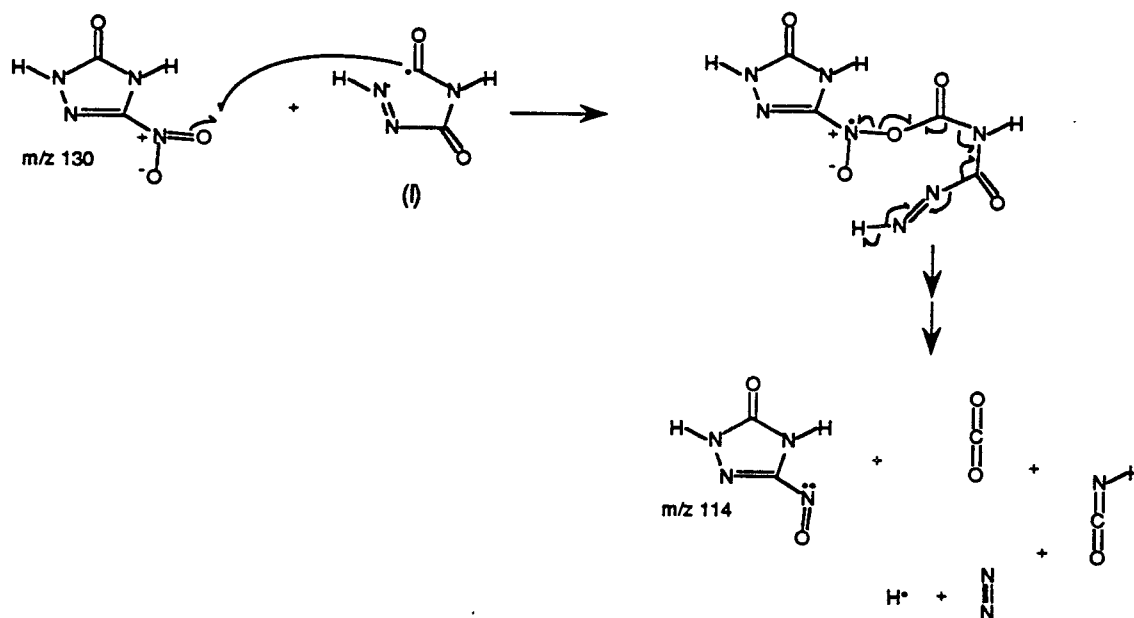


Scheme 3. NTO decomposition by nitro-nitrite rearrangement, O-N bond cleavage, and NO recombination on nitrogen.

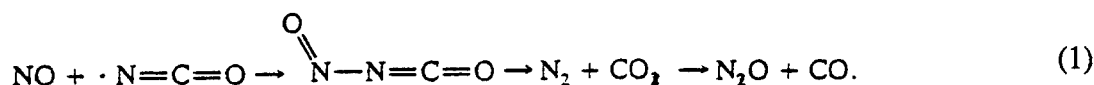
The exact conditions in the laser-desorption environment are not easy to specify. Under the influence of the desorbing laser (at either 279 or 355 nm), an area about 50- $\mu\text{m}$  in diameter is heated and in a few microseconds goes from solid NTO to dilute gas in the upper part of the laser plume. There is clearly a continuous, albeit rapid, transition from solid condensed phase through dense gas phase to dilute gas phase. During this transition, the opportunities for bimolecular reactions will vary widely in a way that depends not only on the laser intensity, but also on the density and heat capacity of the sample and the nature of the ablated surface. In general, one expects that the decomposition sequences that begin as a result of the energy imparted by mechanical stress will have substantial similarities to the sequence observed in the laser plume, but also some differences. The temperatures achieved under shear or impact conditions will probably be less, and the density will be higher. These differences mean that mechanical stress should *relatively* favor bimolecular over unimolecular reactions, and because of higher dielectric constant and/or acidity, perhaps favor ionic- over free-radical reactions.

The connection most easily made between the laser desorption/decomposition we report here and literature data involves the laser-heated thin-film decomposition studies of Botcher et al. [9]. These authors concluded that formation of  $\text{CO}_2$  resulting from direct biomolecular reaction of two NTO molecules, is the first decomposition step that occurs when condensed-phase NTO is rapidly heated. Schemes 1 and 2 above lend themselves very readily to early (albiet not "initial") formation of  $\text{CO}_2$  by an *intermolecular* route involving a radical intermediate and an NTO molecule, rather than two intact NTO molecules. The ring opened, acyl radical intermediate [(I) in Scheme 1] is a prime candidate (provided its lifetime before unimolecular CO elimination is long enough) for the role of  $\text{R}\cdot$  illustrated in Scheme 2, in which a radical intermediate becomes oxidized by adding to the  $\text{N}=\text{O}$  multiple bond in an intact NTO molecule and then re-eliminating as the species  $\text{RO}\cdot$ . In the case of the acyl radical intermediate (I), this would give  $\text{CO}_2$ , as shown in Scheme 4. If the lifetime of intermediate (I) before unimolecular CO elimination is long enough, it will be a much more favorable reductant for an intact NTO molecule than will be the closed-shell CO species.

Oxidation of various radical fragment species by NTO is consistent with the fact that  $m/z$  114 ( $\text{NTO} - \text{O}$ ) is typically the most prominent among the NTO fragment peaks. Nevertheless, an additional route to  $\text{CO}_2$  may be provided by reaction of NO and  $\cdot\text{NCO}$  to yield  $\text{CO}_2$  and  $\text{N}_2$  (Reaction 1). This reaction is key to de- $\text{NO}_x$  processes using cyanuric acid, and in the present case would additionally account for the fact that relatively little NO is observed in most NTO decomposition studies.



Scheme 4. Intermolecular oxidation by NTO of the ring-opened acyl radical intermediate to produce  $\text{CO}_2$ .

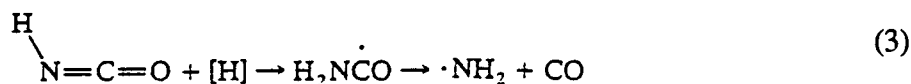
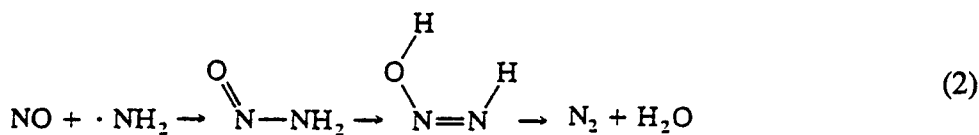


Botcher et al. conclude, from their concentration-independent CO<sub>2</sub> yields, that CO<sub>2</sub> production is bimolecular. Scheme 4 above is clearly bimolecular, in a general sense, but we believe oxidation of radical intermediates by intact NTO molecules represent a much more plausible detailed mode of reaction than the direct interaction of two closed-shell NTO molecules that is suggested by Reaction 4 of Botcher et al. [9]. A truly concerted reaction in which C-N bonds on either side of the carbonyl group are broken while an oxygen is transferred from an adjacent NTO, in a reaction involving a single potential energy maximum with no intermediates, is highly unlikely. On the other hand, oxidation of acyl radical fragments by a nitro compound can occur as an addition-elimination process, a reaction that is about 10 kcal/mol exothermic [20], and is expected to have low intrinsic activation energy [22,23].

The report of Williams et al. [7] of pressure-dependent gas-phase FTIR measurements showing that CO<sub>2</sub> yields increase by a factor of five (and NO yields decrease) as the argon atmosphere is increased from 0.5 to 60 atm certainly support a general picture in which more than one NTO molecule is involved in the generation of CO<sub>2</sub>. Although the absence of a mass spectrometric peak in the face of many potential secondary reactions is hardly definitive, it is interesting that our SALI spectra show no intensity at m/z 102 for the product of direct bimolecular generation of CO<sub>2</sub>, or, for that matter, at m/z 86 for the closed-shell intermediate that would result from *intramolecular* CO<sub>2</sub> loss. Finally, a bimolecular, rate-determining CO<sub>2</sub> elimination that involved two intact NTO molecules would provide no basis for either the commonly reported autocatalytic behavior of NTO, or for observed deuterium isotope effects. Thus we conclude that generation of CO<sub>2</sub> does occur bimolecularly, but through oxidation of an acyl radical intermediate as shown in Scheme 4, or of CO itself, or through reaction of NO and •NCO.

**Nitrogen-Labeling Studies.** The extensive nitrogen-labeling studies of Oxley et al. [8] are complex to interpret, but offer additional insight when considered together with the present results. Through a series of double-labeling experiments they conclude that about 60% of the N<sub>2</sub> is formed from the two adjacent ring nitrogens (N1 and N2). Thus about half of the N<sub>2</sub> derives from the original N-N bond in NTO, and about half comes from formation of a new N-N bond between the nitro nitrogen and the isolated ring nitrogen. This result is consistent with the ring-opening, CO/CO<sub>2</sub> loss sequence shown in Scheme 1 [generating N<sub>2</sub> from N(1) and N(2)], followed by a series of known reactions [24]: reactions of NO from the nitro group either with

•NCO (Reaction 1), or with NH<sub>2</sub> (Reaction 2) produced by reaction of H• with HNCO (Reaction 3), ultimately generating additional N<sub>2</sub> from nitrogens 4 and 6 or 2 and 6.

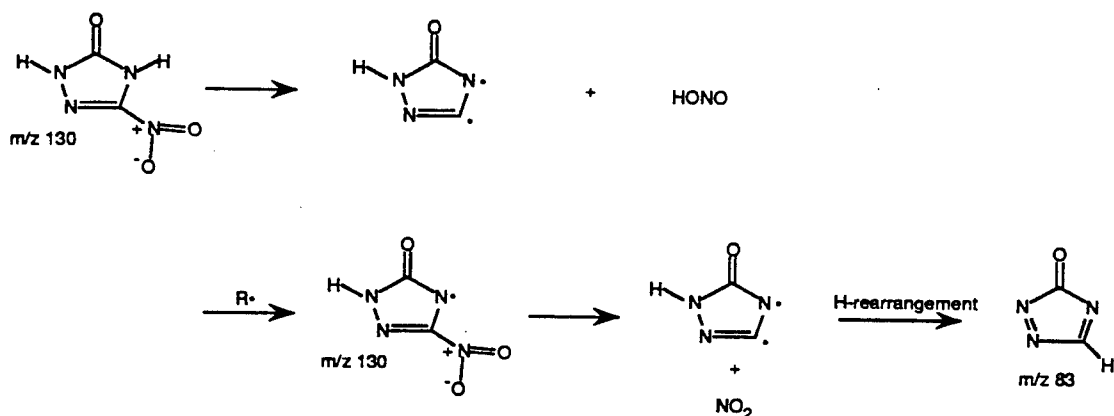


**Deuterium Isotope Effects.** Oxley et al. propose that the N<sub>2</sub> generated from nitrogens 1 and 2 comes as a result of initial HONO loss and subsequent ring-opening [8]. HONO loss *might* result either from a true concerted elimination, or result from NO<sub>2</sub> β-scission following an initial H-loss. In acyclic species with a radical center β- to an NO<sub>2</sub> group, such NO<sub>2</sub> β-scission is extremely rapid, being exothermic, but from a five-membered ring would be considerably less favorable, requiring either formation of an allenic double bond (or a bi-radical), or a hydrogen rearrangement. These routes to HONO elimination and a highly strained intermediate are shown in Scheme 5.

In the case of either HONO elimination route, the breaking of an N-H bond would account for a deuterium isotope effect. However, beyond the point of qualitatively accounting for an isotope effect, it is difficult to see how the proposed HONO loss pathway is consistent with observations. First, without a 1-3 H-rearrangement, it results in a very strained, essentially biradical product. Second, if a coupled H-rearrangement *did* lead to the closed-shell dehydrogenated triazalone (m/z 83), it is therefore harder to see how HONO loss would lead to ring-opening. Third, HONO loss is not supported by our mass spectrometric data, as the SALI spectra show essentially zero intensity at m/z 83.\* Although the absence of a mass spectrometric peak at m/z 83 certainly does not prove that the suggestion of HONO elimination, under different conditions, is wrong, it certainly provides no support for such elimination. Finally, Botcher et al. [9] were unable to find any infrared evidence for the trapping of HONO as an intermediate at 77K. On balance, we conclude that the weakness of the C-NO<sub>2</sub> bond and its proclivity for a nitro-nitrite rearrangement, together with the fact that formation of the alkoxyl radical intermediate (I) in Scheme 1 is all set up for a ring-opening β-scission reaction that paves the way to CO and/or CO<sub>2</sub>, indicate the route we outline in Scheme 1 and Reactions 1, 2, and 4 is more plausible and more consistent with the data.

\* We note that Beard and Sharma do report a thermal desorption, chemical ionization peak that nominally corresponds (see footnote below) to m/z 83 and has about the same intensity as their m/z 85.





Scheme 5. Required products for unimolecular- and H-transfer-promoted bimolecular elimination of HONO.

The consequence of ring opening without H-transfer is that the deuterium isotope effects are left to be accounted for by H-transfers in secondary reactions. This is entirely reasonable, since the reported values ( $k_H/k_D$  ca. 1.7 @ ~240°C) [6] do not seem enough to be clear indicators of a primary effect in a reaction that exerts 100% of the rate control. The species (I) in Scheme 1, which must transfer a hydrogen either unimolecularly or bimolecularly, is one intermediate from which H-transfer could make a contribution to rate control.

The question of whether the reaction sequences outlined in Schemes 1-4 and their enthalpy requirements are consistent with reported temperature dependences for NTO decomposition cannot be precisely answered at this time. First, our data are only a semiquantitative indication of the relative contributions of the various pathways, since there is not direct means of calibrating for detection sensitivity for the various unstable intermediates. Second, experimental "activation energies," particularly for systems that are subject to autocatalysis and autoacceleration through self-heating, are notoriously subject to systemic errors or distortions. Nevertheless, it is interesting to note that the recent report of Williams and Brill [16], which thus far represents the only systematic attempt to separate NTO sublimation from thermal decomposition, describes an apparent activation energy for decomposition of about 87 kcal/mol. This value is about 15 kcal/mol above the expected C-NO<sub>2</sub> bond strength in NTO, and therefore above the estimated enthalpic requirement in the nitronitrite rearrangement that begins the decomposition sequences shown in Schemes 1-4.\*

Williams and Brill describe the 87-kcal/mol value as an "Arrhenius-type" constant and recognize that it applies to global kinetics and not to any particular fundamental step. Even so, both the activation energy and the A-factor ( $10^{32.5} \text{ s}^{-1}$ ) reported by these authors appear high, even for the global chemical process. First, the expected activation energy for chain processes with higher than

\* The energy requirements for nitro-nitrite rearrangement have been found to be not far below those for simple C-NO<sub>2</sub> or N-NO<sub>2</sub> bond scission [19, 25]. That is, the C-NO<sub>2</sub> or N-NO<sub>2</sub> bonds must be substantially lengthened before rotation of the NO<sub>2</sub> group can occur.

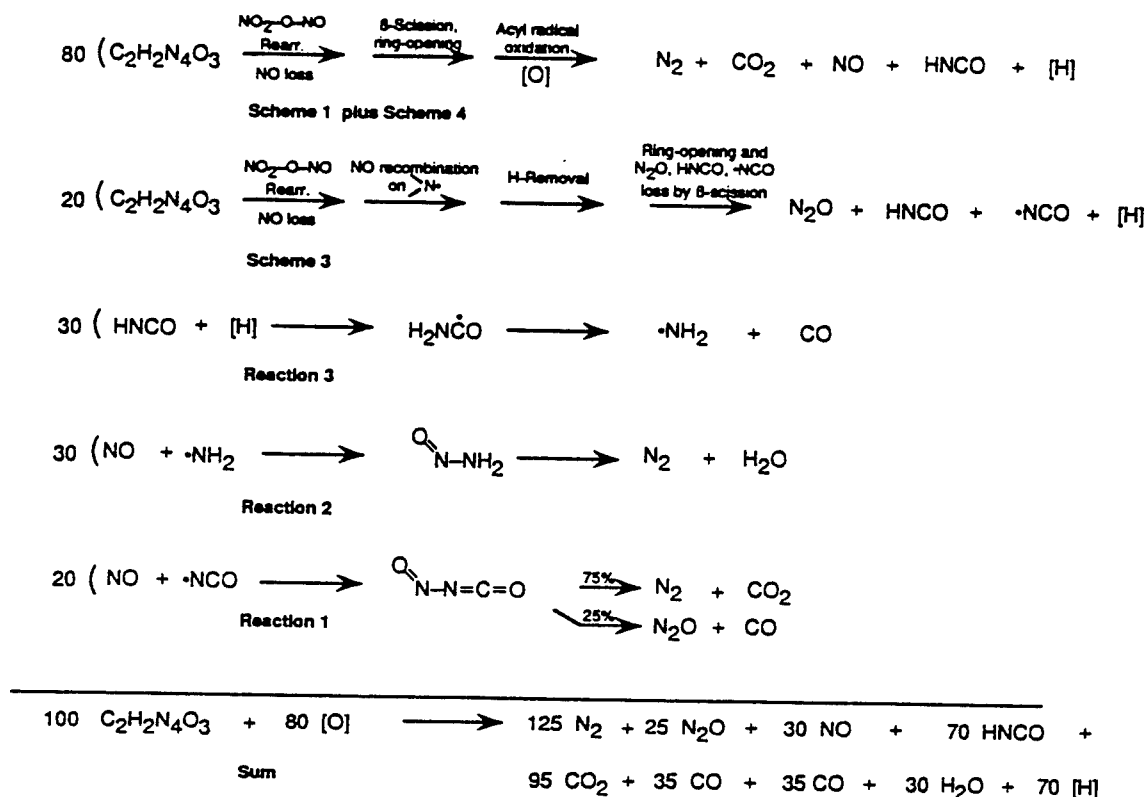
first-order chain-breaking steps tends to be less than that of the initiation step itself. Second, the temperature interval over which this activation energy was measured was only 10°C, and it is therefore subject to even more uncertainty from systematic distortions than is commonly encountered in measurement of activation energies. Considering all these factors, it is not really possible at this time, on the basis of detailed comparisons of observed and anticipated activation energies, to rule either for or against the NTO reaction sequences we suggest here.

We can however, ask whether the reaction sequences shown in Schemes 1, 2, 3, and 4 above, are consistent with stable product yields reported by other researchers. These sequences, which we derived originally from the SALI mass spectral data alone, were combined so as to produce the stoichiometry outlined in Scheme 6 and Table 1. Table 1 compares the yields predicted by the combination of reactions in Scheme 6 with the yields reported by Oxley [8]. This comparison shows that a combination of the reaction pathways involving intermediates actually observed in the laser desorption mass spectra, when combined with known reactions [24] of HNCO, •NCO, and NO, readily match the the gross gas composition. Moreover, that same combination of reactions also does a very good job of matching the isotopic labeling results of Oxley [8] that specify the origin of the nitrogen atoms in N<sub>2</sub> and N<sub>2</sub>O. This result further supports our suggestion that NTO decomposition routes summarized in Scheme 6 offer a more plausible explanation of NTO decomposition than either unimolecular generation of CO<sub>2</sub> or unimolecular HONO elimination.

Table 1. Comparison of the Gas Composition and the N-Compound Origin Predicted from the Reaction Sequence in Scheme 5 with the Analytical Results Reported in Reference 8.

Product	Percent of Gas		Percent of N in Product from N(1) and N(2)					
	Predicted <sup>a</sup>	Observed <sup>b</sup>	N(1) and N(2)		N(4)		N(6)	
			Predicted <sup>a</sup>	Observed <sup>b</sup>	Predicted <sup>a</sup>	Observed <sup>b</sup>	Predicted <sup>a</sup>	Observed <sup>b</sup>
N <sub>2</sub>	40	43	66	61	16	15	18	24
N <sub>2</sub> O	8	6	40	39	10	6	50	55
NO	10	8	0	NR <sup>c</sup>	0	NR	100	NR
CO <sub>2</sub>	31	37	—	—	—	—	—	—
CO	11	6	—	—	—	—	—	—
H <sub>2</sub> O	(9) <sup>d</sup>	NR <sup>c</sup>	—	—	—	—	—	—

- "Prediction" here means the result of adjusting the coefficients in Scheme 5 to give a reasonable (but not unique) fit of the N<sub>2</sub>, N<sub>2</sub>O, NO, CO, and CO<sub>2</sub> data of Reference 8, and then noting the isotopic composition that is dictated by this fitting.
- Product yields as reported in Reference 8.
- "NR" means "not reported."
- H<sub>2</sub>O yields are not reported in Reference 8, so the predicted yields of other gases are given as a percent of the total gas yield, excluding water.



Scheme 6. Stoichiometry of possible combined reaction sequences for NTO decomposition.

While Scheme 6 accounts rather successfully for gas-phase product formation, it is not yet clear how compellingly the reaction schemes suggested here may account for the polymeric residue reported by those who study NTO decomposition. In this work we observed that decomposition of NTO under one-atmosphere flowing argon in a TGA apparatus gave results essentially identical to those reported by Williams et al., namely a residue of  $11 \pm 1$  wt % [7], but significantly different than the 31% observed in sealed-tube experiments.[8]\*. In an extension of the reaction network summarized in Scheme 6 above, this polymeric material would come primarily from polymerization reactions of the HNCO that does not go to gaseous products. If this polymerization consumed all of the HNCO remaining in Scheme 6, but no other intermediates, it would result in a residue weighing 21% and having somewhat less nitrogen, and more oxygen, than the residues reported by Rothgery and by Oxley [5,8].

\* No meaningful measurement of weight loss can be made in the laser-desorption spectra.

Additional information that will enable us to make more definitive statements about the overall temperature dependence expected from the rather involved decomposition sequences outlined here includes confirmation that the peaks observed in the spectra reported here are indeed accounted for by the structures we have shown, particularly where more than one structure can plausibly account for the  $m/z$  value in question (e.g.,  $m/z$  85). Other needed information is a more quantitative determination of branching ratios among the various reaction sequences. This information will come from laser-desorption studies of isotopically labeled NTO, from calibration of relative detection sensitivity for the products (or analogs of the products) seen here, and from more detailed study of the influence of laser-desorption conditions on product ratios.

**Stress-Induced Fragment Emission.** The shear-induced fragment emission reported here for NTO is of course related to the fracture-induced emission, or "fractoemission" reported in recent years by Dickenson and coworkers for many non-explosive- as well as some explosive materials [26,27]. These reports have most commonly described electron- and photon- emission, as well as the measurement of positive and negative ions without mass analysis. As such, they have focused on the general phenomenon, more than on the elucidation of chemical decomposition pathways. The results we describe here appear similar to those reported for the explosive RDX [26] in that the emission can be long-lasting, with decay times of ca 20 ms to hundreds of seconds.

The remarkable observation here is that we are able to detect relatively strong signals on a single-shot basis (single ionizing laser pulse) for up to tens of seconds after a shear event. Although the exact stress to which the NTO pellet is subjected is very complex (partially compressive and partially tensile) and cannot readily be calculated, we can estimate that the upper limit to be about 0.1 kbar, on an average, for a species of molecular weight ca. 100 Da to travel the ~1 mm from the fracture surface to the region traversed by the ionizing laser is only about 1  $\mu$ s, it is very clear that either the intermediates are adsorbed on or within the NTO fracture region for a relatively long time prior to desorption, and/or the reaction time to produce these intermediates is rather long.

The fragment emission that results without laser desorption in the *in-situ* shear experiments is related to, but in part different from, that which occurs under laser desorption. As Figures 10 and 11 show, the dominant fragment is now  $m/z$  99, and all other fragments are much lower. Clearly the shear stress favors formation (or at least emission into the gas phase) of  $m/z$  99, and disfavors its decomposition into lower-mass products. Second, the major peak (within the 99/100/101 grouping) shifts from 100 to 99. These observations can be rationalized by speculating that the nitro-nitrite rearrangement that begins Scheme 1, and which we believe already accounts for the bulk of the NTO behavior under simple thermal decomposition conditions, becomes even more dominant in the case of stress-induced decomposition.

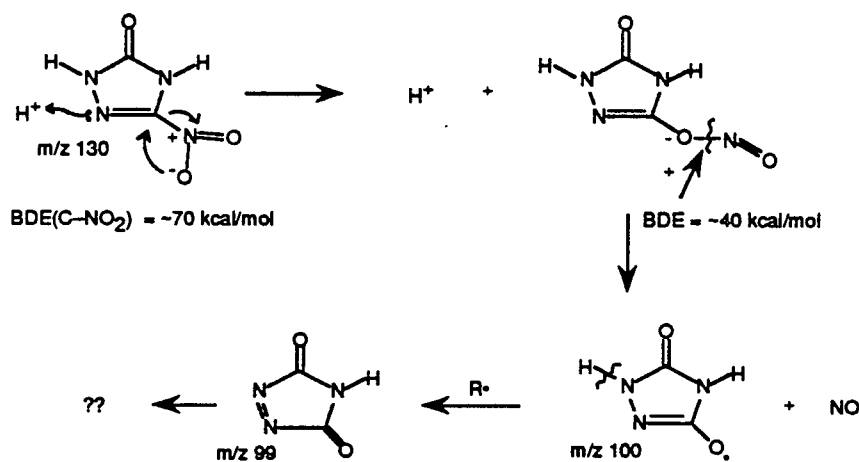
Enhancement of the nitro-nitrite rearrangement under conditions that include condensed-phase-like densities is reasonable, since under those conditions, the acidity of NTO could come into play in self-protonation reactions. As suggested in Scheme 7, association of the imine-nitrogen with an acidic proton will withdraw electron density from the carbon bearing  $\text{NO}_2$  and facilitate the internal attack of a negatively charged oxygen, which must take place during the nitro-nitrite rearrangement. Similarly, the higher concentrations in the condensed phases would favor subsequent bimolecular H-atom loss to produce the closed-shell species  $m/z$  99. This species will be more resistant to ring-opening than its alkoxy radical parent, and therefore might be expected to accumulate behind a ring-opening "bottleneck." Also, the failure of the alkoxy radical to undergo the ring-opening reaction shown in Scheme 1 blocks production of the principal species we have suggested as the reductants that produce the nitroso-triazalone,  $m/z$  114. Thus, the proposed sequence of reactions is entirely consistent with the fact that the shear-induced spectra (Figures 9 and 10), in which  $m/z$  99 is the dominant peak, show almost no intensity at  $m/z$  114.

It is appropriate to ask why the high-concentration conditions would be more likely to promote H-atom transfer *from* as compared to H-transfer *to* the alkoxy radical  $m/z$  100 species. To some extent, this should be a function of the redox nature of the medium, with a more oxidizing medium being more likely to abstract an H-atom from the alkoxy radical and produce  $m/z$  99. The speculation could be tested by determining the effect of selected additives on the  $m/z$  99 peak observed in the shear-induced spectra, and perhaps also comparing the effect on this intermediate with the effect of additives on the NTO sensitivity. Furthermore, recent theoretical and experimental studies [22] of the structure and infrared spectra of NTO provide a good baseline for molecular dynamic calculations that would address alternative reaction modes under thermal and mechanical stress.

The differences we observe between the thermal- or laser-desorption spectra and mass spectra from shear-induced emission (no laser-desorption), appear at first glance much greater than the differences we find between laser desorption spectra of unstressed NTO and post-examination of NTO that has been subjected to much higher (but still sub-critical) stress in a standard drop-hammer apparatus. In large part, this diminished difference simply reflects the fact that the shear-induced peaks tend to be much less intense than the laser-induced peaks, and also the fact that we were not able to examine the impacted samples until about an hour after the drop-weight tests were performed. Nevertheless, differences can be seen: before impact, there is essentially zero intensity at  $m/z$  99 ( $<0.1\%$  of the  $m/z$ -130 intensity), but after impact the relative  $m/z$ -99 intensity was clearly visible at  $\sim 2\%$  (Figure 13). Thus, even though  $m/z$  99 is dwarfed by the normal laser desorption peaks, it can be clearly seen, in contrast to the laser-desorption spectrum in Figure 8b, where  $m/z$  99 does not rise above the baseline. Thus, the appearance of a new peak at  $m/z$  99 is

common to the very modest stress caused during simple shear, and to the much larger stresses resulting during marginally subcritical impact. The fact that no peak at  $m/z$  99 was observed under the conditions of Beard and Sharma [10] could simply reflect lower signal/noise ratios in their chemical ionization mass spectra.

The other significant differences between the fresh and impacted samples appear primarily as relative intensity shifts of the peaks *within* the minor peak groups.\* For instance,  $m/z$  84 increases from an intensity generally less than or equal to  $m/z$  85 (Figures 7-9), to an intensity two-to-three times  $m/z$  85 in Figure 13. These shifts within individual fragment groups are similar, at least in general terms, to those reported by Beard and Sharma [10]. For impacted samples they report enhancements in the relative intensities of fragment peaks 83, 85, 100, and 114 that range from 0.9 to 1.8. However, they see no increase in  $m/z$  85, but report a 70% increase in  $m/z$  83, which we do not see at all.\*\*



Scheme 7. Possible formation of cyclic diketone by acid-promoted nitro-nitrite rearrangement, followed by bimolecular H-atom transfer.

\* Because differences in the relative intensity of any of the fragment groups and the molecular ion can result from sample-to-sample variations in the desorption laser intensity, the higher intensity of fragment groups in general for the previously impacted samples cannot be attributed with any certainty to the subcritical impacts themselves.

\*\* Exact comparison with the reported masses of reference 10 is difficult, because it was assumed in that paper that all peaks observed under chemical ionization conditions result from proton transfer to anolyte species; thus ions at  $m/z$  84 and 101 are assigned to thermal product masses 83, and 100. However, it is not always certain that all ions result from proton transfer to neutral fragments.

## SUMMARY AND CONCLUSIONS

Laser-desorption spectra of NTO powder and pellets give prominent fragments at mass 114, 100/101, 84, 85, 71, and a number of lower masses. This sequence indicates that thermal decomposition, either in the heated surface layers or in the laser plume, proceeds largely by nitro-nitrate rearrangement, NO loss, and ring opening adjacent to the carbonyl group. This sequence satisfactorily explains the initial formation of CO<sub>2</sub> that has been previously reported, as well as the results of nitrogen double-labeling experiments, and also the fact that neither NO<sub>2</sub> nor HONO have been seen as significant initial products. Furthermore, the suggested ring-opening sequence is not inconsistent with reported deuterium isotope effects that can be categorized as "diluted" primary isotope effects.

Real-time measurements of shear-induced NTO fragments were performed by means of a spring-driven shearing device installed in the SALI chamber directly beneath the mass spectrometer sampling region. The shear-induced spectra are dominated by a peak at  $m/z$  99, which is not seen in the thermal- or laser-desorption spectra of fresh NTO. This peak is assigned to the closed-shell triaza-diketone (or triazoline dione) produced by the same sequence of nitro-nitrite rearrangement and NO loss as observed under simple thermal decomposition. However, under the high concentration mechanical rupture conditions, bimolecular H-atom removal to produce the cyclic diketone is more favorable.

It is highly speculative at this early stage, but still worth considering, whether stability of the closed-shell species  $m/z$  99 could contribute to initiation insensitivity by inhibiting further reaction under high-concentration (i.e., condensed-phase), low-temperature (i.e., thermally marginal) conditions. In any case, SALI measurements and the capability for performing *in-situ* shear experiments have provided us a new window on NTO decomposition chemistry, allowing observation of intermediate molecular weight species not previously detected. We believe these results are providing a good foundation for addressing the coupled questions of what makes NTO so insensitive and what makes it reluctant to achieve high-order detonation. In ongoing work, we are attempting to shorten the time period between the application of the stress and observation of the evolved fragments as well as to increase the intensity of the stress. In the results reported here, the ca. 3 ms time delay was dictated by the time required for the small spring-driven shearing blade to clear the region normal to the fracture surface. We are shortening the delay time by three orders of magnitude by modifying the fracture platform to collect, within a few microseconds of

the completion of crack propagation, fragments that are emitted normal to the side of the cylindrical specimen, and essentially parallel to the fracture surfaces.

*Support for this reasearch by the Air Force Office of Scientific Research, under AFOSR Contract No. F49620-94-C0055 is gratefully acknowledged. We thank Program Manager Dr. Michael Berman for helping to maximize the connection between this work and other fundamental and applied studies of NTO. We also thank J. Oxley, C.A. Wight, and D. L. Thompson for sending us copies of in-press manuscripts describing the recent results of their respective research groups with NTO. We also appreciate the courtesy of Mr. Stephen Aubert and Gary Parsons of Eglin Air Force Base in supplying us with samples of the same material used in the the USAF NTO formulation studies, as well as guidance in the hot-pressing of NTO.*



## REFERENCES

1. Lee, K.-Y.; Chapman, L. B.; Coburn, M. D. *J. Energetic Materials*, 5:27 (1987).
2. Aubert, S.; Corley, J. D.; Glenn, J. G. "Development of TNTO Composite Explosives," Final Report WL-TR-92-7073 for Wright Laboratory, Armament Directorate, June 1993.
3. Nielsen, A. T. "Correlation of the Chemical Structure of Organic High Explosives with Sensitivity," Working Group Meeting on Sensitivity of Explosives, Mar 15-18, 1987, Socorro, NM.
4. Aubert, S., "Characterization of the Hydrodynamic Performance Properties for NTO and TNTO Composite Explosives," Final Report WL-TR-94-7037 for Wright Laboratory, Armament Directorate, May 1994.
5. Rothgery, E. F.; Audette, D. E.; Wedlich, R. C.; Csejka, D. A. *Thermochemica Acta*, 185:235 (1991).
6. Menapace, J. A.; Marlin, J. E.; Bruss, D. R.; Dascher, R. V. *J. Phys. Chem.* 95:5509 (1991).
7. Williams, G. K.; Palopoli, S. F.; Brill, T. B. *Combustion and Flame*, 98:197 (1994).
8.
  - a. Oxley, J.; Smith, J. L.; Zhou, Z.-L.; McKenney, R. L. *J. Phys. Chem.* 99:10383 (1995).
  - b. Oxley, J.; Smith, J. L.; Yeager, K. E.; Rogers, E.; Dong, X. X., "NTO Decomposition Studies," *Materials Research Society Proceedings*, 418:315 (1996).
  - c. Oxley, J.; Smith, J. L.; Yeager, K. E.; Rogers, E.; Dong, X. X., "NTO Decomposition Products Tracked With  $^{15}\text{N}$  Labels," *J. Phys. Chem. A*, 101:3531 (1997).
9. Botcher, T. R.; Beardall, D. J.; Wight, C. A., "Thermal Decomposition Mechanism of NTO," *J. Phys. Chem.*, 100:8802 (1996).
10. Beard, B. C.; Sharma, J. *J. Energetic Materials*, 11:325 (1993).
11. Becker, C. H.; Gillen, K. T. *Anal. Chem.*, 56: 1671 (1984).
12. Pallix, J. B.; Schule, U.; Becker, C. H.; Huestis, D. L. *Anal. Chem.* 61:805 (1989).
13. Berkowitz, J., *Photoabsorption, Photonionization, and Photoelectron Spectroscopy*, Academic Press, New York, 1979.
14. Driscoll, J. N., in *Detectors for Capillary Chromatography*, (H. H. Hill and R. H. McMinn, Eds.) John Wiley & Sons, Inc. New York, 1992, Chap. 4.
15.
  - a. Sharma, J.; Hoffsommer, J. C.; Glover, D. J.; Coffey, C. S.; Forbes, J. W.; Liddiard, T. P.; Elban, W. L.; Santiago, F. *Proceedings of Eighth Symposium (International) on Detonation*, Albuquerque, New Mexico, July 15-19, 1985, p. 725.
  - b. Sharma, J.; Forbes, J. W.; Coffey, C. S.; Liddiard, T. P. *J. Phys. Chem.*, 91:5139 (1987).

- c. Sharma, J.; Beard, B. C.; Forbes, J. ; Coffey, C. S.; Boyle, V. M. *Proceedings of the Ninth Symposium (International) on Detonation*, Portland, Oregon, 1989, p. 897.
16. Williams, G. K., and Brill, T. B., *J. Phys. Chem.* 99:12536 (1995).
17. He, H. Y., Ciu, J. P., Mallard, W. G., and Tsang, W., *J. Am. Chem. Soc.* 110:3574 (1988).
18. Jeffries, J. B.; Zellweger, J.-M.; McMillen, D. F.; Golden, D. M.; Steward, P. H. *J. Phys. Chem.*, 93:3557 (1989).
19. Nigenda, S. E.; McMillen, D. F.; Golden, D. M. *J. Phys. Chem.*, 93:1124 (1989).
20. a. Batt., L.; Robinson, G. N. "Thermochemistry of Nitro Compounds, Amines, and Nitroso Compounds," in *Chem. of Functional Groups*, Suppl. F, Ed., S. Patai, John Wiley and Sons, Ltd., London, 1981.
- b. Benson, S. W. *Thermochemical Kinetics, Second Edition*, John Wiley and Sons, New York, 1976.
21. Hoffsommer, J. C.; Glover, D. J., *Combustion and Flame* , 59:303 (1985).
22. Schroder, M. A., "Critical Analysis of Nitramine Decomposition Results: Some Comments on Chemical Mechanisms," *Proceedings of the 16th JANNAF Combustion Meeting*, 14 September 2:17 (1979).
23. Melius, C. F., and Binkley, J. S., *Proceedings of Eighth Symposium (International) on Detonation*, Albuquerque, New Mexico, July 15-19, 1988, p. 1953.
24. Bozzelli, J. W.; Dean, A. M. "Combustion Chemistry of Nitrogen Compounds: A Comprehensive Review and Analysis of Selected Reactions," in *Combustion Chemistry, 2nd Edition*, Edited by W. C. Gardiner, Jr., in press.
25. Saxon, R. P., and Yoshimine, M., *J. Phys. Chem.*, 91:2376 (1989).
26. Dickenson, J. T.; Miles, M. H.; Elban, W. L.; Rosemeier, R. G. *J. Appl. Phys.*, 55:3994 (1984).
27. Dickenson, J. T.; Jensen, L. C.; Langford, S. C. *Phys. Rev. Lett.*, 66:2120 (1991).
28. Sorescu, D. C.; Sutton, T. R. L.; Thompson, D. L.; Beardal; Wight, C. A. *J. Mol. Struct.*, 384:87 (1997).

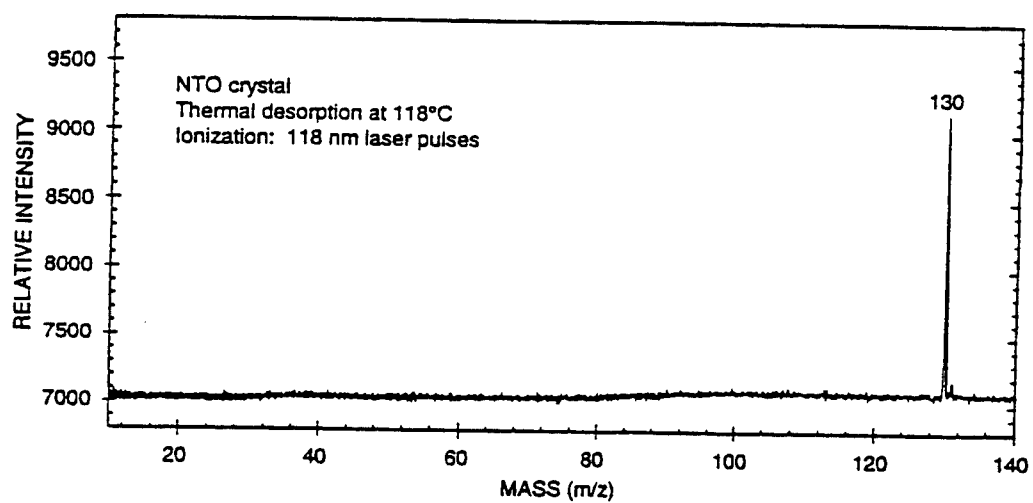
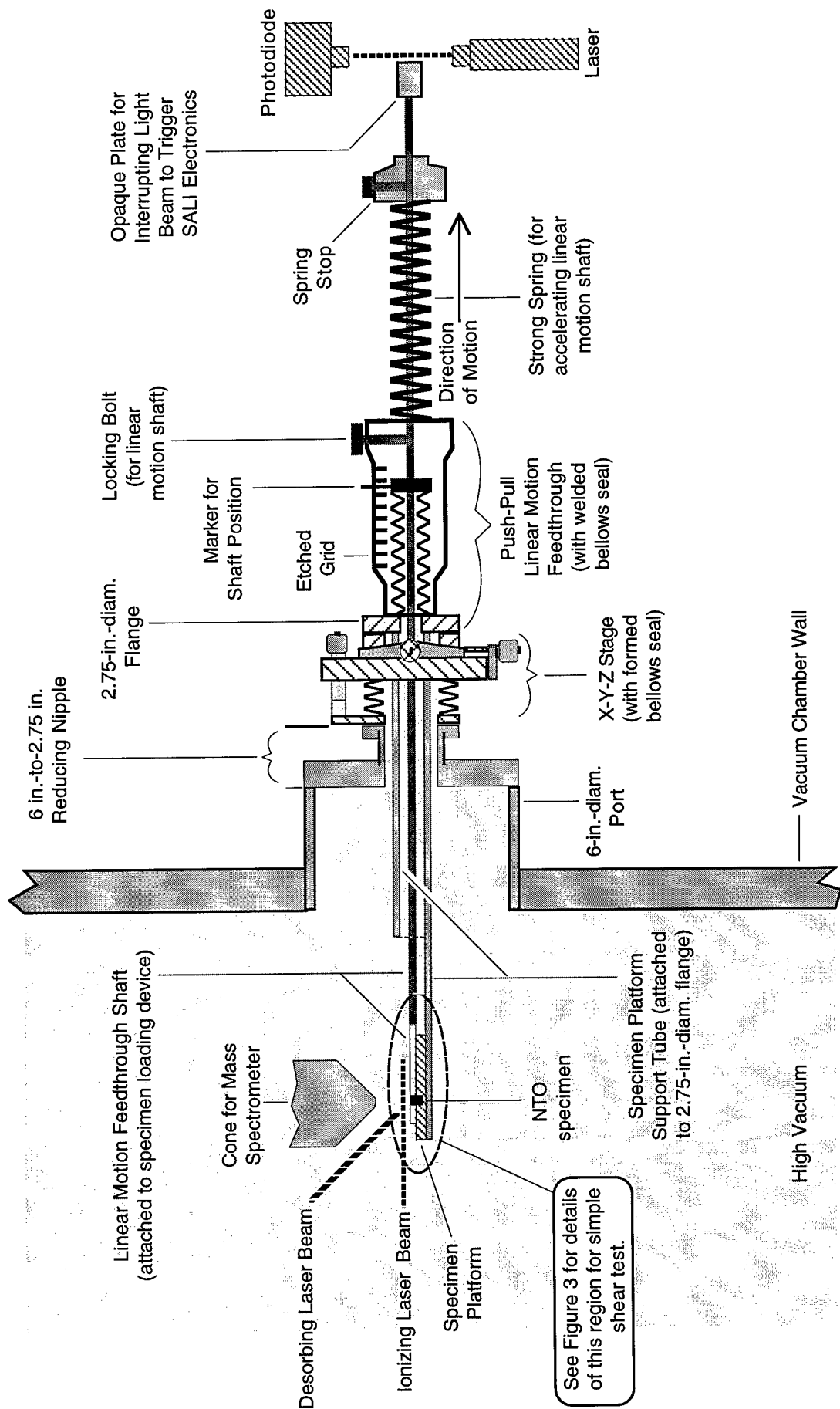


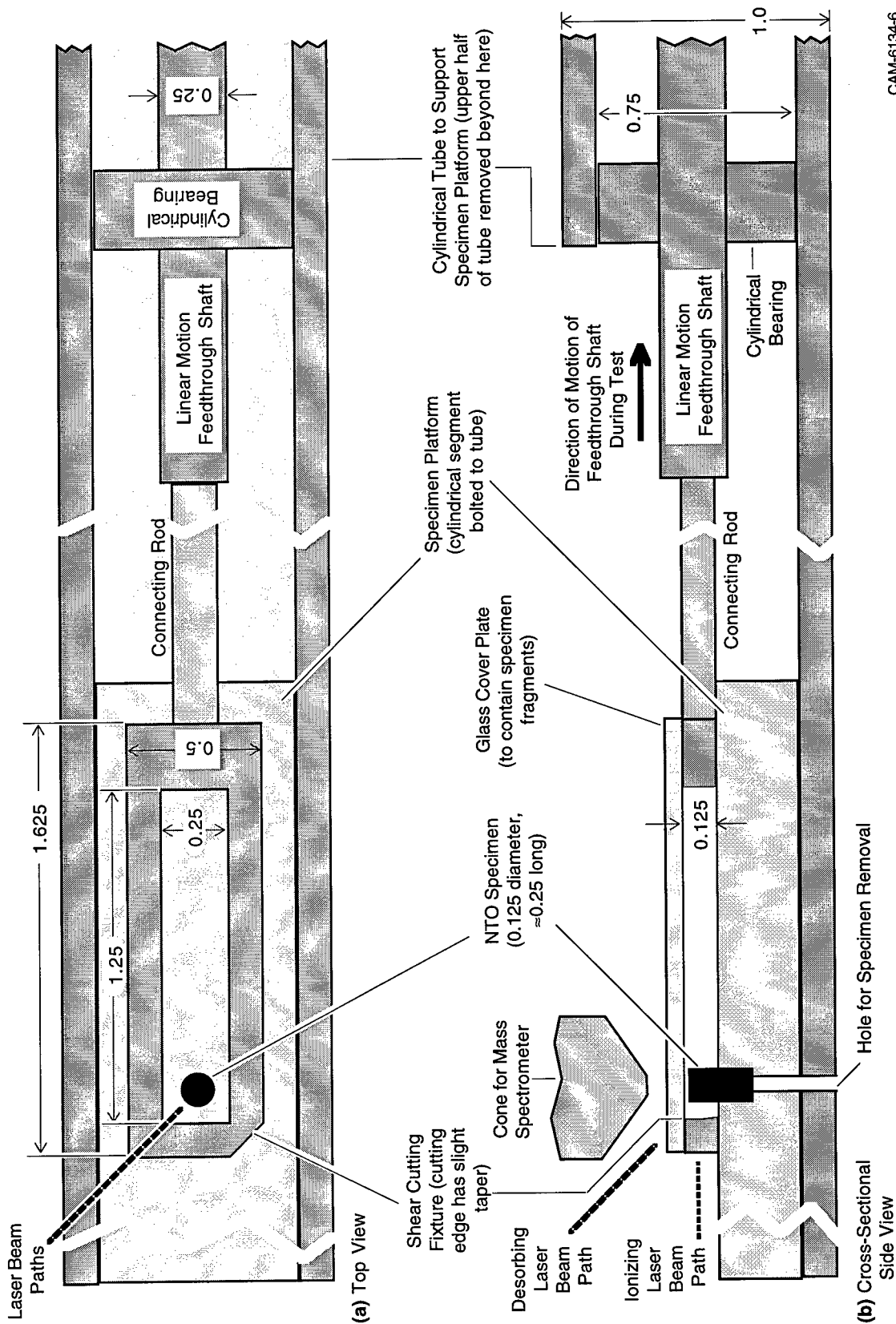
Figure 1. Temperature-programmed thermal desorption SALI spectrum of NTO crystals at 118°C.



CAM-6134-5

Figure 2. Schematic view of *in-situ* test fixture on SALI apparatus for use in dynamic fracture tests.

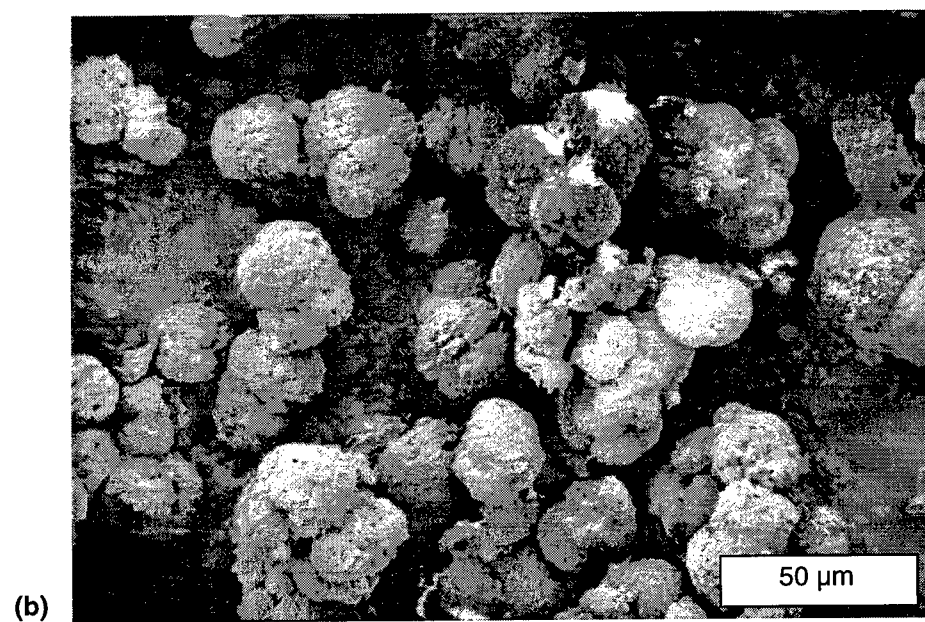
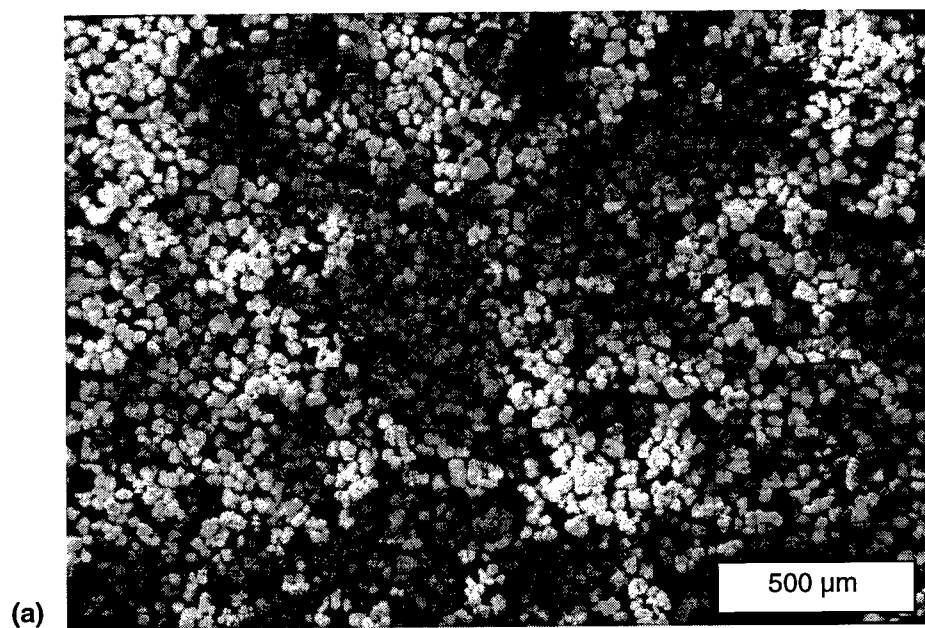
Note: Both ionizing and desorbing laser beams enter at  $\approx 45^\circ$  from the plane of the paper.



CAM-6134-6

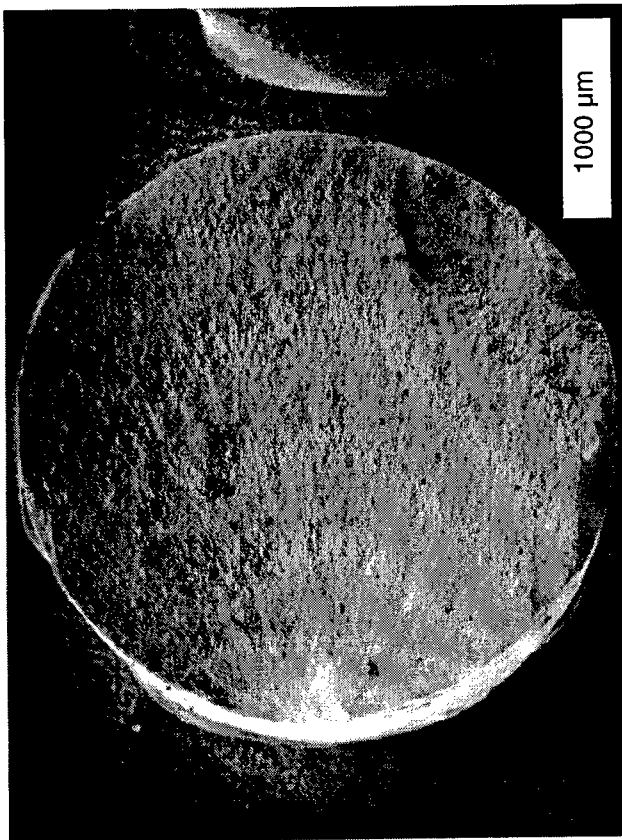
Figure 3. Detail of SALI *in-situ* test fixture for simple-shear tests with millisecond delay times.

All dimensions in inches.

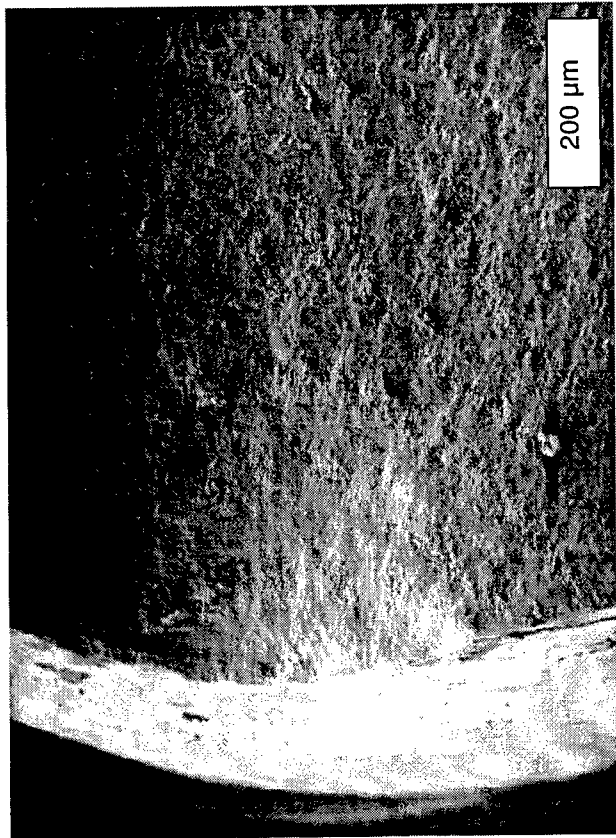


CAM-6134-3

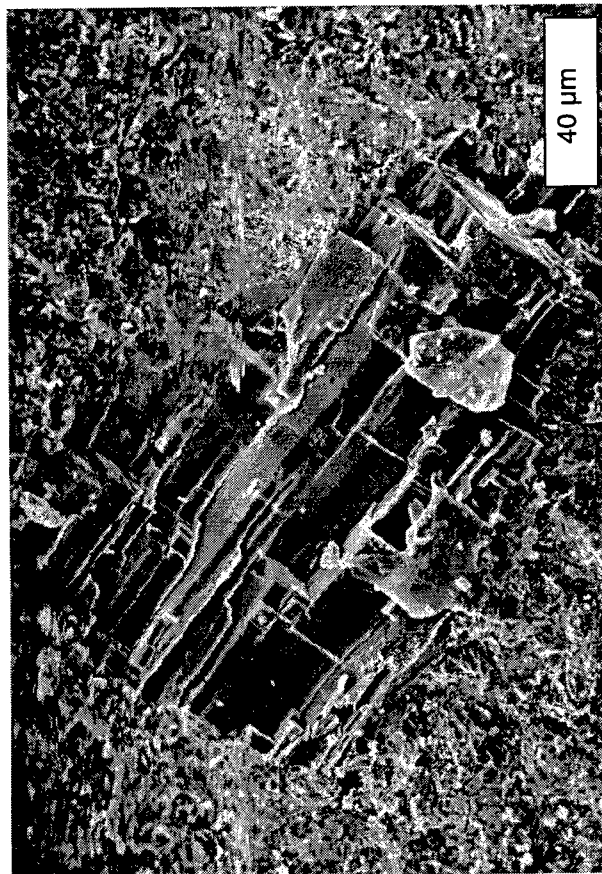
Figure 4. SEM views of fine-grained NTO.



(a)



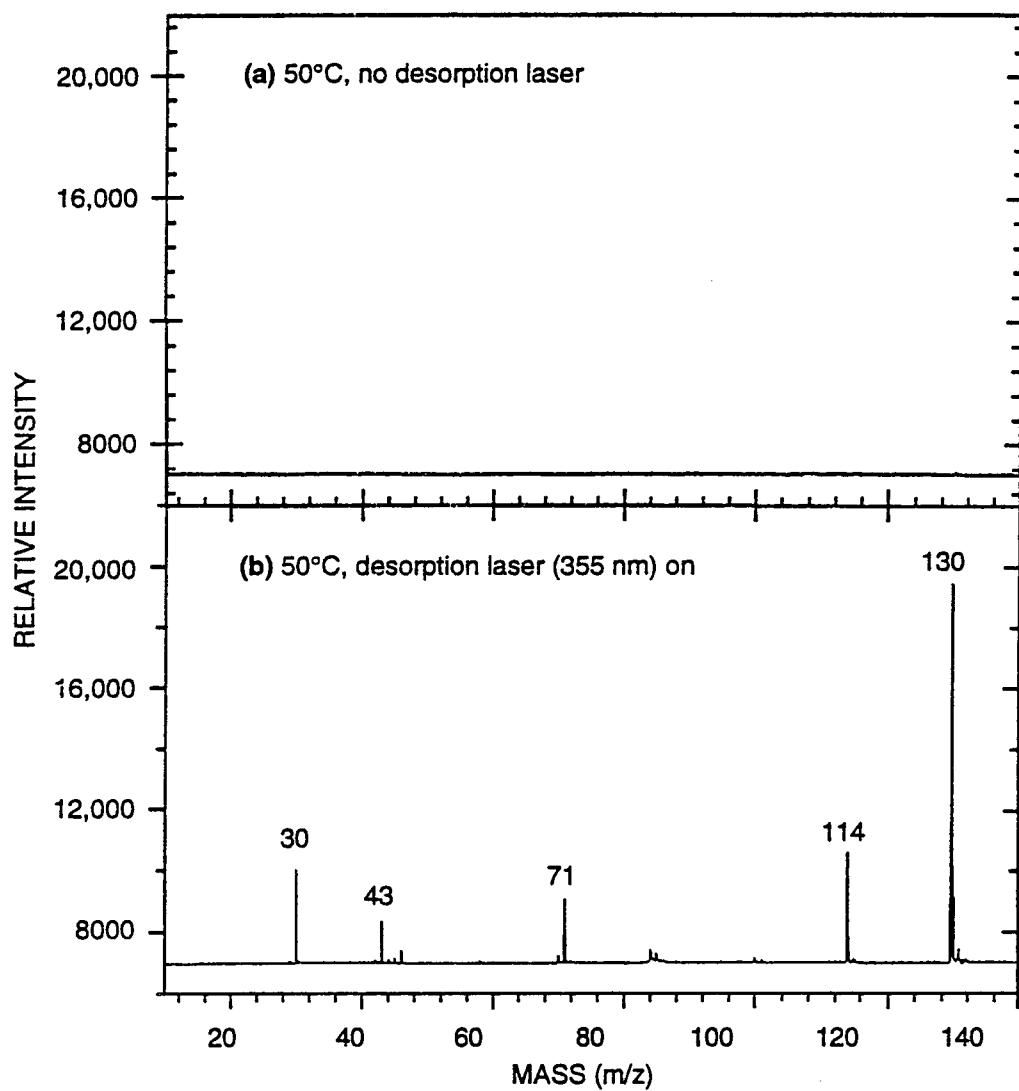
(b)



(c)

CAM-6134-8

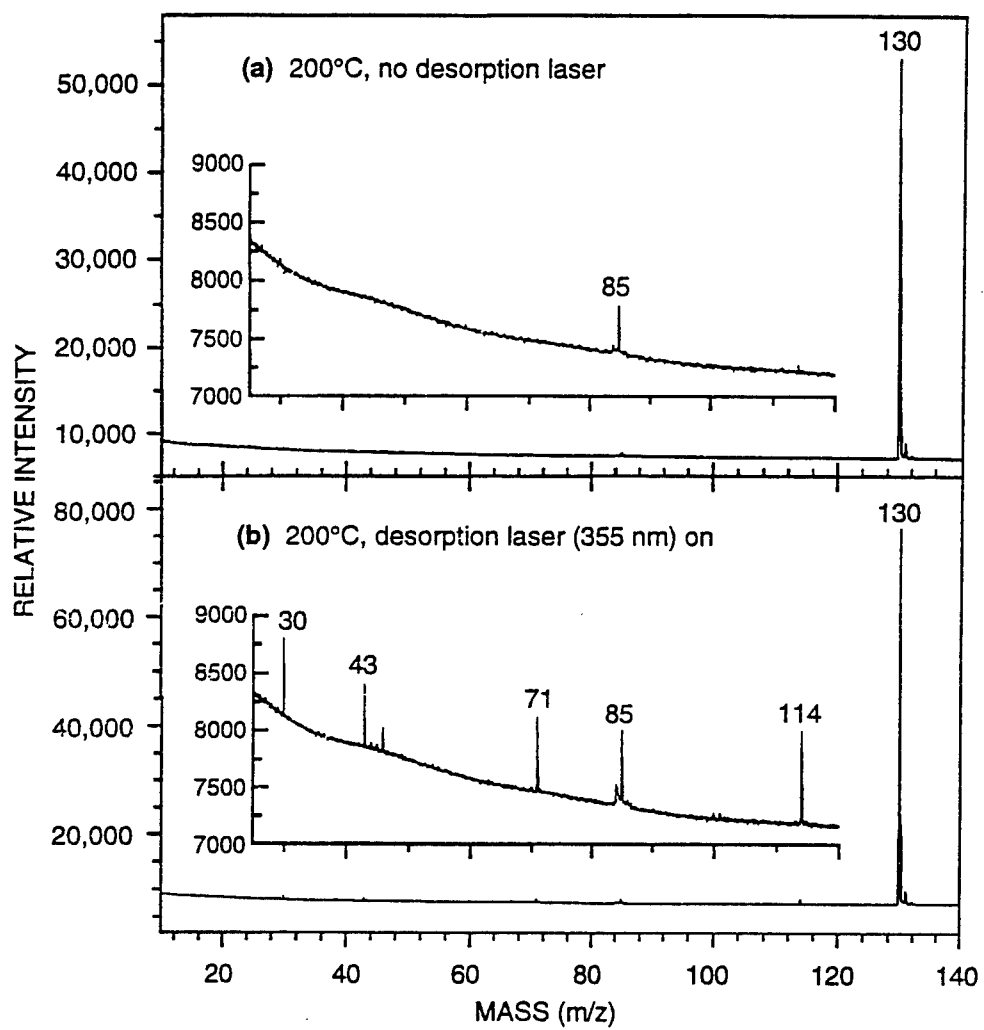
Figure 5. SEM views of various regions of the fracture surfaces from *in-situ* simple shear-tests onNTO pellet.



CAM-6134-12

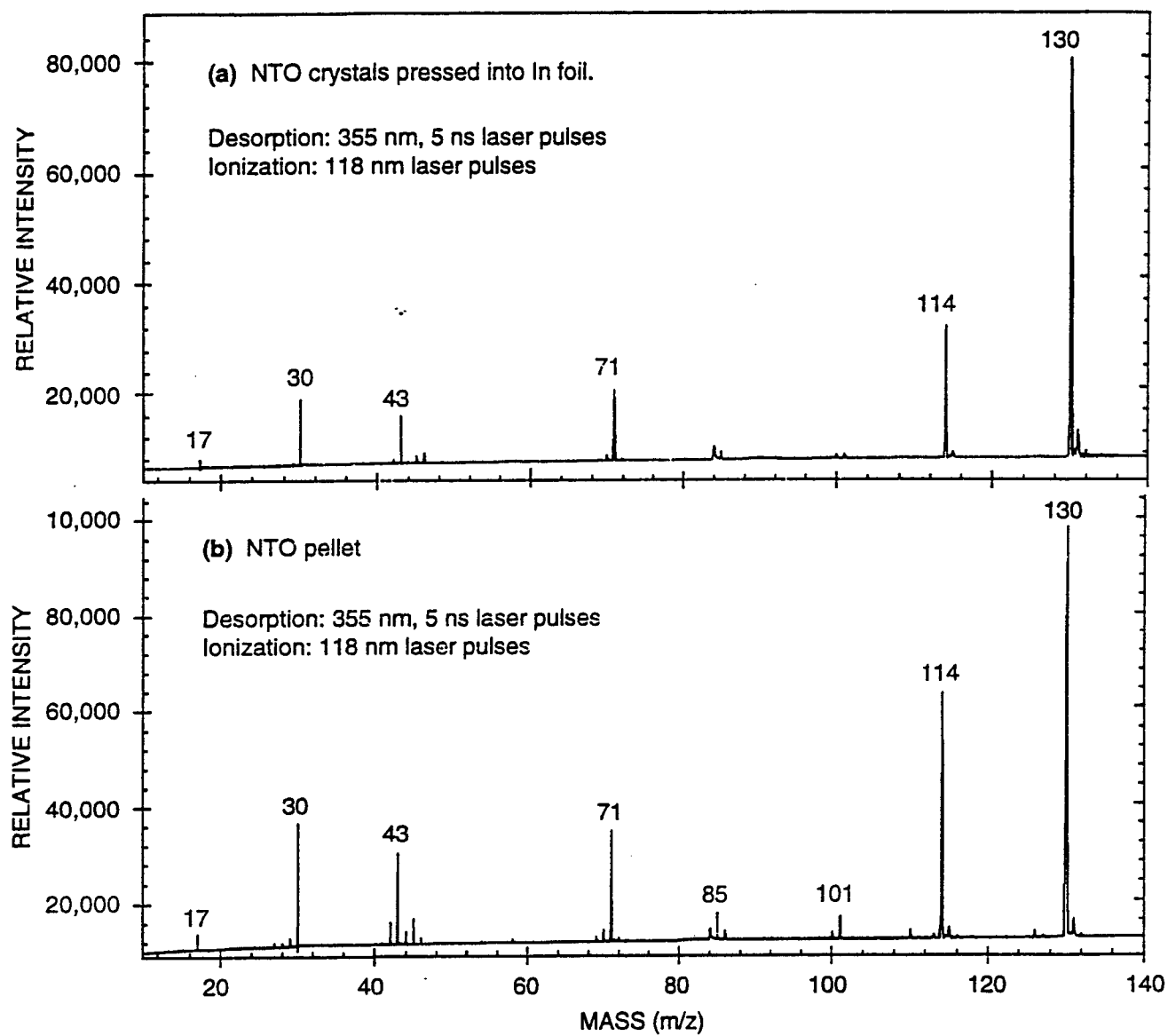
Figure 6. SALI spectra of NTO crystals during slow heating in copper grid. (a) 50°C, no desorption laser.  
(b) 50°C, desorption laser on.





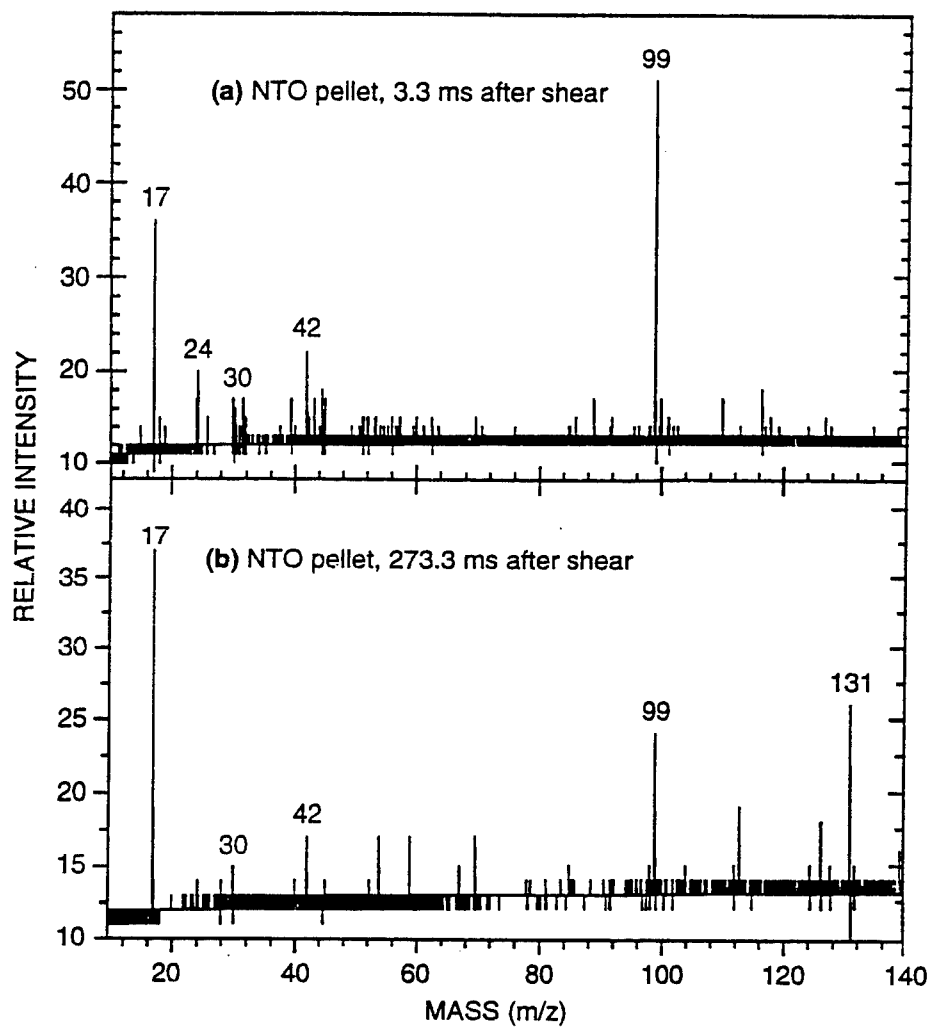
CAM-6134-13

Figure 7. SALI spectra of NTO crystals during slow heating in copper grid. (a) 200°C, no desorption laser. (b) 200°C, desorption laser on.



CAM-6134-11A

Figure 8. Laser-desorption SALI spectrum of NTO. (a) Crystals pressed into indium foil. (b) Surface of pressed pellet.



CAM-6134-14

Figure 9. Single-shot SALI spectra of shear-induced fragment emission taken 3.3 and 273.3 ms after shear.

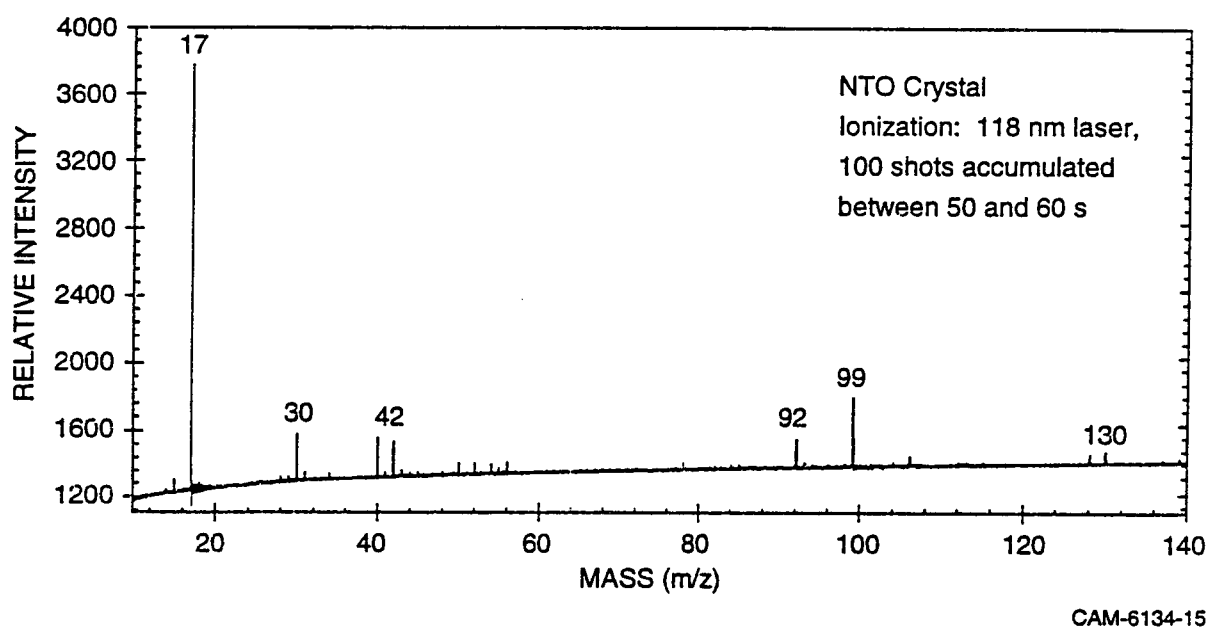


Figure 10. 100-shot average SALI spectrum of shear-induced fragment emission accumulated between 50 and 60 s after shear.

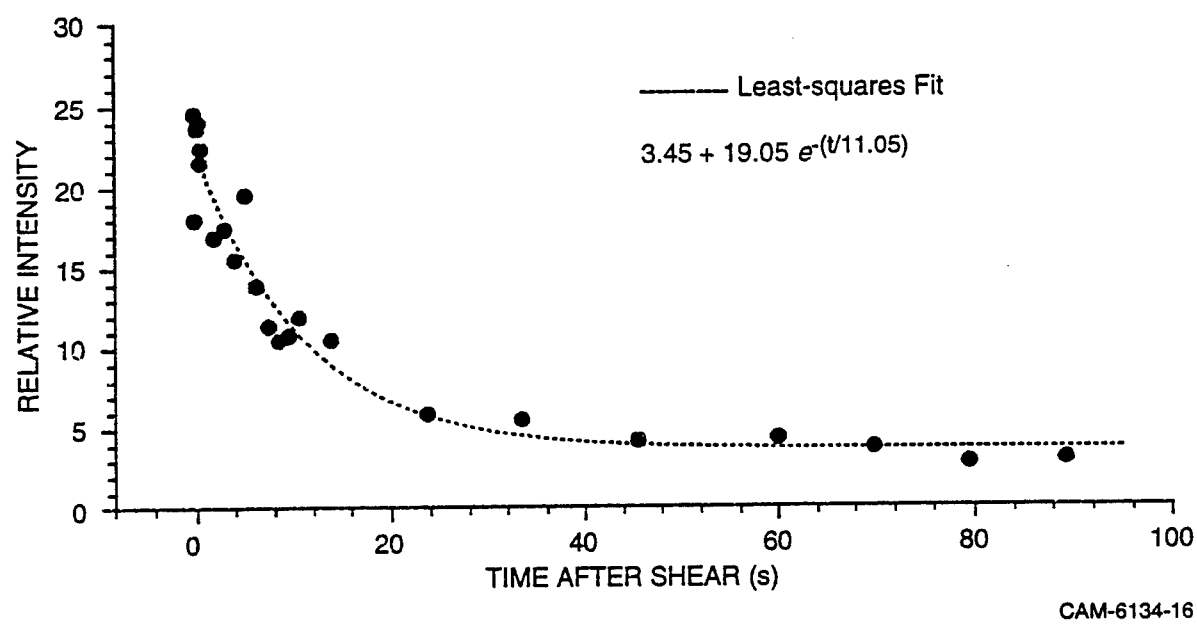


Figure 11. Decay of m/z 99 intensity following simple-shear test.

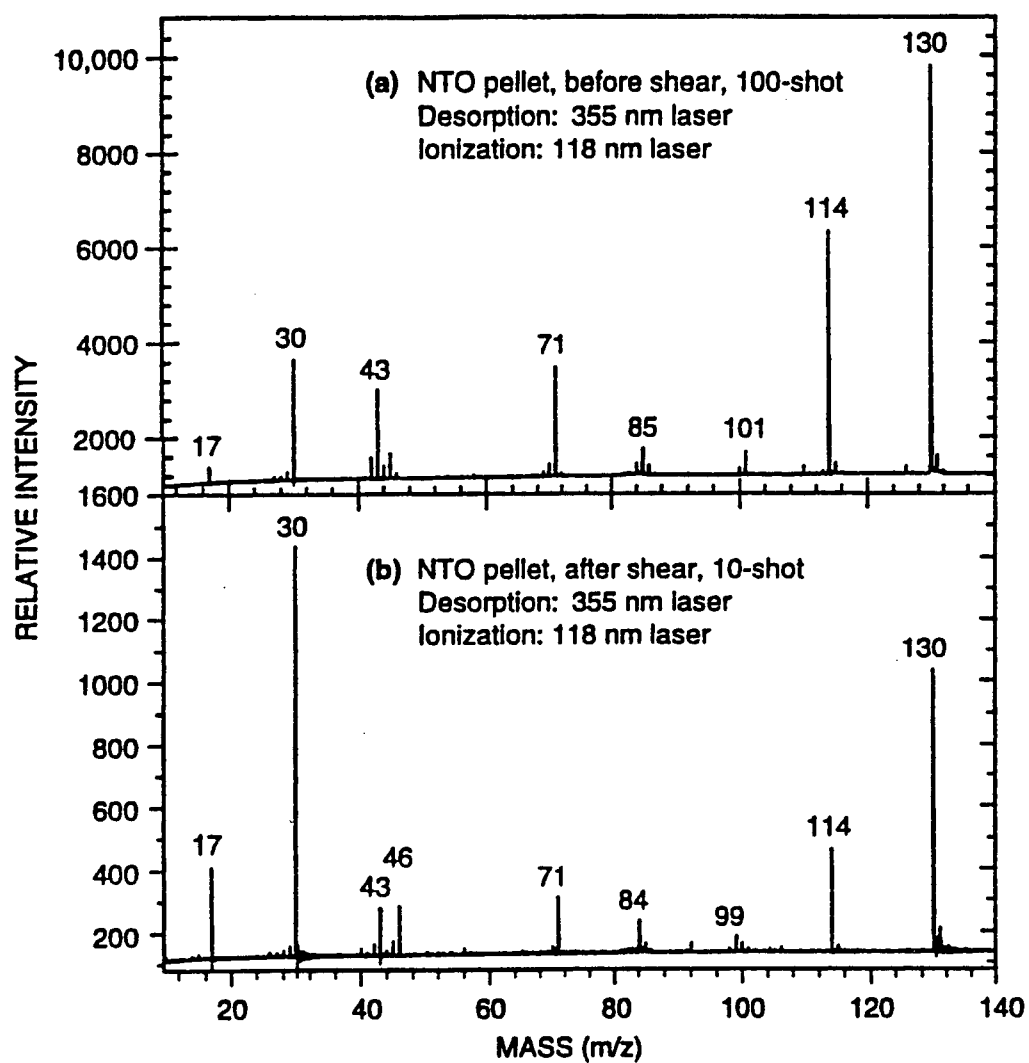


Figure 12. Comparison of laser-desorption SALI spectra taken before and after shear test.

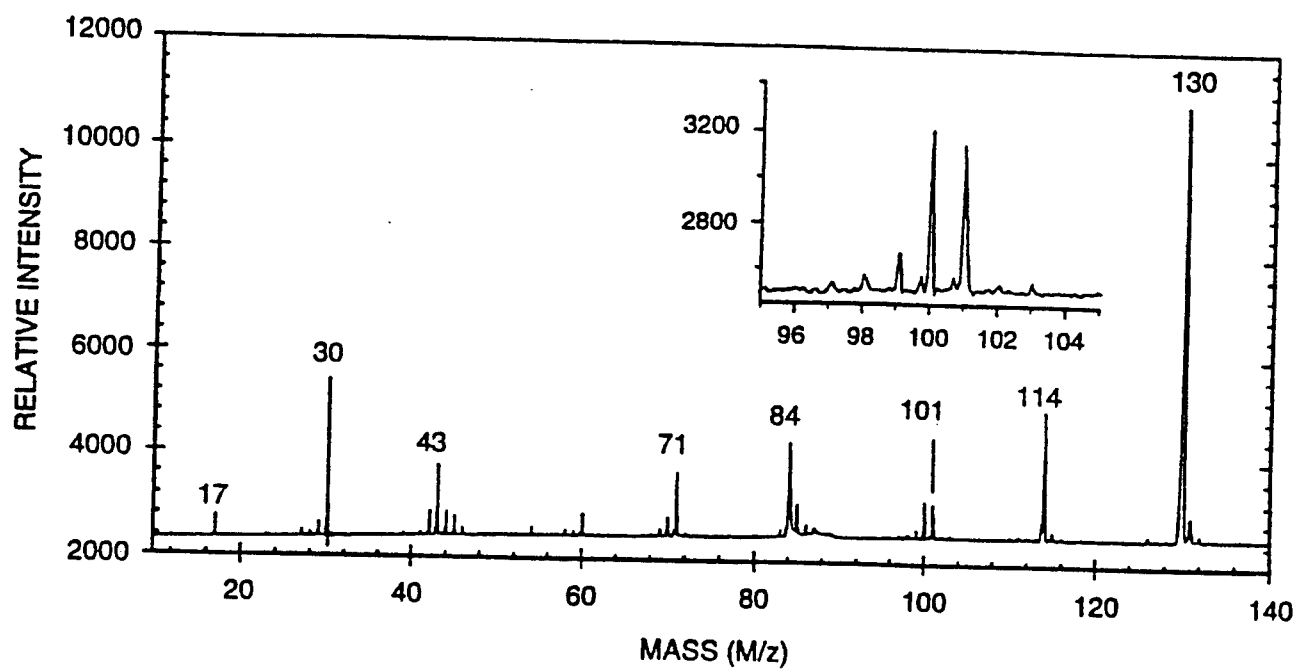


Figure 13. Laser-desorption SALI spectrum of NTO recovered from a sub-critical impact test.

## **APPENDIX B**

### **REAL-TIME PHOTOIONIZATION MASS SPECTROMETRY OF FRACTURE-INDUCED DECOMPOSITION OF A HIGH EXPLOSIVE**



# REAL-TIME PHOTOIONIZATION MASS SPECTROMETRY OF FRACTURE-INDUCED DECOMPOSITION OF A HIGH EXPLOSIVE

Chun He, D. F. McMillen\*, D. C. Erlich, C. H. Becker, and D. A. Shockey  
SRI International  
Molecular Physics and Poulter Laboratories  
333 Ravenswood Avenue, Menlo Park, CA 94025

## ABSTRACT

The chemical factors that affect the sensitivity of the explosive initiation process have been the subject of study for many years. However, the task of determining the sequence of chemical steps that leads to rapid self-sustaining decomposition – either deflagration or detonation – has proven extremely daunting, due to the need for highly sensitive, essentially simultaneous detection of transient intermediates. We report development of a powerful analytical tool for *in-situ*, real-time measurement of the thermally and mechanically induced transient decomposition processes of energetic materials and its application to a new explosive material, nitro-1,2,4-triazol-5-one (NTO).

## INTRODUCTION

NTO (nitro-1,2,4-triazol-5-one, see Figure 1) potentially represents a new generation of insensitive, high-explosive materials: it is energetically comparable to RDX (hexahydro-1,3,5-trinitro-1,3,5-triazine), a widely used military high explosive, but much less sensitive to shock- and impact-induced initiation than RDX, or even TNT (2,4,6-trinitrotoluene) (1,2). The stability characteristics are vitally important with respect to hazards in transportation, storage, or preparation for use. NTO has a heat of detonation higher than that of TNT, and a comparable C-NO<sub>2</sub> bond strength, but its sensitivity is substantially lower. Thus, it is unusual among high explosives in that it does not fall in the traditional correlation between detonation sensitivity and a combined function of the heat of detonation and the X-NO<sub>2</sub> bond strength. The cause of its unusual insensitivity is not understood, raising once again the difficult-to-answer-questions of what sequence of decomposition reactions is responsible for initiation of an explosives event, and what are the chemical and/or physical bottlenecks that make it much more difficult for some explosives to achieve self-sustaining decomposition.

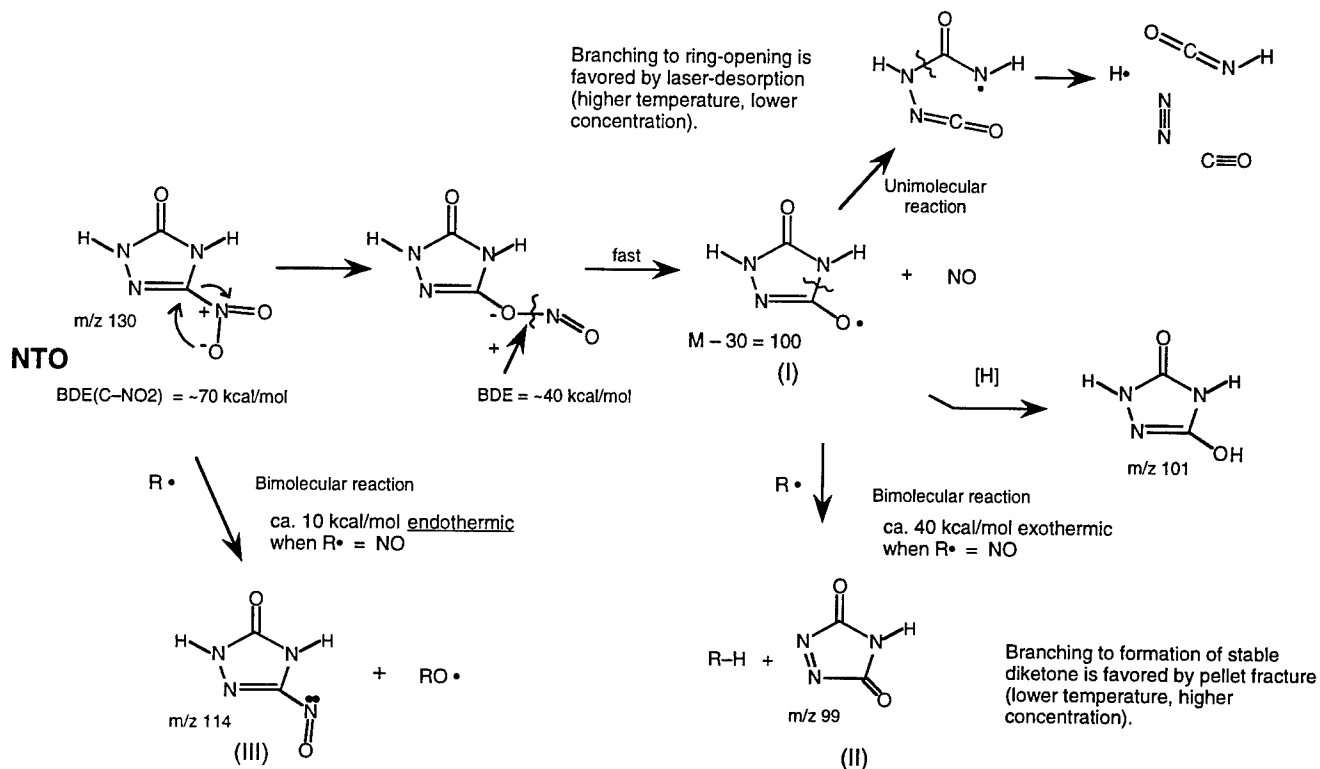


Figure 1. Summary of proposed NTO decomposition pathways.

Since its introduction in 1987, NTO has received the attention of various research groups. Studies have been performed to detect products of NTO thermal decomposition during either slow- or rapid heating, using various techniques such as differential scanning calorimetry (DSC), thermogravimetric analysis (TGA) (3), GC-MS (4), electron spin resonance (ESR) (5), Fourier transform infrared (FTIR) (3), X-ray photoelectron spectroscopy (XPS) (6), and chemical ionization mass spectrometry (CIMS) (6). In almost all cases, the dominant identifiable products of autocatalytic decomposition (which becomes significant at about 220°C) were small molecules, such as O, NO, CO<sub>2</sub>, HONO, N<sub>2</sub>O, etc., rather than larger identifiable intermediates. A small amount of structurally ill-defined polymeric materials is also produced in slow thermal decomposition (4,7). Thus, even for decomposition during slow heating, the literature data provide a very incomplete picture of the actual intermediates that precede the final gaseous products. Furthermore, even if the mechanism of thermal decomposition during slow heating were understood, very little information is available to relate this slow decomposition to the mechanical-

stress-initiated decomposition of NTO. The ultimate solution, obvious in principle but difficult in practice, is to perform a real-time detection of the chemical intermediates during the mechanical-stress-initiated decomposition or detonation of NTO.

We have performed, for the first time, real-time molecular detection of intermediates during fracture-induced decomposition of NTO and have coupled these results with those from slow-heating and laser ablation-induced thermal decomposition, obtained in the same apparatus. Particles emitted from sheared NTO pellets were measured by single-photon ionization (SPI) mass spectrometry *in-situ*. The intermediates were ionized without photofragmentation under conditions that provide true relative concentrations of registered masses.

## EXPERIMENTAL PROCEDURE

NTO samples were obtained from Eglin Air Force Base in roughly spherical polycrystalline grains 20  $\mu\text{m}$  in diameter and were hot-pressed into cylindrical specimens 3.0-mm in diameter by 6.0-mm long. The fracture-induced spectra were obtained in a high-vacuum ( $7 \times 10^{-8}$  torr) chamber designed for laser-desorption mass spectrometry (8), but were acquired *without* use of the desorption laser. The specimen is inserted into a close-fitting hole 4-cm deep on a stainless steel platform mounted to an xyz precision manipulator stage. The platform is placed perpendicular to the axis of the mass spectrometer 4 mm below the extractor of a time-of-flight (ToF) mass spectrometer (mass resolution  $>1000$ ) for which the platform also functions as a repeller plate. Photoion detection is by ion impact on dual chevron microchannel plates at 2 keV impact energy, followed by a variable amplification/attenuation electronics combination. The output analog signal is digitized by a 100-MHz transient digitizer.

When the pellet is to be fractured in a "simple-shear" motion, the fixture holds the pellet so that it is directly below the sampling cone of the mass spectrometer, with the long axis of the pellet on the axis of the mass spectrometer flight tube. A linear motion, bellows-sealed feedthrough shaft is used to apply a simple shearing force with a near-90° blade. A coil spring attached to the shaft outside the vacuum chamber accelerates the blade, which shears the pellet essentially perpendicular to the long cylindrical axis, providing a fracture surface perpendicular to the ToF axis and initiating the mass spectrometer scan(s). Laser-desorption spectra can be obtained before and after fracture of the pellet.

The speed of the shaft during an impact event is monitored by a high speed video camera capable of 2000 frames per second. At an impact speed of 2.25 m/s, the pellet cracks and breaks into two pieces approximately 80  $\mu\text{s}$  (0.18 mm of blade travel) after the contact of the shaft on the front surface of the pellet. In the simple shear mode, the cutting blade clears the new fracture

surface and the collection of spectra begins at ~3 ms after first contact. Modifications of the fixture allow spectra to be taken within a few microseconds of crack completion following simple shear (albiet with a less ideal exposure of the fracture surface) or following compressive impact.

To achieve non-selective photoionization of molecules without photofragmentation, a 118-nm SPI scheme was used for molecular ionization followed by mass detection. The coherent vacuum-ultraviolet (VUV) light generation, based on the 9th harmonic of a 35-ps Nd:YAG laser at 1064 nm, is passed 0.5 mm above and parallel to the fracture surface of the sample, intersecting the axis of the mass spectrometer at the point of focus. The 118-nm (10.5-eV) photons can ionize (with similar cross-sections) virtually any molecule excluding noble gases and a few atoms and small molecules (e.g., C, N, N<sub>2</sub>, N<sub>2</sub>O, O, CO, and CO<sub>2</sub>).

In the experiments on NTO, we specifically tested whether significant photofragmentation resulted from the photoionization. Figure 2 shows the VUV SPI mass spectrum of NTO vapor obtained via by heating the NTO grains to 120°C, a temperature too low for thermal decomposition to compete with vaporization. The single peak for the molecular ion of NTO at  $m/z$  130 confirms that phtofragmentation does not occur, even for this class of substrates where electronegative substitution makes postive ions more prone to fragmentation. Figure 2 also illustrates the high signal-noise ratios routinely achieved for materials of low-to-moderate volatility.

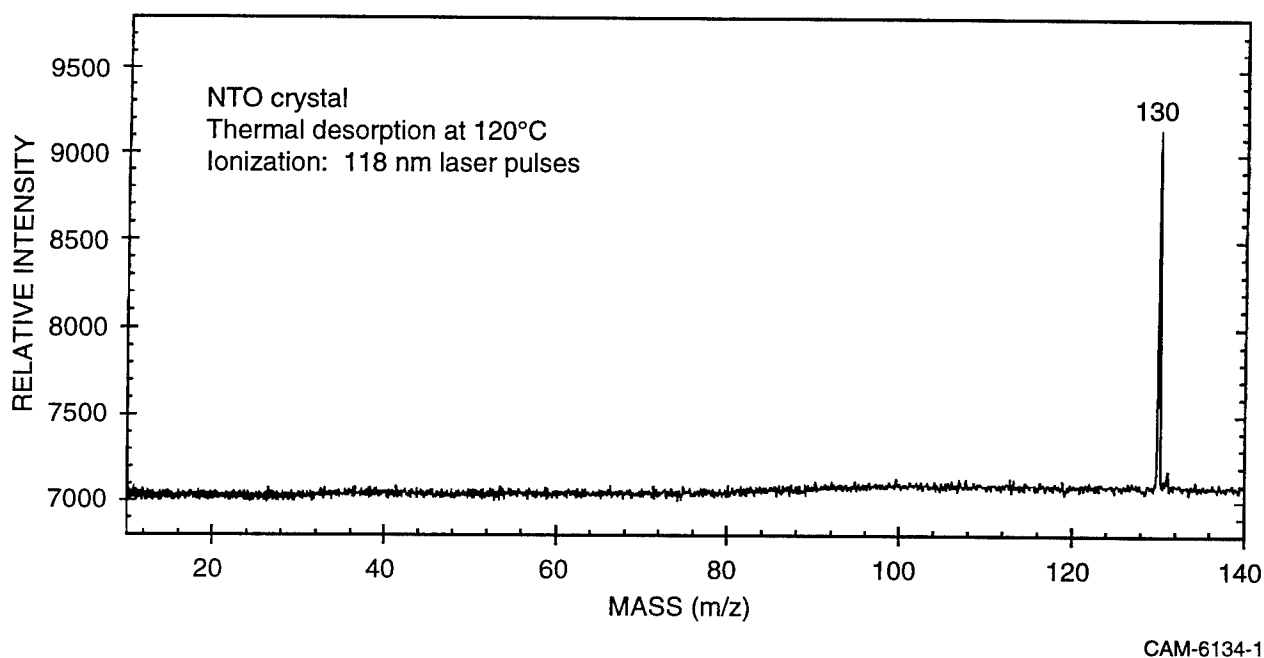


Figure 2. Temperature-programmed desorption SALI spectrum of NTO crystals at 120°C.

To initiate a measurement, the time at the release of the spring loaded shaft is sensed by an emitter-photodiode setup and defined as zero. The laser fire command is issued after a given time following the contact of the shearing blade with the NTO pellet. The transient digitizer is triggered by a photodiode that senses the laser output. The timing sequence is controlled by a four-channel programmable delay generator which, together with the data acquisition system, is controlled by a laboratory computer through a CAMAC interface.

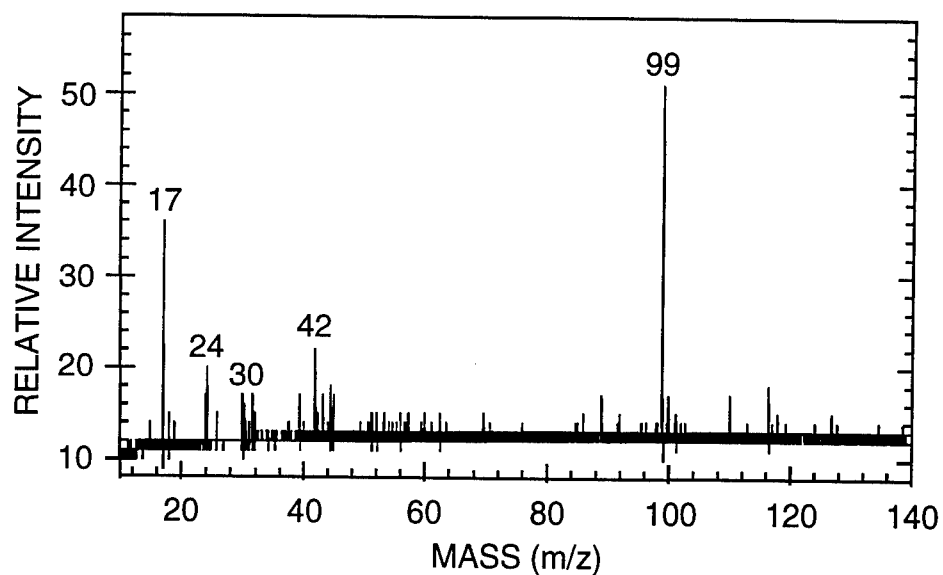
## RESULTS AND DISCUSSION

Figure 3 shows single-shot and averaged mass spectra of the shear-induced emission from an NTO pellet. For comparison, we also obtained spectra under either slow-heating (Figure 2) or rapid pulsed-laser heating conditions (Figure 4), where the fragments are products of rapid thermal decomposition in the laser plume. The time decay of the shear-induced emission is similar to earlier "fractoemission" studies of the explosive RDX, which were performed without mass-analysis (9).

Two differences between the fracture-induced spectra and the laser-desorption thermal decomposition spectra are immediately apparent. First, the shear-induced fragments are dominated by a single peak,  $m/z$  99, which is completely absent in either the laser- or thermal-desorption spectra (where  $m/z$  100 and 101 are significant, though minor, peaks). Second, those minor fragment peaks that do occur as a result of shear have lower intensities and come at somewhat different masses than those that appear under laser-desorption conditions. Third, the dominant thermal-decomposition intermediate, at  $m/z$  114, is not observed at all under the mechanical fracture conditions.

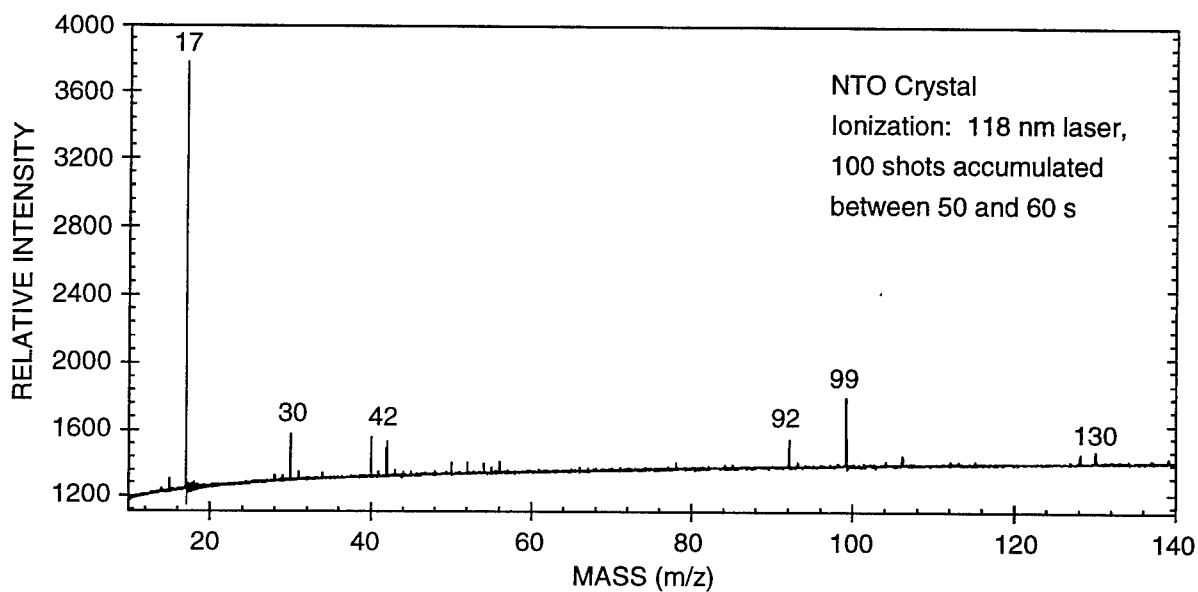
The chemical interpretations of the spectra obtained under these various conditions are briefly outlined below. They lead to the hypothesis that, under the stress of mechanical fracture, intermediates of mass 100 and/or 101 are diverted to mass 99, which then tends to accumulate, rather than going on to produce the next generation of decomposition intermediates at  $m/z$  85, 71, and 43.

Figure 1 shows a set of fundamental reaction steps that are consistent with the observed fragments, and whose literature precedents in other contexts help to provide a plausible accounting for the various intermediates and the variation in branching that occurs under different decomposition conditions. The nitro-nitrite rearrangement of NTO converts the weakest bond in the original molecule ( $C-NO_2$ ) to the still weaker  $O-NO$  bond and leads directly to loss of NO and generation of the alkoxy radical at  $m/z$  100 (I), which can either be scavenged to produce mass 101, undergo



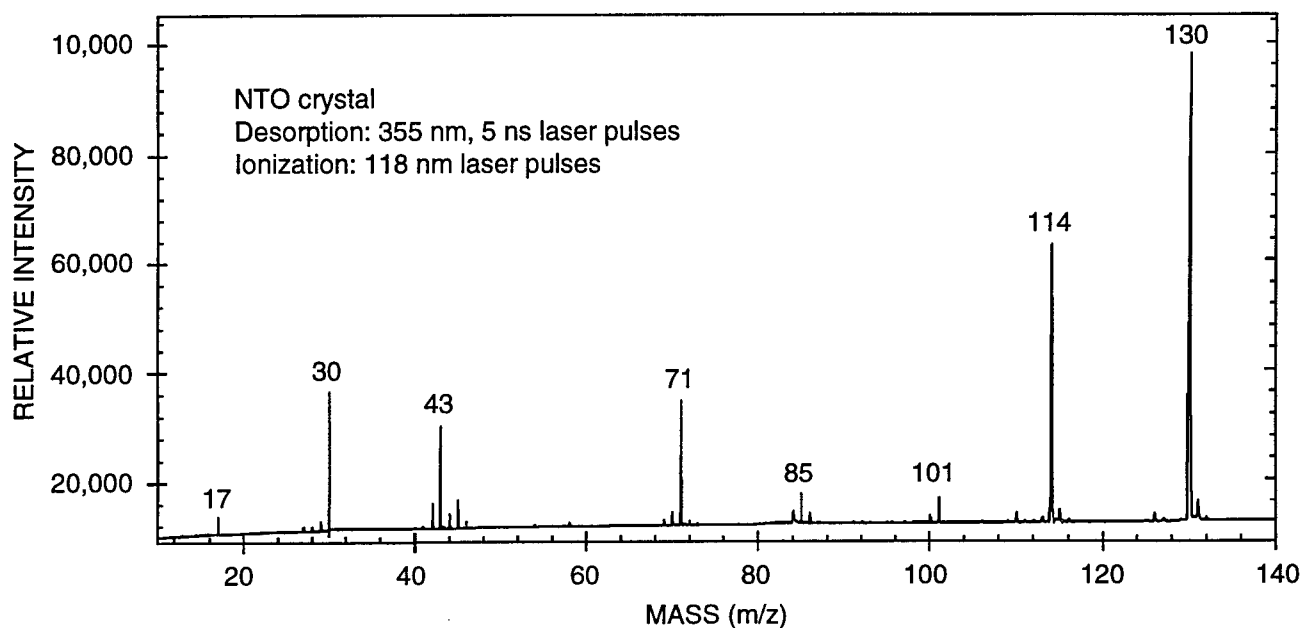
CAM-6134-14A

Figure 3a. Single-shot SALI spectra of shear-induced fragment emission taken 3.3 and 273.3 ms after shear.



CAM-6134-15

Figure 3b. 100-shot SALI average SALI spectrum of shear-induced fragment emission accumulated between 50 and 60 seconds after shear.



CAM-6134-11

Figure 4. Laser-desorption SALI spectrum of NTO pellet.

ring-opening to lead to smaller fragments, or lose a hydrogen to form the triaza-diketone structure  $m/z$  99 structure (II). The only intermediate that clearly does *not* arise from the original nitro-nitrite rearrangement and NO loss is  $m/z$  114 (III), the most abundant single intermediate observed under laser-desorption conditions. The formation of  $m/z$  114 must involve bimolecular reactions with radical fragments, since the  $\Delta H^\circ$  for simple unimolecular loss of oxygen atom from a nitro group is prohibitively high (10). However, oxygen loss should easily occur via addition of any carbon-centered radical  $R^\bullet$  to one of the N–O multiple bonds, followed by elimination of the the oxidized species  $RO^\bullet$ .

We suggest that formation of  $m/z$  99 by rapid *bimolecular* H-atom removal from (I) may be favored under conditions of subcritical mechanical stress by relatively low-temperatures and high-densities (i.e., high concentrations). The stability of this closed shell, relatively unstrained intermediate could help explain the shock insensitivity of NTO. In contrast, higher-temperature, more dilute-phase decomposition during laser desorption should favor unimolecular ring-opening of  $m/z$  100, followed by a sequence of  $\beta$ -scission reactions that leads to the various smaller fragments. A forthcoming publication describes this hypothesis and the factors that dictate shifts in the other intermediates as decomposition conditions change from slow thermal heating, to rapid laser-heating, to shear- and impact initiated decomposition, to laser-heated decomposition of previously shocked NTO.

In summary, without understating the complexity of the explosives initiation process, we believe the capability outlined in this communication offers the potential for sensitive and very direct monitoring of the sequence of reactions that occur as a result of mechanical energy input to various explosive and nonexplosive materials. In the first use of this technique, we have demonstrated (1) monitoring of a relatively new explosive under both thermal- and fracture-induced decomposition conditions, (2) observation of intermediates not previously detected, and (3) use of these data to propose a reasonable sequence of reactions that involves all these intermediates, reconciles a substantial portion of previous slow thermal decomposition data, and potentially explains the initiation insensitivity of NTO.



## REFERENCES

1. K.-Y. Lee, M. D. Coburn, J. Energ. Mater. **5**, 27 (1987).
2. S. Aubert, J. D. Corley, J. G. Glenn, "Development of TNTO Composite Explosives," Final Report WL-TR-92-7073 for Wright Laboratory, Armament Directorate, June 1993; S. Aubert, "Characterization of the Hydrodynamic Performance Properties for NTO and TNTO Composite Explosives," Final Report WL-TR-94-7037 for Wright Laboratory, Armament Directorate, May 1994.
3. G. K. Williams, T. B. Brill, J. Phys. Chem. **99**, 12536 (1995).
4. J. Oxley, J. L. Smith, K. E. Yeager, E. Rogers, X. X. Dong, "NTO Decomposition Products Tracked With  $^{15}\text{N}$  Labels," J. Phys. Chem. A, **101**, 3531 (1997).
5. Menapace, J. A.; Marlin, J. E.; Bruss, D. R.; Dascher, R. V. J. Phys. Chem. **1991**, **95**, 5509.
6. B. C., Beard, J. Sharma, J. Energetic Materials, **11**, 325 (1993)
7. G. K. Williams, S. F. Palopoli, T. B. Brill, Combustion and Flame, **98**, 197 (1994).
8. Pallix, J. B.; Schule, U.; Becker, C. H.; Huestis, D. L. Anal. Chem. **1989**, **61**, 805.
9. Dickinson, J. T.; Miles, M. H.; Elban, W. L.; Rosemeier, R. G.; J. Appl. Phy. **1984**, **55**, 3994.
10. Batt., L.; Robinson, G. N. "Thermochemistry of Nitro Compounds, Amines, and Nitroso Compounds," in Chem. of Functional Groups, Suppl. F, Ed., S. Patai, John Wiley and Sons, Ltd., London, 1981.

## **APPENDIX C**

**MANUSCRIPT FOR REVIEW OF SCIENTIFIC INSTRUMENTS**

# AN APPARATUS FOR STUDY OF STRESS-INDUCED CHEMISTRY IN EXPLOSIVE AND NON-EXPLOSIVE MATERIALS

D. F. McMillen\*, D. C. Erlich, C. He, C. H. Becker, and D. A. Shockey  
Molecular Physics and Poulter Laboratories  
SRI International, Menlo Park, CA

## ABSTRACT

A spring-driven shearing device has been installed in a surface analysis by laser ionization (SALI) apparatus and used to obtain, for the first time, real-time photoionization mass spectra of the fracture-induced molecular-fragment emission from the explosive NTO (5-nitro-1,2,4-triazol-3-one). NTO was chosen for these experiments because of its potential utility as an energetic, but unusually insensitive, explosive. Using vacuum ultraviolet single photon ionization, the shear-induced and impact-induced NTO spectra were obtained with the fracturing fixture installed in the SALI chamber directly beneath the mass spectrometer sampling region. For comparison, spectra were also obtained in the same apparatus under either slow-heating or rapid pulsed-laser heating conditions. The combination of these results has allowed us to (1) identify previously unreported intermediates from NTO decomposition, (2) observe differences in branching between fracture-induced and thermally-induced decomposition, and (3) to postulate a molecular origin for the marked insensitivity of NTO.

## INTRODUCTION

The elucidation of the steps in a rapid stress-initiated chemical reaction sequence, such as the detonation or deflagration of an explosive, has proven to be an extremely daunting task, even with the aid of modern analytical tools. Furthermore, even if the decomposition sequence of an energetic material is known under a particular thermal input, there has been very little basis for understanding how that chemical sequence determines the sensitivity of the material to mechanical stress. In spite of much effort over the years to examine the nature of "hot spots," scientists have not yet achieved a full understanding of the coupling of mechanical energy to chemical reaction.<sup>1</sup> Moreover, it has not yet been possible for any of the organic explosive materials in common use to determine the critical chemical steps that determine whether self-sustaining reaction is achieved. Therefore, we wished to devise an apparatus for analyzing the products that result from the decomposition of an explosive under an applied "mechanical" stress, as well as under the influence of various thermal inputs. We have applied this technique to the new and unusually insensitive high explosive, 5-nitro-1,2,4-triazol-3-one (NTO).<sup>2</sup>

This work derives in part from the "fracto-emission" studies of Dickinson and coworkers,<sup>3,4</sup> who have shown that both explosive and non-explosive materials spontaneously emit neutral

molecules, ions, electrons, and electromagnetic signals when fractured by mechanical stress. Their studies have focused on the general nature of the fractoemission phenomenon and dealt relatively little with the distribution of chemical products. In this work our intention is to characterize the emitted molecules and use that information to help determine the sequence of chemical steps that begin with "mechanical" stress and lead to self-sustaining decomposition. It should be emphasized that we are *not* attempting to characterize the products of an actual detonation or deflagration: not only is there a potential problem of damage to the apparatus, but the products would be dominated by species that are the late products of any explosive decomposition, namely CO, CO<sub>2</sub>, N<sub>2</sub>, NO, NO<sub>2</sub>, N<sub>2</sub>O, etc., and therefore which would give little or no information about the initiation process of any particular explosive. Our desire was to characterize the products under sub-critical mechanical stresses, where initiation sequences had begun, but where there was not enough energy feedback to result in fully self-sustaining decomposition, and to use this information to help determine why some high-explosives are much more difficult to initiate than others.

## APPARATUS AND EXPERIMENTAL PROCEDURES

### Analytical Rationale

In the study of explosive decomposition, the need for highly sensitive, essentially simultaneous, and preferably *in-situ* detection of transient intermediates is such that even tools having the sensitivity and universal detection ability of GC-MS are not sufficient, because the requirement for extraction and chromatographic separation often precludes detection of a mixture of intermediates without further reaction under the conditions of the transfer. Mass spectrometry by itself can sometimes provide a virtually *in-situ* analysis, but the fragmenting nature of electron-impact ionization limits the complexity of the mixture that can be analyzed, particularly where unstable intermediates are involved and there is no possibility of "authentic" standards. The use of essentially non-fragmenting ionization techniques, such as field ionization, field desorption, chemical ionization, and photoionization can be a major help in this regard. The first three of these ionization techniques are very gentle, but generally involve substantial opportunity for secondary reactions while the analyte species are transported to the ionization region. A better approach to *in-situ* analysis, and only slightly less non-fragmenting than field ionization, is provided by single-photon ionization (SPI), at for example 10.5 eV. When coupled with laser-desorption and reflecting time of flight (ToF) mass spectrometry, post-ionization with SPI provides an extremely sensitive surface-analysis technique with nearly universal detection capabilities. Surface analysis by laser ionization (SALI), as developed at SRI,<sup>5-7</sup> is one example of such a combination.

The SALI method offers high sensitivity (< ppm) and wide dynamic range ( $\geq 10^5$ ) and is equally well-suited to either spontaneous or stimulated desorption from the sample surface. In the present work we used a single-photon ionization (SPI) scheme for the ionization step. The coherent

vacuum-ultraviolet (VUV) light generation is based on the 9th harmonic of a 35-psi Nd:YAG laser at 118 nm (10.5 eV). At this wavelength, photo-fragmentation is generally not observed.

SALI differs from standard secondary-ion mass spectrometry (SIMS) principally in that, rather than relying on the so-called secondary ions generated in the highly energetic ion-beam- or laser-beam-ablation process, emitted neutral species are ionized by a 118-nm laser beam that passes directly over the sample surface and under the sampling cone (see Figure 1). The 10.5-eV photons of this beam have enough energy to ionize almost any organic compound, but generally not enough excess energy to cause significant fragmentation. Furthermore, the ionization efficiencies differ very little from structure to structure, and SALI is not subject to the matrix effects that make for very large differences in sensitivities in SIMS analysis. Most importantly, since the desorption and ionization steps are separate, SALI is inherently suited to study of chemistry induced by mechanical generation of fracture surfaces where the decomposition products are spontaneously emitted from those surfaces and an additional desorption input is not needed.

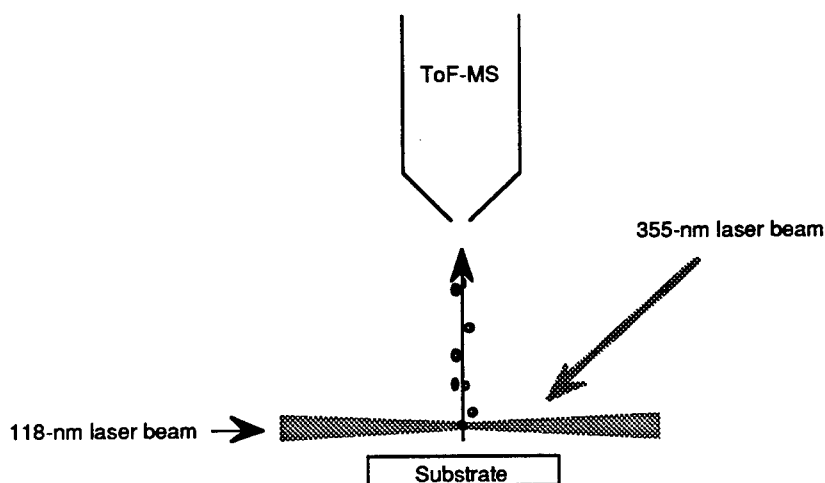


Figure 1. Generalized schematic of SALI technique.

In this paper, we describe results obtained with SALI in the thermal and the laser-desorption modes, and also in this new modification in which there is no laser or thermal pulse but in which a sample is mechanically fractured immediately below the point of focus of the ionizing laser. This modification has allowed us to perform, for the first time, real-time molecular detection of intermediates during fracture-induced decomposition of the new explosive material, nitro-1,2,4-triazol-5-one (NTO) and to couple these results with those from slow-heating and laser ablation-induced thermal decomposition, obtained in the same apparatus. The chemical interpretation of these results are presented in detail in a forthcoming publication;<sup>8</sup> such discussion in this paper is limited to a summary so that the reader can see how this new capability has allowed us to (1) detect and identify transient intermediates that have not been previously reported, (2) assemble a plausible

decomposition sequence that encompasses both thermal and stress-induced decomposition, (3) see how changes in reaction conditions change branching ratios within this sequence, and (4) see how some of the intermediates in these sequences may account for the remarkable insensitivity of NTO.

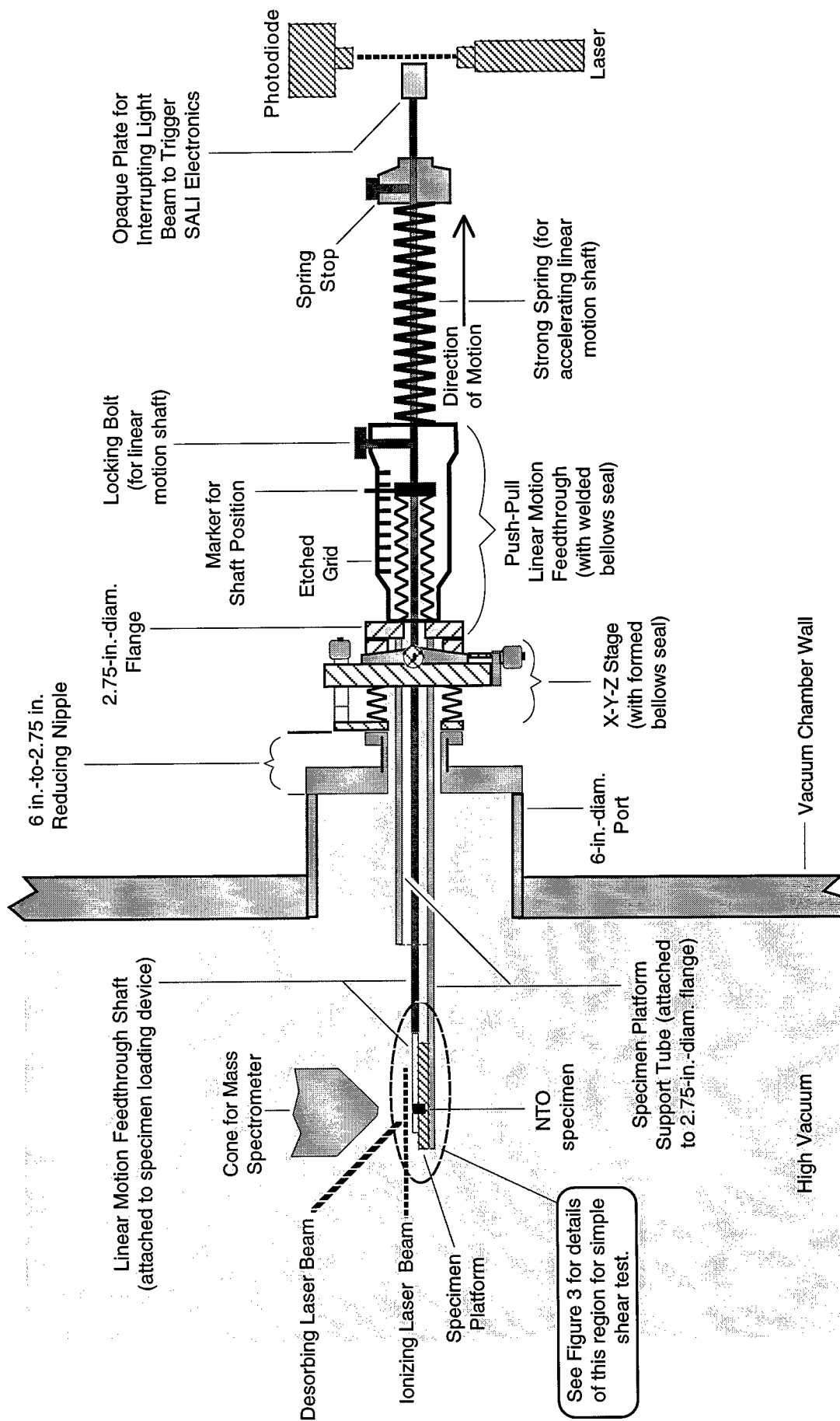
### **Modification of the SALI Chamber for *in-situ* Detection of Fragments Generated by Mechanical Fracture**

A simplified schematic for the SALI method itself is shown in Figure 1. The SALI instrument is housed in a high-vacuum chamber ( $1 \times 10^{-7}$  torr), which is pumped from below and has the ToF mass spectrometer extending from the top. The section we modified for the present work, involving both simple-shear and compressive impact, is a 8-in.-diameter cylindrical section equipped with one 6-in. port and several smaller ports, in addition to ports for ion guns, laser-beam entry, observation, and standard sample introduction.

*In situ* testing in the SALI facility required a fixture that would hold a small NTO specimen near the center of the 8-in.-diameter high-vacuum chamber (so that the surface to be examined was generated within a few mm of the mass spectrometry sampling cone), and could load the specimen along a variety of load paths with a device that could be controlled from outside the chamber (i.e., by means of a high-vacuum motion feedthrough). Furthermore, the geometry of the fixture had to be such that each of the two lasers involved in the SALI technique had a clear path either onto the specimen's surface of interest (in the case of the desorbing laser) or slightly above the surface (in the case of the ionizing laser), either during the loading process (in the case of quasistatic loading) or very shortly afterwards (in the case of dynamic loading).

A schematic diagram of the generalized *in situ* test fixture is shown in Figure 2. The foundation of the fixture is provided by an X-Y-Z precision manipulator stage and a push-pull motion, bellows-sealed feedthrough, which were attached via a reducing nipple to a 6-in.-diameter port that is approximately 6 in. from the center of the SALI chamber. The linear motion feedthrough was modified by: (1) welding a 1-in.-O.D. tube to the inside of the 2.75-in.-diameter flange to provide rigid support for a platform into which the NTO specimen is inserted, (2) bolting a specimen loading device to the inside end of the linear motion feedthrough shaft, and (3) extending the outside end of the shaft to allow for attachment of a spring to provide an accelerating force to the shaft and an opaque plate to provide a means for triggering the SALI electronics.

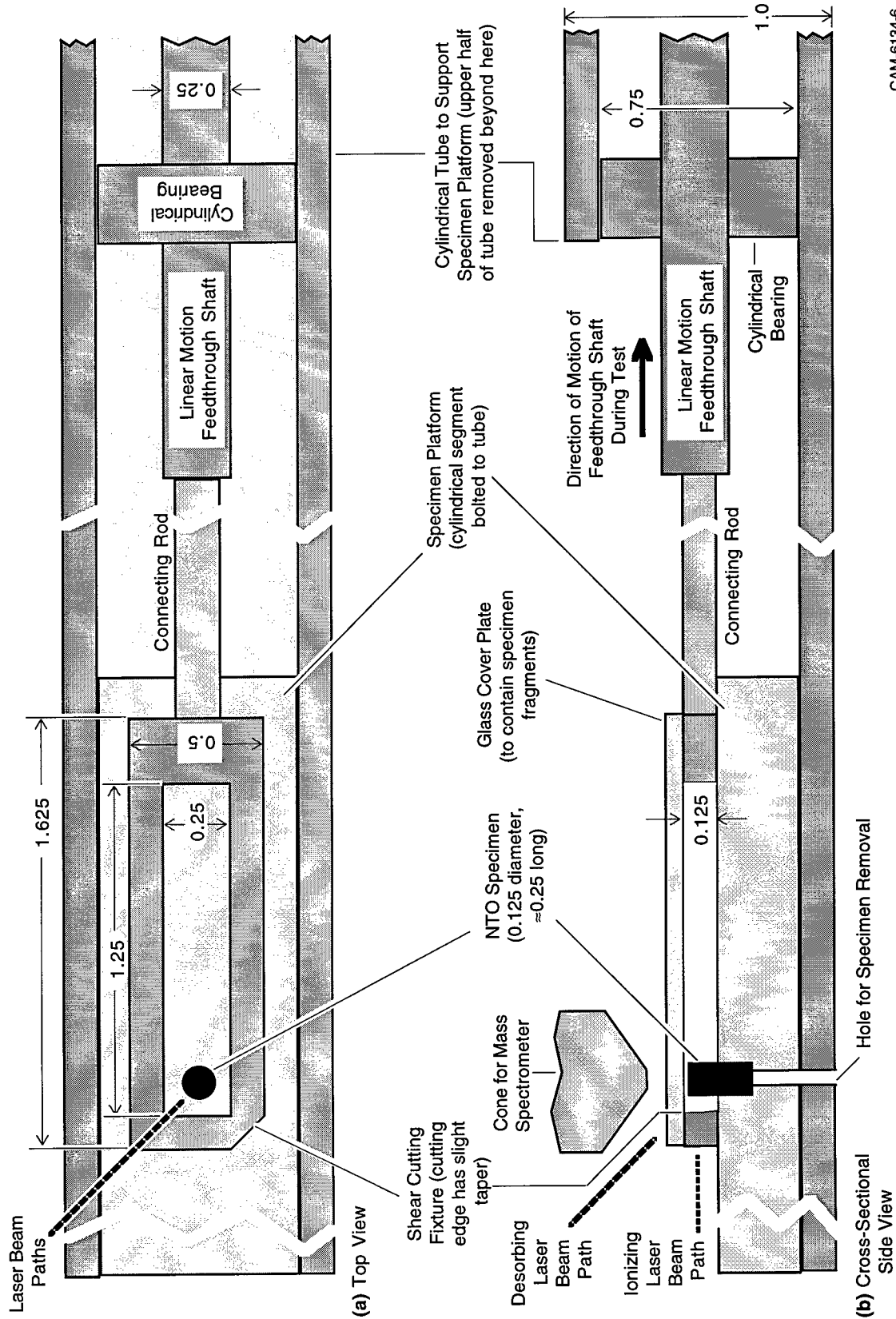
The position of the specimen platform with respect to the mass spectrometer cone is controlled by the X-Y-Z stage, while movement of the feedthrough shaft applies the load to the specimen. The X-Y-Z stage positioning controls remain attached to the high-vacuum chamber during the course of a test series, while the heavily-modified linear motion feedthrough (holding the sample platform itself) is unbolted and removed for each test to allow insertion of the NTO



CAM-6134-5

Figure 2. Schematic view of *in-situ* test fixture on SALI apparatus for use in dynamic fracture tests.

Note: Both ionizing and desorbing laser beams enter at  $\approx 45^\circ$  from the plane of the paper.



CAM-6134-6

Figure 3. Detail of SALL *in-situ* test fixture for simple-shear tests with millisecond delay times.

All dimensions in inches.



specimens. When the linear motion feedthrough and the sample platform are reconnected to the X-Y-Z stage, they return to the originally aligned position within a few thousandths of an inch.

**Fixture for *In-Situ* Simple Shear with Millisecond Delay Times.** The first series of dynamic *in-situ* mechanical fracture tests we performed involved application of a simple shearing force at 90° to the long axis of the cylindrical pellet. As shown in Figure 3, the NTO specimen, a cylinder 0.125 in. (3.2 mm) in diameter by approximately 0.25 in. (6.4 mm) is inserted into a 0.125 -in.-(2.3 mm)-deep hole in the specimen platform, with the upper half sticking above the surface of the platform (Figure 3). A cutting tool attached to the linear motion feedthrough shaft, traveling at about 1.25 m/s, shears a nearly horizontal slice through the specimen, and then continues in the same direction until the tool and the sheared upper half of the specimen are clear of the SALI lasers and the mass spectrometer cone. In this manner the new fracture surface is generated essentially 90° to the mass spectrometer flight axis, presumably the optimum angle for maximum intensity of any decomposition products that would be emitted from the surface, but this arrangement requires the cutter blade to clear the sheared face of the specimen before the ionizing laser can be triggered, a motion that requires 3 milliseconds. A thin glass cover plate atop the shear cutting fixture and a thin brass cylindrical sleeve surrounding the support tube and extending out to the platform region (not shown in Figure 3) contain the sheared NTO fragments after the test.

**Fixture for *In-Situ* Simple Shear with Microsecond Delay Times.** With a viewing angle normal to the newly generated surface, practical limits on spring strength mean the soonest the shearing blade can clear the sheared surface and the collecting of SALI spectra can begin is about 3 milliseconds after initial contact. Since molecular velocities are of the order of mm/ $\mu$ s, the unobstructed travel provided by a high vacuum means that species departing from the fracture surface at the instant fracture is completed would travel beyond the mass spectrometer range in only a few microseconds. To be able to view the sheared surface and detect products much sooner than a few milliseconds after impact, we redesigned the test fixture with different geometry so that we could observe the sheared face without having to wait for the shear cutter to clear the specimen,\* allowing a 10- to 100-fold shortening of the delay time.

---

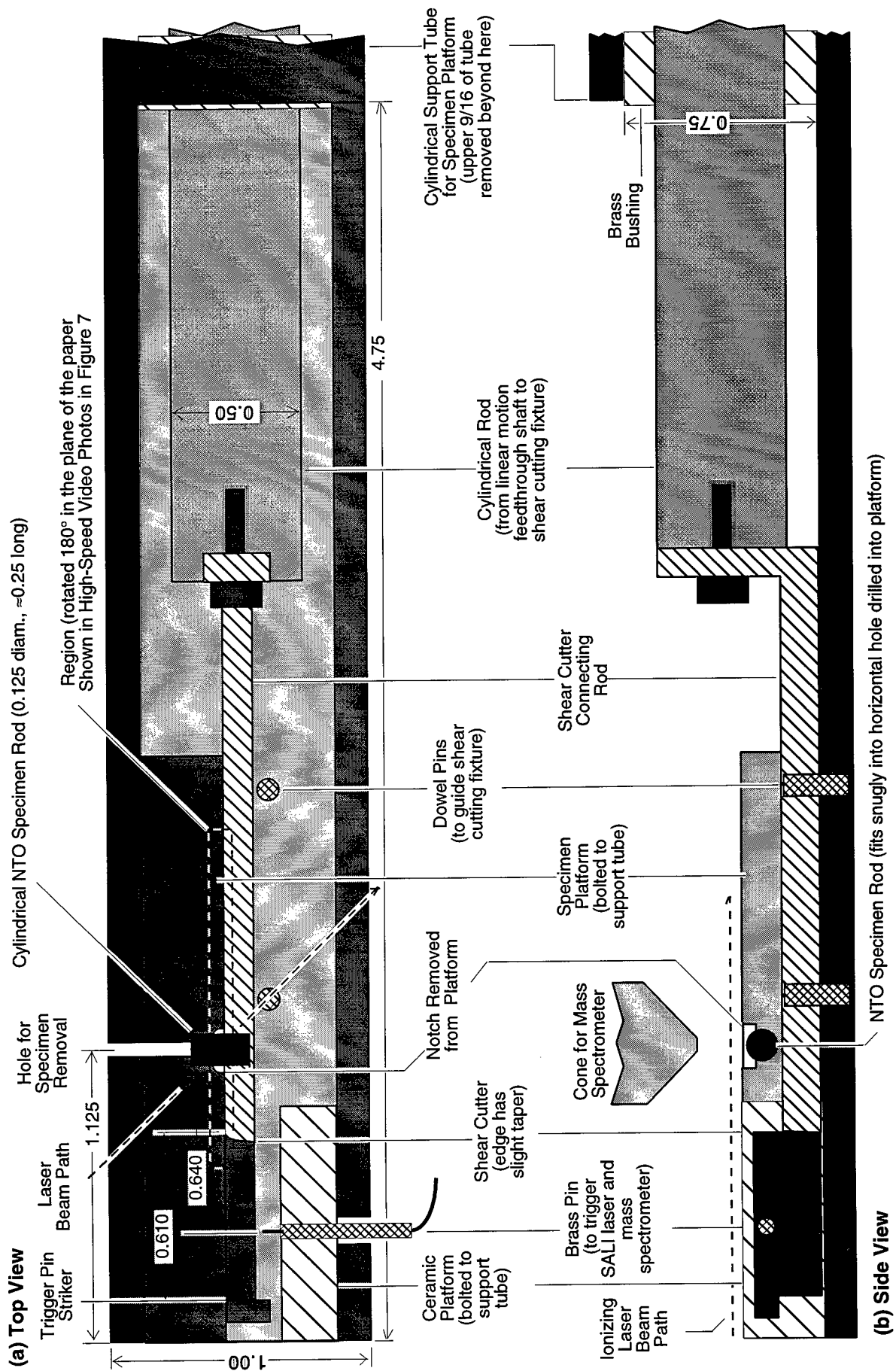
\*Given that the blade speed required to clear the specimen in microseconds is roughly 1000 times faster than the currently achieved 2.25 m/s (faster than the speed of sound in air) and not practically achievable under the present conditions, the only option for acquiring data with shorter delay times was to view the pellet, in effect, from the side, as the end is sheared off. It should also be noted that the crack moves much faster than the blade, and even if a substantially faster blade speed could have been achieved, it would not have resulted in a substantially more energetic crack propagation.

In this mode, the cylindrical specimen (having the same dimensions as in the tests with millisecond-delays) is inserted, as shown in Figure 4, to its midpoint in a hole with its axis in the horizontal, rather than the vertical, direction. The cutter now shears a nearly vertical slice through the middle of the specimen  $\approx$  mm below the ionizing laser and mass spectrometry cone, which means that the line of sight from the crack to the ionization/extraction region is unobstructed almost immediately after the crack was formed, although the viewing angle is far from ideal: the mass spectrometer axis is now almost  $90^\circ$  from normal to the new fracture surfaces. With this new configuration, we did not know whether the net effect on signal strength (vis-a-vis the arrangement shown in Figure 3) would be a net loss of intensity because the MS axis was so far from normal to the crack surface, or a net increase, because we were examining the fracture surface so much earlier.

On the other side of the support tube from the specimen platform is bolted an insulating machinable ceramic (Micor) block into which is inserted a brass rod with a 0.010-in.-diameter brass whisker that acts as a trigger pin. The front edge of the pin is located 0.640 in. (16.26 mm) from the front edge of the NTO specimen. The rod is electrically isolated from the rest of the support tube and is attached to a lead that travels through an electrical feedthrough in the SALI chamber out to the trigger circuitry box.

The steel shear cutting fixture is attached to a guide bar, which in turn is bolted to the linear motion feedthrough shaft through the connecting rod. The guide bar travels between the specimen platform and a pair of steel dowel pins protruding from the bottom of the support tube. On one end of the cutting fixture is the cutting edge (slightly tapered to minimize any tensile component), which impacts the specimen near its axial midpoint. At the other end, located 0.610 in. (15.49 mm) along the direction of motion from the cutting edge, is the protruding shoulder, which strikes the trigger pin.

**Fixture for *In-Situ* Compressive Impact Tests.** The simple-shear tests, in which a crack was caused to propagate across the specimen diameter, splitting the specimen roughly in half, involved relatively little energy being absorbed by the NTO specimen. The shear cutting fixture, traveling at around 2 m/s, loses negligible velocity, and hence negligible kinetic energy, as it drives a shear crack through the thin NTO specimen. The objective in the compressive tests was to substantially increase the energy absorbed by the specimen in the fracturing process. One way to achieve that is to impact the NTO specimen in a compressive (or crushing) mode, with the impactor coming to a complete stop during the process of fracturing the specimen, thereby



CAM-6134-20

Figure 4. Detail of SALI *in situ* test fixtures for simple-shear tests with microsecond delay times. All dimensions in inches.

imparting all its kinetic energy to the fracturing process.\* We therefore modified our *in-situ* fixture to allow for end-on impacts of the cylindrical NTO specimens. We also decided to modify the die we used for pressing the specimens so as to obtain a conical shape for the impacted end of the specimen, judging that impact on a cone would cause more surface fragmentation than impact on a flat-ended specimen.

Details of the specimen loading geometry for the *in-situ* compressive tests are shown in Figure 5. The aluminum specimen platform (a cylindrical quarter-segment) is bolted to the inside of the support tube, and a hardened steel specimen holder is attached to the platform. The conical-tipped, cylindrical NTO specimen is inserted (with its axis horizontal and parallel to the axis of the feedthrough shaft) into a 0.125 -in.-diameter (3.2 mm) by 0.125 -in.-deep (3.2 mm) hole in the side of the specimen platform. Approximately half of the length of the specimen protrudes from the hole, including all of the conical tip and a small portion of the cylindrical segment. The conical tip section is centered directly beneath the ionizing laser beam path; the apex of the cone lies  $\approx 2.5$  mm below the beam path.

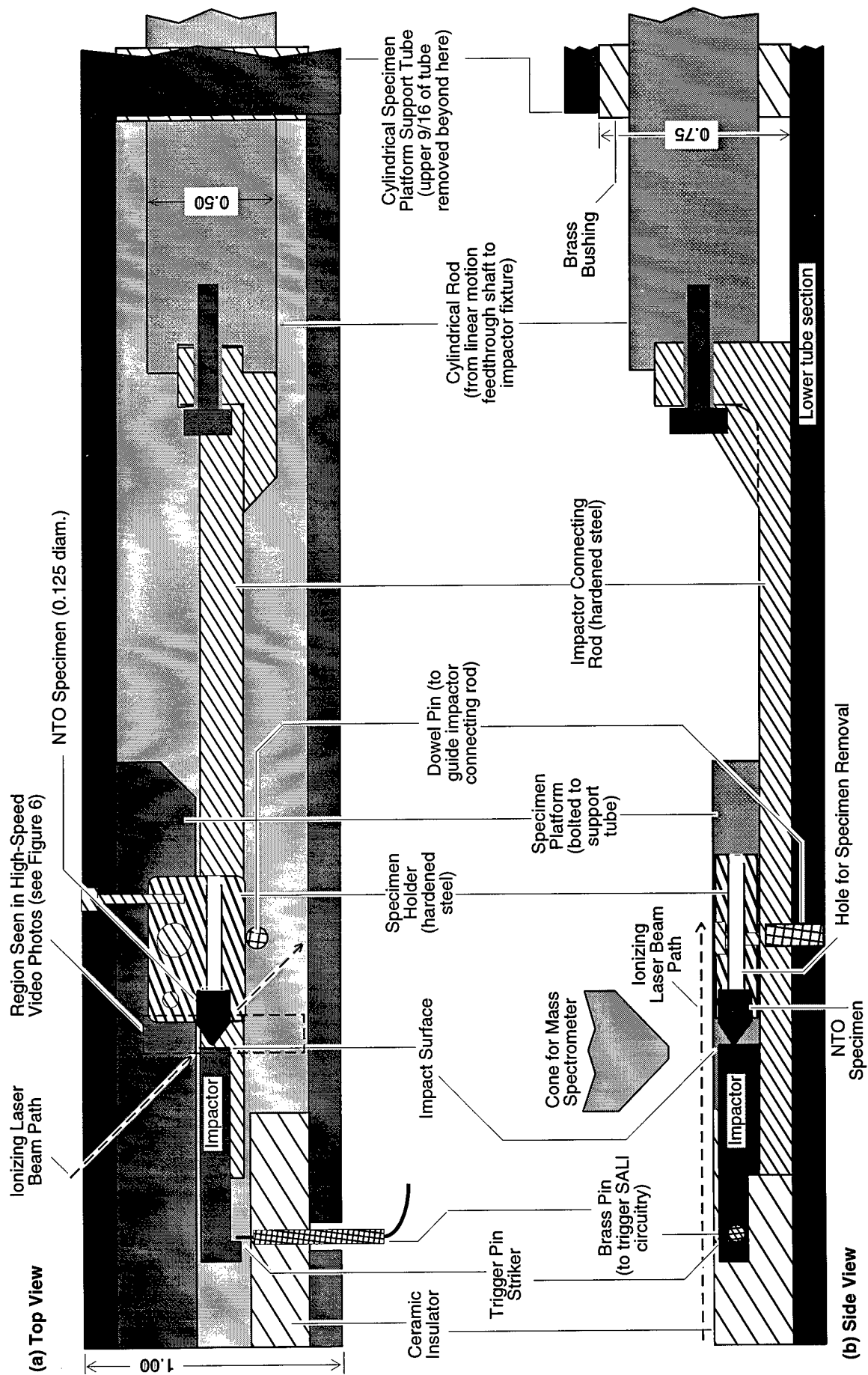
The same Micor ceramic block used for the shear tests was used here to hold the brass trigger pin that closes a connection to the ionizing laser trigger circuitry. The impactor is now attached to a hardened steel connecting bar, which in turn is bolted to the linear motion feedthrough shaft through the connecting rod. The hardened steel material and the reinforcements near the bolt end became necessary in the compressive-impact mode to eliminate bending of the connecting bar during the rapid deceleration. Such rapid deceleration was not encountered in the earlier shear-test modes, where the drive spring, once it passed its equilibrium point, simply slowed the shaft in a more gradual fashion.

### Diagnostic Tests for Pellet-Fracture Fixtures

Before each of the categories of *in-situ* NTO testing, we performed several diagnostic tests to assess the functioning of the fixtures themselves. We needed to determine accurately the relevant distances and velocities, so we could calculate the time interval between the shear crack formation or compressive impact and the SALI measurements. We also wanted to examine the motion of the sheared sections of the specimens to better understand the shearing mechanics. In the compressive impact tests, we also wanted to examine the motion of impactor as it fractured the conical end of the specimen and came to a complete stop.

---

\*More precisely, some of the kinetic energy of the impactor goes to the fracturing process in the target, and some goes to lateral acceleration of the fractured fragments.



CAM-6134-28

Figure 5. Detail of SALL *in-situ* test fixture for compressive impact tests.  
All dimensions in inches.

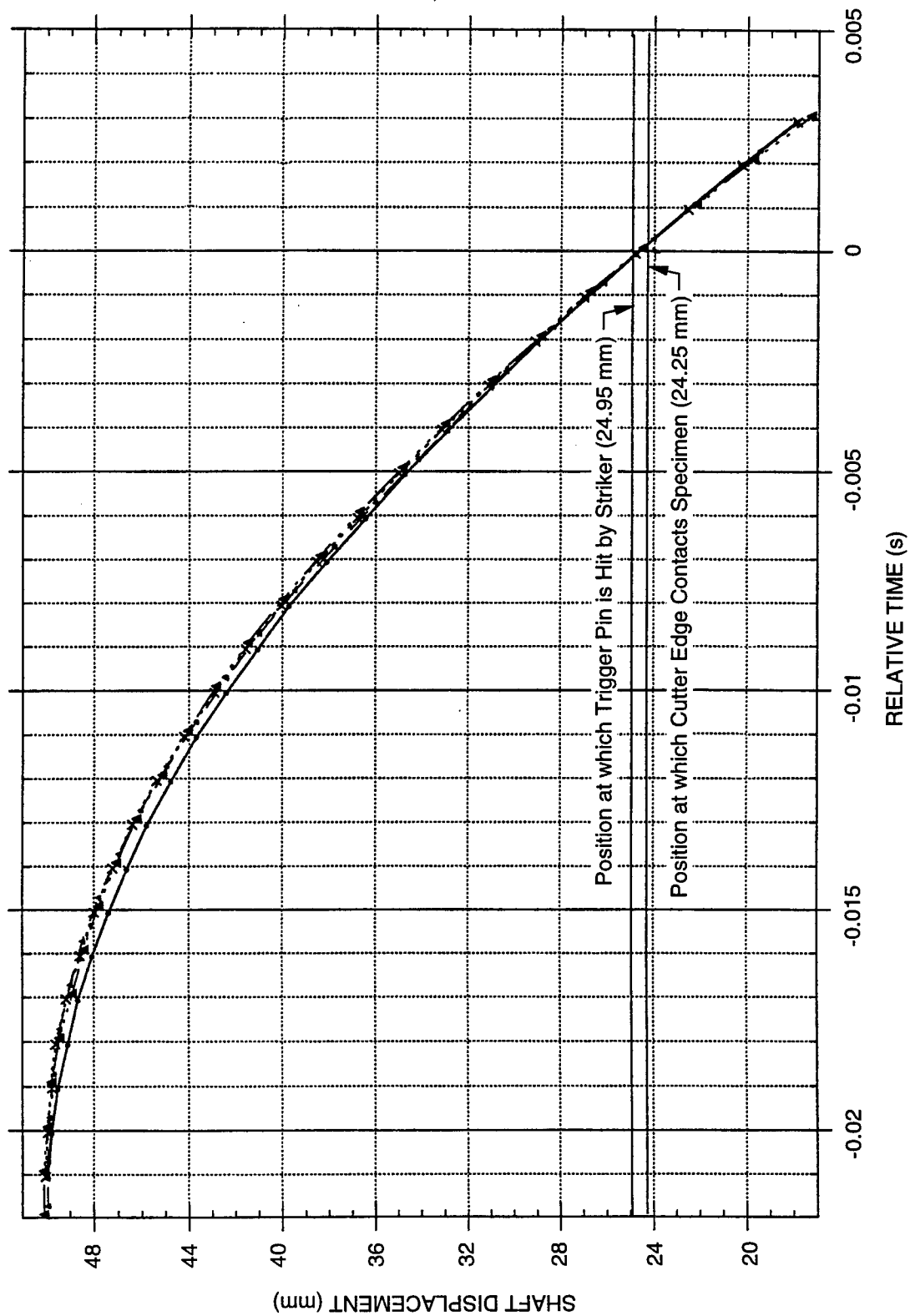
**Simple-Shear Fixture.** For the simple-shear tests with millisecond delay times, timing is simple because the sum of all electronic and inadvertent mechanical delays is well under a millisecond. For the modified shear with  $\sim 100 \mu\text{s}$  delay times, the timing became more critical, and the following approach was used.

First, we positioned the linear motion feedthrough device on a machinist's mill, and while moving the shaft, very accurately measured the distance traveled after the shoulder strikes the trigger pin whisker, before the edge of the shear cutter reaches the specimen. The result was  $0.0302 \pm 0.0002 \text{ in.}$  ( $0.767 \pm 0.005 \text{ mm}$ ). We then measured the additional distance that the shear cutter needed to travel into the NTO specimen after impact before the specimen sheared. This test was performed at the very slow rate of less than  $0.0002 \text{ in./s}$  ( $0.005 \text{ mm/s}$ ), and the result was brittle shear crack failure at  $0.007 \pm 0.001 \text{ in.}$  ( $0.175 \pm 0.025 \text{ mm}$ ). The cutter edge appeared at first to penetrate the specimen without any observable cracking, and then at a depth that ranged between  $0.0060$  and  $0.0078 \text{ in.}$  ( $0.15$  and  $0.20 \text{ mm}$ ) over several tests, a shear crack began and traveled all the way through the specimen at a speed faster than the eye could follow, splitting the specimen in two.\* The distance of penetration of the cutter before specimen shearing may be a function of cutter velocity (at very high velocities, there may be more or less penetration, depending on the mechanism involved). However, we do not expect the penetration distance before fracture to change significantly at the rates for the *in-situ* shear test ( $2 \text{ m/s}$ ), because that is still very slow compared with typical crack propagation velocities in brittle materials.

Next, we used a high-speed (up to 12,000 frames per second) videocamera to record the displacement history of the linear motion feedthrough shaft in actual operation, so we could determine the velocity of the cutting edge as it shears through the specimen. Because we wanted to duplicate the exact conditions of the shear tests, the device was first bolted in place on the X-Y-Z stage, and a vacuum was pulled in the SALI chamber (the pressure in the chamber affects the motion of the shaft by acting over the cross-section area of the bellows seal). The shaft motion was then locked in its maximum inward position, just beyond the 50-mm mark, and then released, with the video camera recording the motion of the shaft marker on the stationary etched grid (see Figure 2). The results of four typical tests are shown in Figure 6, with the time for all the curves shifted so that zero time occurs in the vicinity of the trigger pin closure (near the 25-mm mark). The displacement histories were quite repeatable; the velocity of the cutter as it reaches the position of specimen impact (near the 24-mm mark) was  $2.25 \pm 0.05 \text{ mm/s}$ .

---

\*This brittle shear crack was in marked contrast to the case of an acrylic specimen, for a which a small crack was observed to form in the vicinity of the shear cutter edge at a penetration depth of  $\approx 0.018 \text{ in.}$  ( $0.45 \text{ mm}$ ) and then, without any further motion of the cutter, to slowly grow across the specimen over tens of seconds until it reached the far edge.



CAM-6134-21

Figure 6. Displacement histories of spring-driven linear-motion feedthrough shaft for four velocity tests of shear fixture.

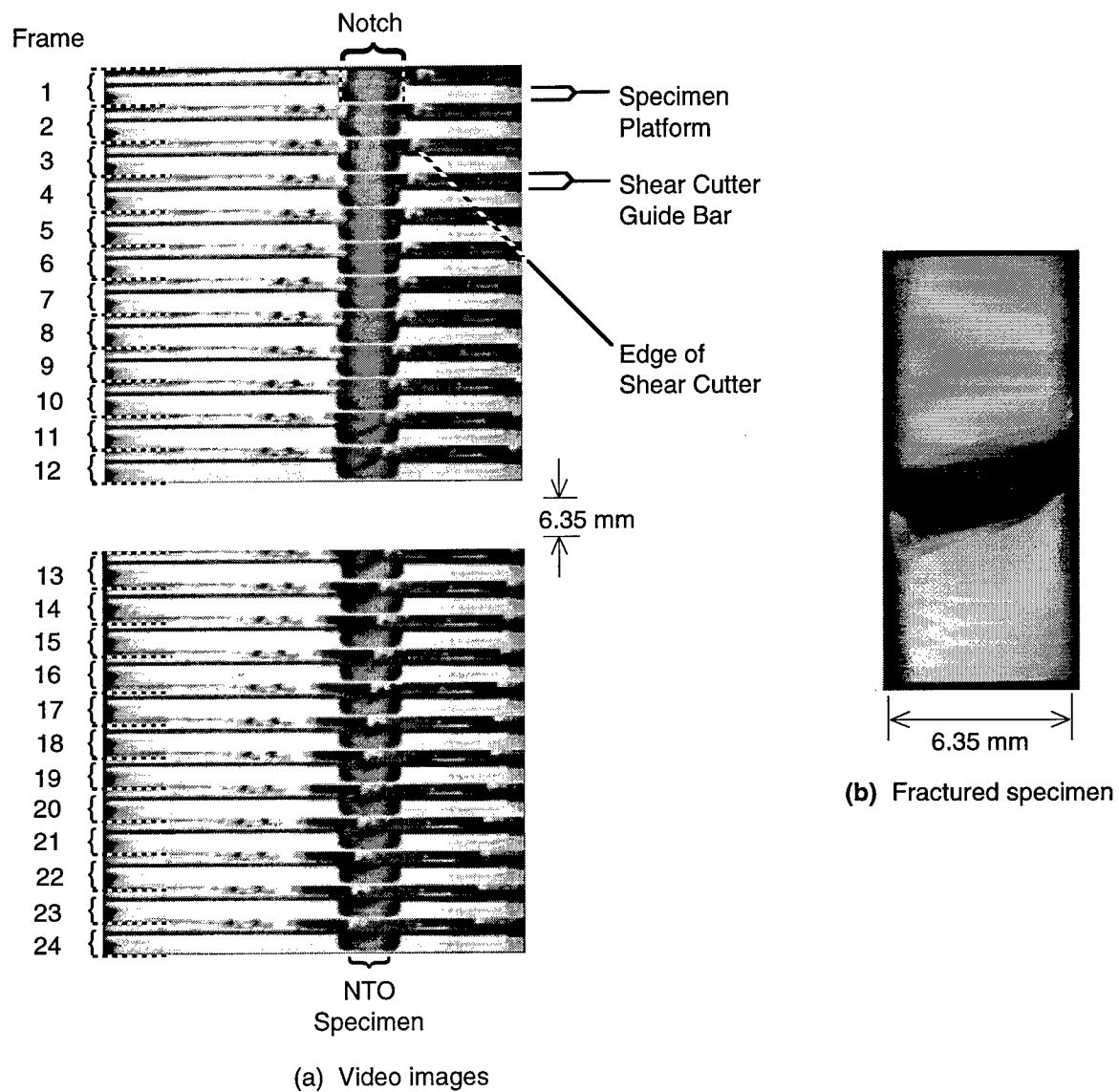
For the final diagnostic test of the shear fixture, we set up the linear motion feedthrough device outside the SALI chamber (so that a closeup lens could be readily used to view the pellet itself), repositioned the spring stop to attain the same shaft velocity (2.25 m/s) at specimen impact that had been obtained with the fixture inside the vacuum chamber (the velocity is faster without the vacuum retarding the motion of the shaft and bellows), and focused the high-speed videocamera on the NTO specimen as it was being contacted and sheared. Typical results are seen in Figure 7(a), which shows 24 frames (in 2 groups of 12 frames) taken at 12,000 frames per second (successive frames are thus 83.3  $\mu$ s apart).

The region shown in each of the long and narrow frames is the region within the dashed rectangle in Figure 4(a), but is rotated 180° in the plane of the paper. The whitish region on both the left and right sides of each frame is the top of the specimen platform on either side of the bowl-shaped notch, and the gray region near the center of each frame is the mid-axial region of the NTO specimen protruding from the notch. The thin gray band moving from right to left across the upper portion of each frame is the shear cutter guide bar. The shear cutter edge is the white, roughly triangular shape that appears to hang from the specimen platform and contacts the NTO specimen at about frame 10.

By frame 11, less than 83  $\mu$ s and 0.008 in. (0.2 mm) of cutter travel after the first contact, the crack appears to have grown all (or very nearly all) the way across the specimen. This gives us further evidence that the  $0.007 \pm 0.001$  in. ( $0.175 \pm 0.025$  mm) value we measured quasi-statically for the cutter penetration before shear cracking is a good approximation to the value at the actual *in-situ* test velocities. By frame 12, less than 166  $\mu$ s after first contact, the NTO has clearly separated into two pieces, and the sheared piece is rotating up and to the left, completely disappearing from view by frame 16.

The shear crack does not propagate exactly transversely across the specimen, but as shown in Figure 7(a), angles downward into the notch at  $\approx 15^\circ$  to the transverse direction. Then as the crack nears the back surface, it changes direction and cuts sharply back towards the specimen midplane. Figure 7(b), a photograph of the two halves of a sheared NTO pellet, shows the typical shape of the shear crack. This behavior has been observed to be quite repeatable, based on both the high-speed video camera images and examination of the recovered specimens. Kalthoff and Winkler<sup>9</sup> showed that angled shear cracks are a natural result of the stress field in the material ahead of a sharp shear cutter. The presence of the notch may also affect the shape of the sheared surface.





CPM-6134-22

Figure 7. High-speed video images of NTO dynamic shear test and photograph of fractured specimen. Frames are 83.3  $\mu$ s apart.

The timing of the mass spectra acquisition for simple shear with microsecond delay times is as follows. The ionizing laser has an inherent firing delay of  $351\ \mu\text{s}$  after its trigger contact, whereas the specimen shears at  $420 \pm 20\ \mu\text{s}$  after this contact. So the time between specimen shearing and SALI measurement is  $T - 69 \pm 20\ \mu\text{s}$ , where  $T$  is any additional time set on the delay generator. In this series of tests,  $T$  spanned a range from 100 to 900  $\mu\text{s}$ , which means that our measurements nominally spanned a range from 31 to  $831 \pm 20\ \mu\text{s}$  after completion of the shear crack.

**Compressive Impact Fixture.** We again used a high-speed video camera to record the displacement history of the linear motion feedthrough shaft, so that we could determine the velocity of the impactor as it contacts the specimen and also observe the fragmentation process. As with the shear tests, the displacement histories were quite repeatable; the velocity of the impactor as it reaches the position of specimen impact was determined to be  $2.37 \pm 0.05\ \text{m/s}$ . The results obtained when the camera is focused on the conical end of the NTO specimen as it was being impacted and crushed are seen in Figure 8.

The region in each of the long and narrow frames is the region within the dashed rectangle in Figure 5(a), but rotated  $90^\circ$  counter-clockwise in the plane of the paper. The long thin gray region on the top of each frame is the edge of the specimen holder. The end of the cylindrical portion and all of the conical-tipped portion of the NTO specimen can be seen protruding from the holder [a magnified view of the protruding region, taken through a microscope, is shown in Figure 8(b)].

Beginning approximately at Frame 0, the impactor can be seen as a black line moving upward into the conical end of the NTO pellet. The impactor motion appears to stop approximately at frame 10, at which point essentially the entire conical section of the specimen has been crushed. Due to the presence of NTO fragments traveling outward in the region between the impactor and the specimen holder, the impactor stops before contacting the specimen holder, so all the kinetic energy of the impactor fixture (including the connecting rod, feedthrough shaft, and so on) is absorbed by the specimen and its fragments. (Because the impactor fixture has a mass of  $\approx 460\ \text{g}$ , roughly  $1.3\ \text{J}$  is absorbed in crushing the conical tip of the specimen. We believe this is several orders of magnitude more energy than is absorbed during an *in-situ* shear test.) NTO fragments can be seen in Figure 8(a) emerging at right angles to the impact direction, traveling from 4 to 9 m/s.

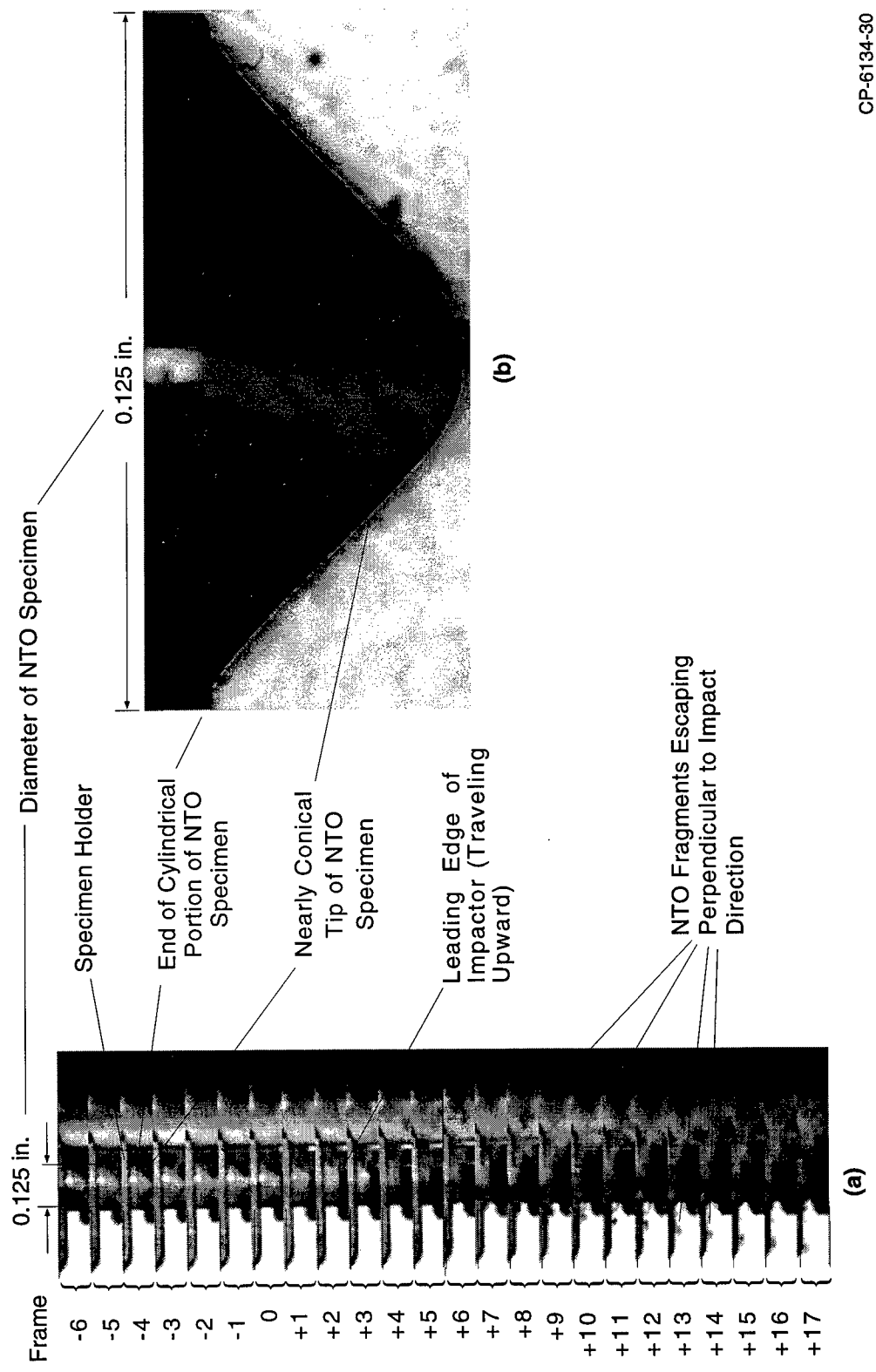


Figure 8. High-speed video images of NTO SALI impact test and microphotograph of conical NTO specimen tip. Successive frames are 83  $\mu$ s apart; impact (at  $2.37 \pm 0.05$  m/s) occurs approximately at Frame 0.

CP-6134-30

## NTO Sample Preparation

**Pressing the NTO Specimens for the *In Situ* Tests.** The fine-grained NTO powder, obtained courtesy of the U.S. Air Force, appears to consist of rough spheres, from  $\approx 15$  to  $\approx 25\ \mu\text{m}$  in diameter. These spheres are in fact bundles of very fine crystals that radiate outward from the center of the sphere.

Our goal for pressing the NTO specimens was to attain densities of  $1.85\ \text{g/cm}^3$  ( $\approx 96\%$  of the TMD of  $1.83\ \text{g/cm}^3$ ) or slightly lower, since higher densities are not reported to produce a higher explosive yield.<sup>10</sup> We used a modification of the procedure described by Aubert<sup>11</sup> for pressing NTO specimens that calls for one cycle at 24,000 to 28,000 psi for 5 minutes at a temperature of  $105^\circ\text{C}$ . The fixture we used consists of a stainless steel die, two alloy steel rods, a base plate, and shims that allow us to press the specimen from both sides and thereby minimize density gradients along the specimen. Electrical heating tape is wrapped around the die to allow for hot pressing. A thermocouple inserted in the die to within 0.25 in. of the specimen recorded the temperature.

We first tried to press cylindrical specimens with an aspect ratio of about 5 [0.080 in. (2 mm) diameter by  $\approx 0.375$  in. (9.5 mm) long], but found that these specimens could not be easily removed from the press or handled without being damaged. We then lowered the aspect ratio to about 2 [0.125 in. (3.2 mm) diameter by  $\approx 0.25$  in. (6.35 mm) long] successfully obtained specimens of good material integrity, such that the fracture surface generated by the shearing blade is relatively smooth, and does not appear to have simply formed along grain boundaries between the original crystallites.

For the simple-shear tests with millisecond delays and for the reoriented shear tests with microsecond delays, we used identical cylindrical pellets, pressed to the dimensions indicated above, using a peak specimen pressure of  $\approx 19$  ksi. In one set of pellets pressed for shear tests, the density of the specimens ranged only from 1.871 to  $1.897\ \text{g/cm}^3$ , a variation of less than 1.5%, corresponding to approximately 97% to 98% of the theoretical maximum density (TMD) of  $1.93\ \text{g/cm}^3$ .

For the *in-situ* compressive tests, we modified the pressing fixture to produce specimens with one roughly conical tip (the cone angle is  $\approx 90^\circ$ ; microphotographs (Figure 8(b)) reveal a rounded apex with a radius of curvature of about 0.025-in.). The hot-pressing procedure itself was not changed from that used for the simple cylindrical pellets. The densities of these pellets are virtually identical to those prepared earlier for the shear tests: ten pressed specimens had densities of  $1.880 \pm 0.013\ \text{g/cm}^3$ , again 97% to 98% of the TMD. The specimens had the same diameter as

before, a conical tip length (distance from the cone apex to the closer end of the cylindrical section) of 0.0536 in. (1.36 mm), and a total length from 0.167 in. (4.24 mm) to 0.203 in. (5.16 mm).

### ***In-Situ* Fracture Procedures**

With the exception of timing and sequence of single- and averaged multiple shot spectra, the procedures used for obtaining SALI spectra are essentially those that have been developed over the last six years in our laboratory using the SRI prototype instrument.<sup>5-7</sup> These include laser-desorption spectra at room temperature and under temperature-programmed heating, as well as spectra with no laser desorption. Mass calibration is achieved by interpolation between the ubiquitous background peak at  $m/z$  17 ( $\text{NH}_3$ ) and a small residual vapor pressure of anthracene ( $m/a$  178) deliberately introduced into the chamber. The uncertainty of interpolation and peak assignment throughout the range is  $< 0.2$  amu. The *in-situ* fracture tests on NTO pellets required the construction of the special modifications to the SALI chamber described above and involve non-standard procedures in which no desorption laser is used. The general procedure for the modified *in-situ* pellet fracture experiments, each of which required 1 to 2 hours, is given below.

Before inserting the sample platform and motion feedthrough into the SALI chamber, we (1) lock the shaft at its most inward possible position (spring fully compressed), just beyond the 50-mm mark, (2) insert an NTO specimen into the platform hole, and (3) position a trigger pin in the Micor block and attach the lead to the back of the pin. We then bolt the shaft onto the X-Y-Z stage, manipulate the stage until the specimen is positioned properly beneath the mass spectrometer cone, pump the chamber down to a high vacuum, and attach the lead from the trigger pin to the trigger circuit.

To begin a test, the thumbscrew on the locking shaft bolt is quickly turned, freeing the shaft to accelerate in the outward direction. After 1.0 or 1.6 in. (25 or 40.5 mm) of travel (for shear tests and compressive impact tests, respectively), the pin striker hits the trigger pin, sending a signal to activate a delay generator. After further shaft travel, depending on the specimen length and test type, the shear cutter or impactor strikes the NTO pellet, at which time the impactor has reached a velocity of  $2.25 \pm 0.05$  m/s or  $2.37 \pm 0.05$  m/s. The delay generator is set to trigger the SALI electronics (ionizing laser and mass spectrometer circuitry) at the desired delay after contact. For the shear tests with millisecond delays, the firing of the ionizing laser is keyed to the time the sheared section flies away from the confined portion of the pellet. For the shear tests with microsecond delays and the compressive impact tests, the ionization laser firing is keyed to the time the impactor has traveled approximately half way into the conical section (i.e., about half of the ultimate travel) and has produced a significant volume of fractured NTO.

## RESULTS AND DISCUSSION

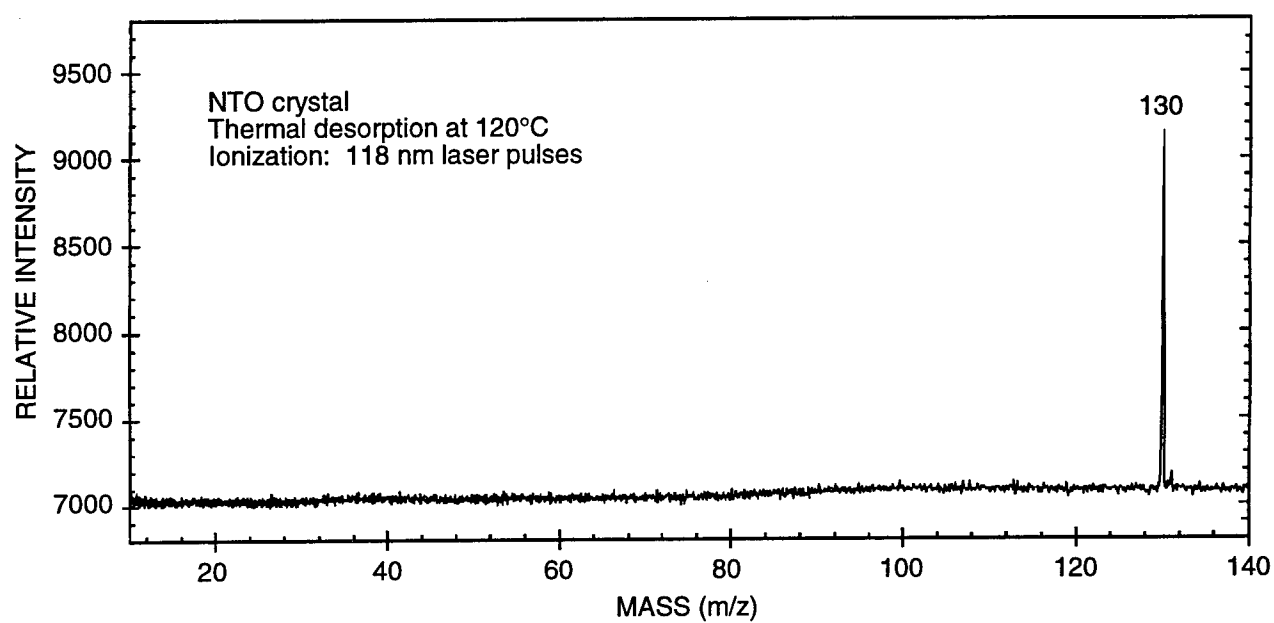
In this section, we describe some of the results obtained for shear- and compressive-impact-induced decomposition of NTO, as well as for simple thermal decomposition under both slow heating and with the sharp thermal pulse resulting from 355-nm laser ablation. Our primary emphasis in this presentation of the results is on the quality of the spectra that are obtainable with this technique and on the pronounced differences we have observed between the fractoemission spectra and normal thermal or laser desorption spectra. A detailed chemical interpretation for the thermal- and shear-induced results is being presented elsewhere, and will only be briefly summarized here. We present the thermal- and laser-desorption spectra first, to provide a background for presentation of the fracture-induced spectra. In all cases, the 118-nm laser radiation provides the ionization source.

We first sought to establish whether significant photofragmentation is induced by the ionization laser. At 120°C, where the vapor pressure of NTO is appreciable but where thermal decomposition is very slow, the spectrum obtained without laser desorption (Figure 9) shows the NTO molecular ion at  $m/z$  130, but no other peaks. Clearly, no fragmentation results here from the ionization process. The absence of fragmentation of the parent also makes it very probable that the various decomposition intermediates of NTO are also ionized without substantial fragmentation, since all of those intermediates have been stripped of the electron-withdrawing NO<sub>2</sub> group, one of the features that makes the positive molecular ions of many nitro-compounds so susceptible to ion-fragmentation in the first place.

Varying the temperature of the NTO substrate provides additional information about the effects of the desorption and ionization lasers. Figure 10 shows that at lower temperatures (50°C) there is no significant ion intensity at *any* mass without the desorption laser, while with the desorption laser on, the dominant molecular ion is accompanied by a number of fragment peaks at 1%-30% of the base peak. At substrate temperatures much closer to the ca. 230°C NTO decomposition temperature, some fragments (principally  $m/z$  85) begin to appear at very low intensities even without the desorption laser [Figure 11(a)], and addition of the desorption laser increases the relative intensity of other fragment peaks at  $m/z$  30, 43, 71, and 114 roughly tenfold [Figure 11(b)] from their thermal background levels. However, the intensities of these latter peaks were still only about 1% of the molecular ion, less even than in the 50°C laser-desorption spectra obtained under nominally identical fluence conditions for both the desorption and ionizing lasers.\*

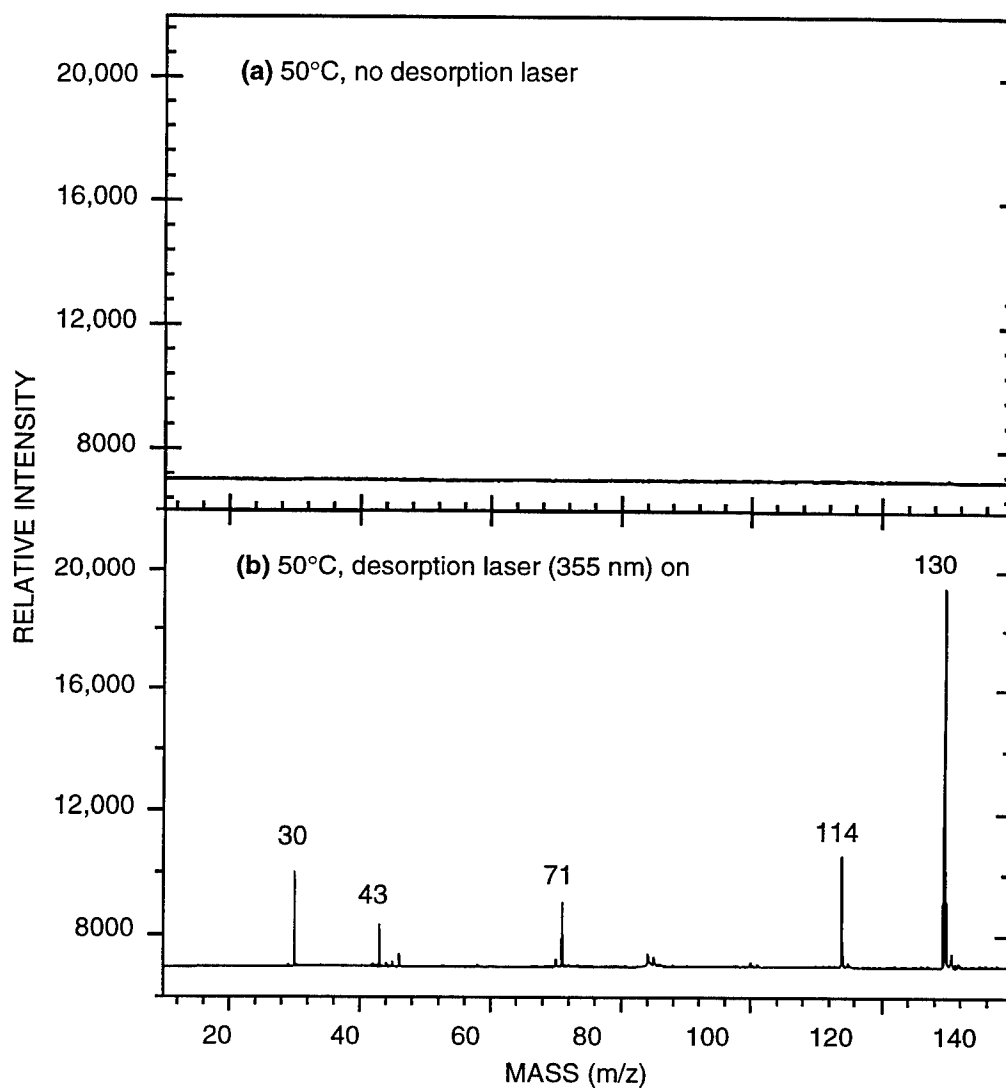
---

\*This remains true even if we subtract the thermal "background" intensity at  $m/z$  130 from the laser desorption spectrum obtained at 200°C, and assign *all* of a given fragment-peak intensity (e.g. @  $m/z$  114) to the laser-desorption contribution.



CAM-6134-1

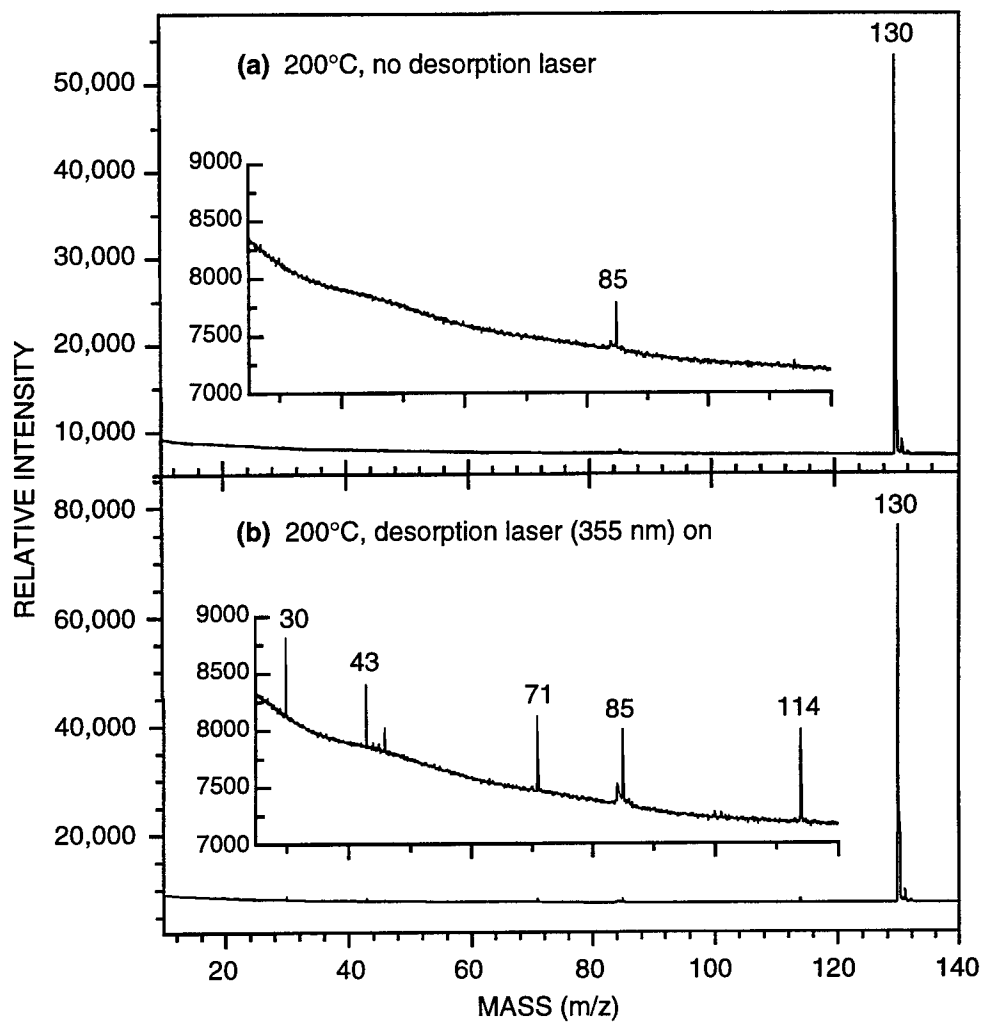
Figure 9. Temperature-programmed desorption SALI spectrum of NTO crystals at 120°C.



CAM-6134-12

Figure 10. SALI spectra of NTO crystals at 50°C during temperature-programmed desorption in copper grid.





CAM-6134-13

Figure 11. SALI spectra of NTO crystals at 200°C during temperature-programmed desorption in copper grid.

Thus, under all conditions tested, the overall fragmentation (thermal plus any possible ion fragmentation) ranges only from modest to inconsequential, does *not* increase with temperature, and provides no suggestion at *any* temperature that any significant portion of this is fragmentation after ionization. Clearly, the single photon ionization as used here provides a very good measure of the distribution of neutrals, either when they are thermally desorbing or being laser ablated from the NTO surface.

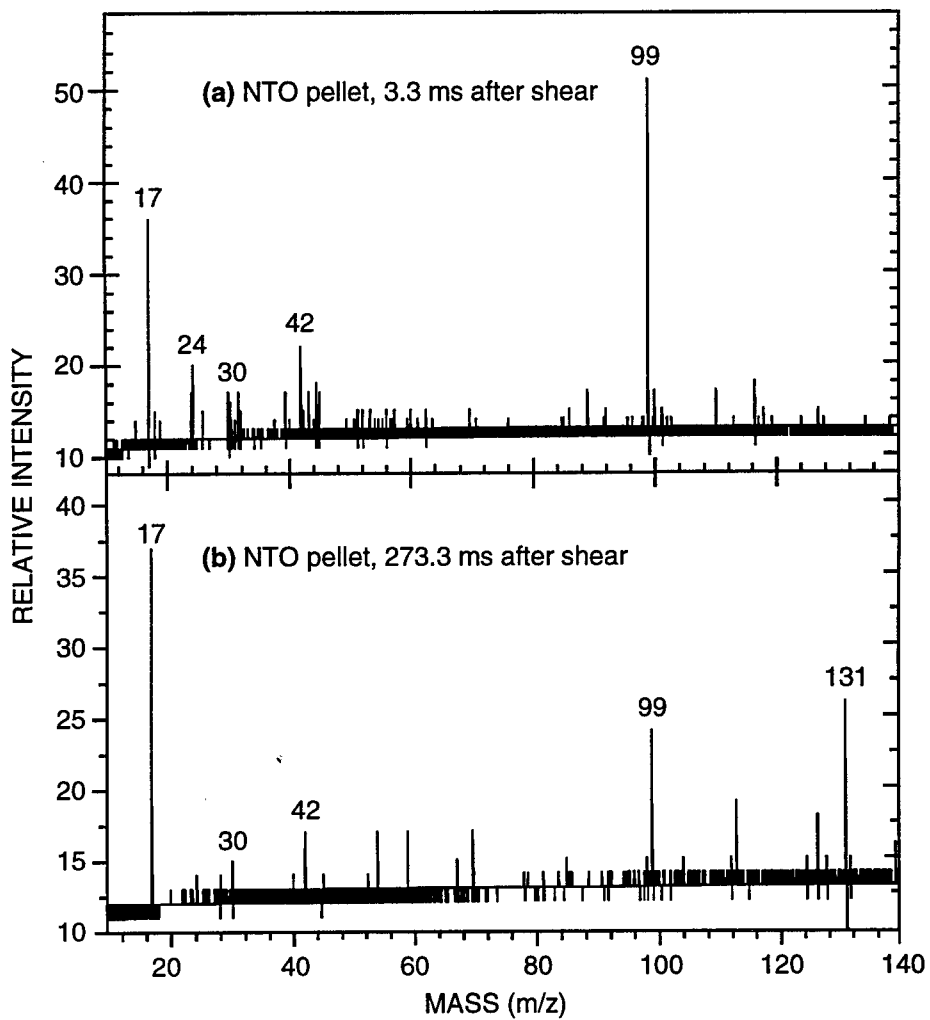
Above 240°C, the temperature at which literature studies show 50% to 90% decomposition in 200 minutes [6], the NTO molecular ion continues to be observed, but at much diminished intensity, and the molecular ions of intermediates decline roughly proportionately. Most of the NTO that has not sublimed has decomposed, and the thermal decomposition intermediates that we observe appear to be transient: under these conditions they do not accumulate to any appreciable extent in the bulk NTO.

The thermal- and laser-desorption mass spectra of NTO can be summarized by saying that the relative intensities of the molecular ion and various fragment peaks differ somewhat under these two sets of conditions.  $M/z$  84, 85, 86 are more important under thermal desorption conditions, and the  $m/z$  43, 71, 101, and 114 peaks tend to be more important under laser desorption conditions. Still other shifts in decomposition intermediates result when decomposition is induced by mechanical stress, as outlined in the following section.

### **Detection of Shear-Induced Fragments with no Laser Desorption**

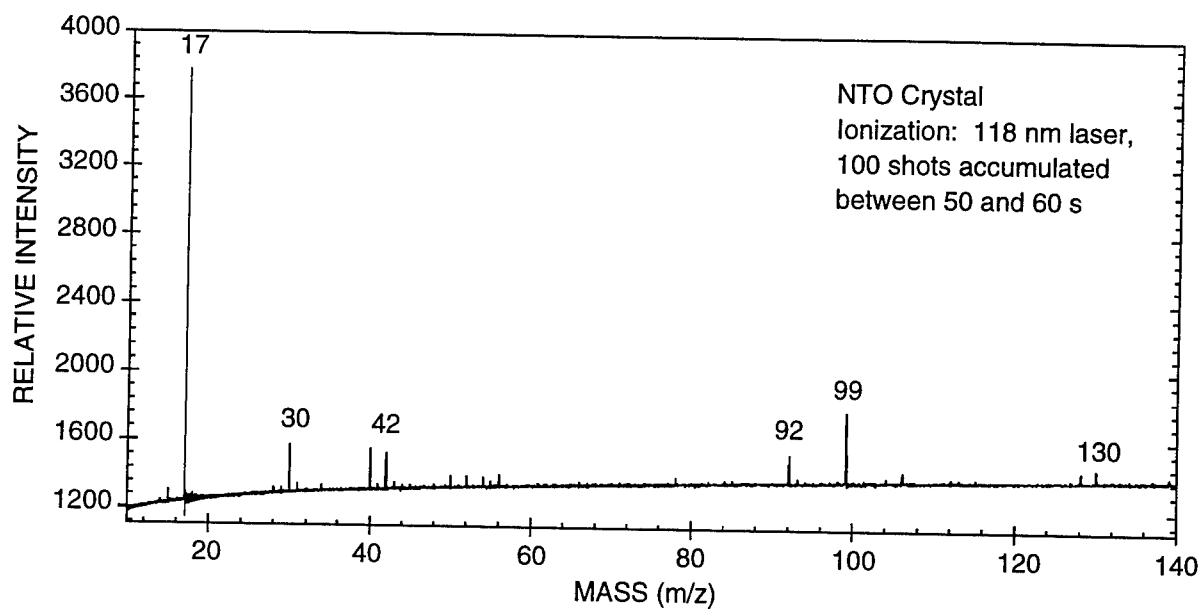
Figure 12 shows single-shot spectra recorded 3.3 and 273.3 ms after initial contact of the shear cutting tool. Figure 13 is the sum of 100 ionizing laser shots, recorded in the interval between 50 to 60 seconds after shear. The decay of  $m/z$  99, the dominant peak in these spectra, is plotted in Figure 14. The intensity of this peak fluctuates initially (on the millisecond time scale) after pellet fracture and then decays slowly over the next 100 seconds.

These shear-induced spectra contrast markedly with laser-desorption spectra obtained without the shear stress. In the shear-induced spectra,  $m/z$  71 and 114 are gone.  $M/z$  100 and 101 are also gone, having been replaced by  $m/z$  99, which dominates the spectra to an extent that no single fragment peak did under laser-desorption conditions. Since  $m/z$  99 was *completely* absent ( $< 0.05\%$  of the base peak) in the laser-desorption mass spectra, it is clear that under conditions of mechanical stress there has been a very profound shift towards this intermediate.



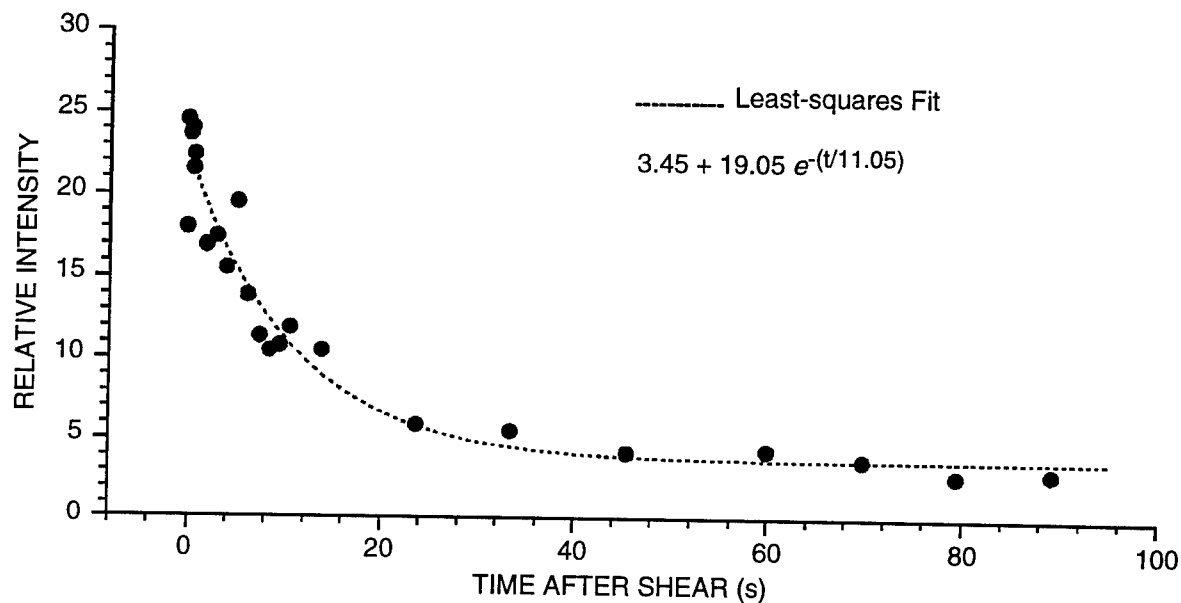
CAM-6134-14

Figure 12. Single-shot SALI spectra of shear-induced fragment emission taken 3.3 and 273.3 ms after shear.



CAM-6134-15

Figure 13. 100-shot SALI average SALI spectrum of shear-induced fragment emission accumulated between 50 and 60 seconds after shear.



CAM-6134-16

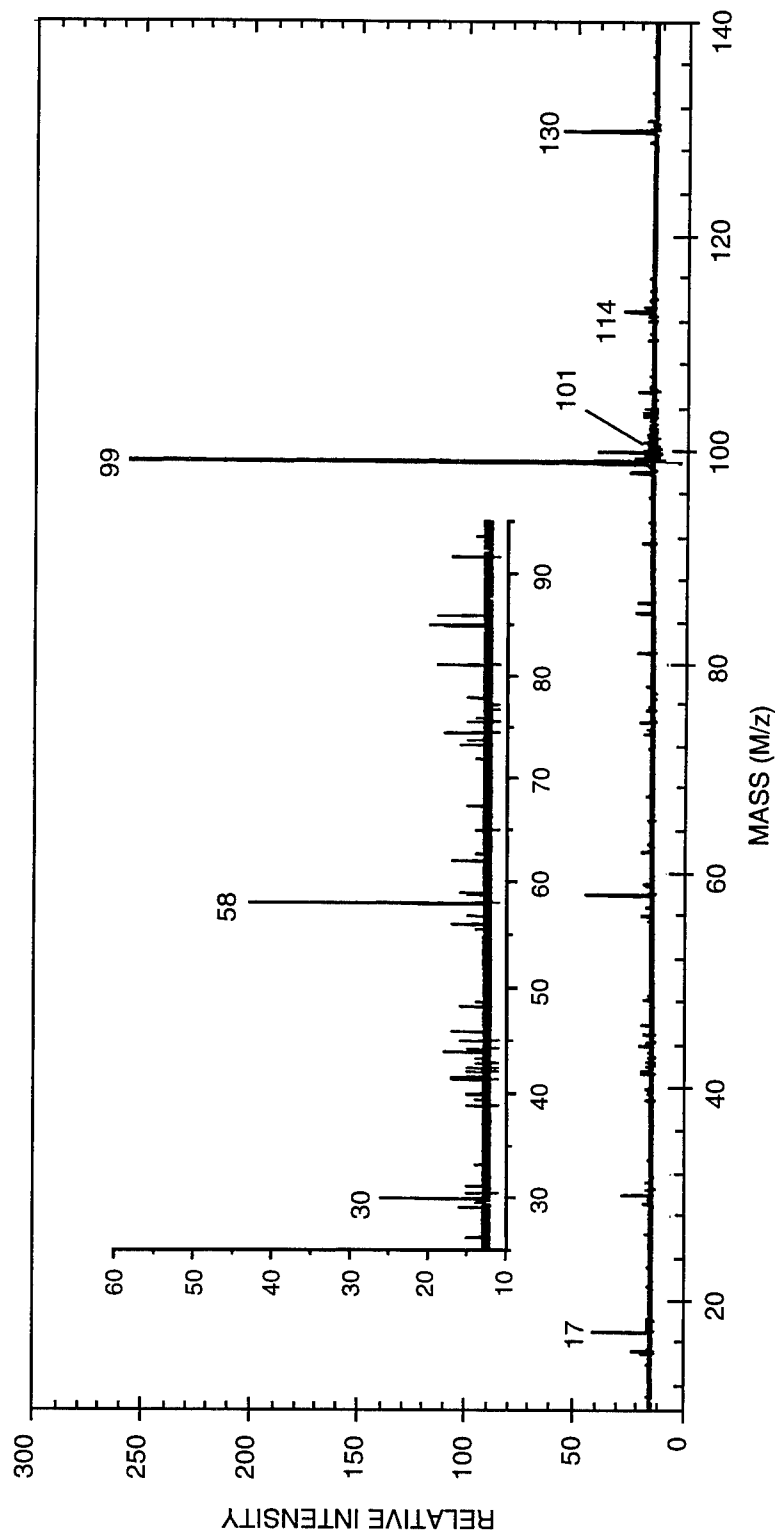
Figure 14. Decay of m/z 99 intensity following simple-shear test.

## Shear-Induced NTO Decomposition on the 100- $\mu$ s Time Scale

As indicated in the experimental section, 3 milliseconds is roughly 1000 times longer than required for thermal fragments to travel the roughly 1 mm from the fracture surface to the ionization region. The shear-induced spectra shown above cannot arise from fragments that depart the shear surface anytime close to the time of fracture completion. We wished to examine fragments emitted from the fracture surfaces within as short a delay time as possible after the shearing took place, in order to determine how the decomposition intermediates may have evolved since crack completion. Because practical limits on spring-applied force prevented the cutter from traveling fast enough to clear the specimen face in microseconds, rather than milliseconds, we modified the shear fixture to view the sheared pellet from the long cylindrical side, at an angle far from normal to the crack surface.

Shear-induced decomposition mass spectra of NTO were obtained with nominal delays (from the time of fracture completion) ranging from 30 to 830  $\mu$ s. These spectra varied widely, from essentially noise only to a signal/noise ratio of 200/1 for the peak at  $m/z$  99. In the latter case (Figure 15), there was a five-fold increase from the best single-shot signal/noise ratio we had observed with millisecond-time-scale viewing normal to the fracture surface and a similar increase in the intensity ratio for  $m/z$  99 and the ubiquitous  $\text{NH}_3$  peak at  $m/z$  17. Thus, in terms of signal strength, the results appeared to benefit more from going to shorter delays times than they were hurt by poor viewing angle.

Although the "better" shear-induced spectra with 100- $\mu$ s delay have substantially higher signal/noise ratios than the 3-ms delay spectra, in the "worst" cases at short delay times, there was no intensity above noise level, even at  $m/z$  99. Our attempts to reliably map the time dependence of the shear fragments have not yet been successful, with the strongest signals appearing at a nominal 30 and 630  $\mu$ s after crack completion, but with some much lower intensities at intermediate delay times. The uncertainties in velocity, position, and time indicate that the nominal time of fracture completion is accurate within  $\pm 20$   $\mu$ s. The high speed video observations (Figure 7) indicate that pellet fracture *and* separation are reproducible, at least on the resolution scale of the video ( $\sim 100$   $\mu$ m) and in the plane of observation. It is possible to have variable rotation of the separating pellet half not only in the plane of the paper, as seen in Figure 7, but also in another plane. This rotation in another plane would change the deviation of the viewing angle from  $90^\circ$  off-normal. If the emission of fragments were to follow, for instance, a  $(\cos)^2$  distribution, such variability could cause large changes in the signal intensity. Thus, the variations in signal intensity we observed could have little to do with timing uncertainty, but reflect instead varying degrees of rotation to turn a sheared face more toward the mass spectrometer.



CAM-6124-24

Figure 15. Single-shot SALI spectrum of shear-induced fragment emission of NTO, with nominal 30- $\mu$ s delay after crack completion.

Notwithstanding the uncertainties in the time dependence of the emission of the shear-induced fragments, these results show that very strong signals can be observed, on a single-shot basis, even when observing almost 90° off-normal to the nominal plane of the fracture surface(s). In the most intense single-shot spectrum we obtained (Figure 15), the intensity of  $m/z$  99 is now much greater than that of  $m/z$  17 for background  $\text{NH}_3$ , in contrast to the averaged spectrum acquired from 100 shots of the ionizing laser 50 to 60 s after shear (fracture face perpendicular to the mass spectrometer flight axis, Figure 13). Also,  $m/z$  58, which is hardly visible in the millisecond delay spectra, now clearly rises out of the background and is more intense than  $m/z$  17.

### Compressive-Impact-Induced NTO Decomposition

Compressive-impact-induced decomposition mass spectra of NTO were obtained with a 300- $\mu\text{s}$  delay after initial contact with the conical tip. At this point, the impactor has traveled roughly halfway into the conical section and produced a significant volume of fractured NTO. As with the 100- $\mu\text{s}$  delay shear spectra, these impact-induced spectra varied widely, from essentially noise only to a signal/noise ratio of 200/1 for the peak at  $m/z$  99. Figure 16 shows the most intense of these spectra. The total number of counts at  $m/z$  99 is about 200, quite similar to the results in Figure 15 for the 100- $\mu\text{s}$  delay shear-induced spectra. Also similar is that the only significant secondary peaks are  $m/z$  58, 30, and 17. As with the 100- $\mu\text{s}$  delay shear-induced spectra, a third to a half of the compressive fracture tests produced no significant intensity at  $m/z$  99,\* under conditions nominally identical to those that provided very strong  $m/z$  99 peaks.

The most striking difference in these compressive-impact-induced spectra from the shear-induced spectra taken earlier is that the molecular ion,  $m/z$  130, is now *completely* absent. The absence of  $m/z$  130 cannot simply be accounted for by an uncontrolled lowering of chamber temperature and therefore a lowering of a peak due to thermal desorption: while the chamber temperature is not specifically controlled, it does not differ appreciably from room temperature, which is always  $24 \pm 2^\circ\text{C}$ . However, the absence of any intensity at  $m/z$  130 may reflect the fact that, for species to be emitted in the compressive impact mode, they effectively need to squeeze out from the cracks in a "pile of rubble." Under these conditions, any NTO molecules that are "bumped" off the surface by movement stemming from the fracture process will have a high probability of encountering another NTO surface and being reabsorbed or condensed.

---

\*In these cases there was no intensity other than chamber background at  $m/z$  17 and anthracene mass marker at  $m/z$  178.

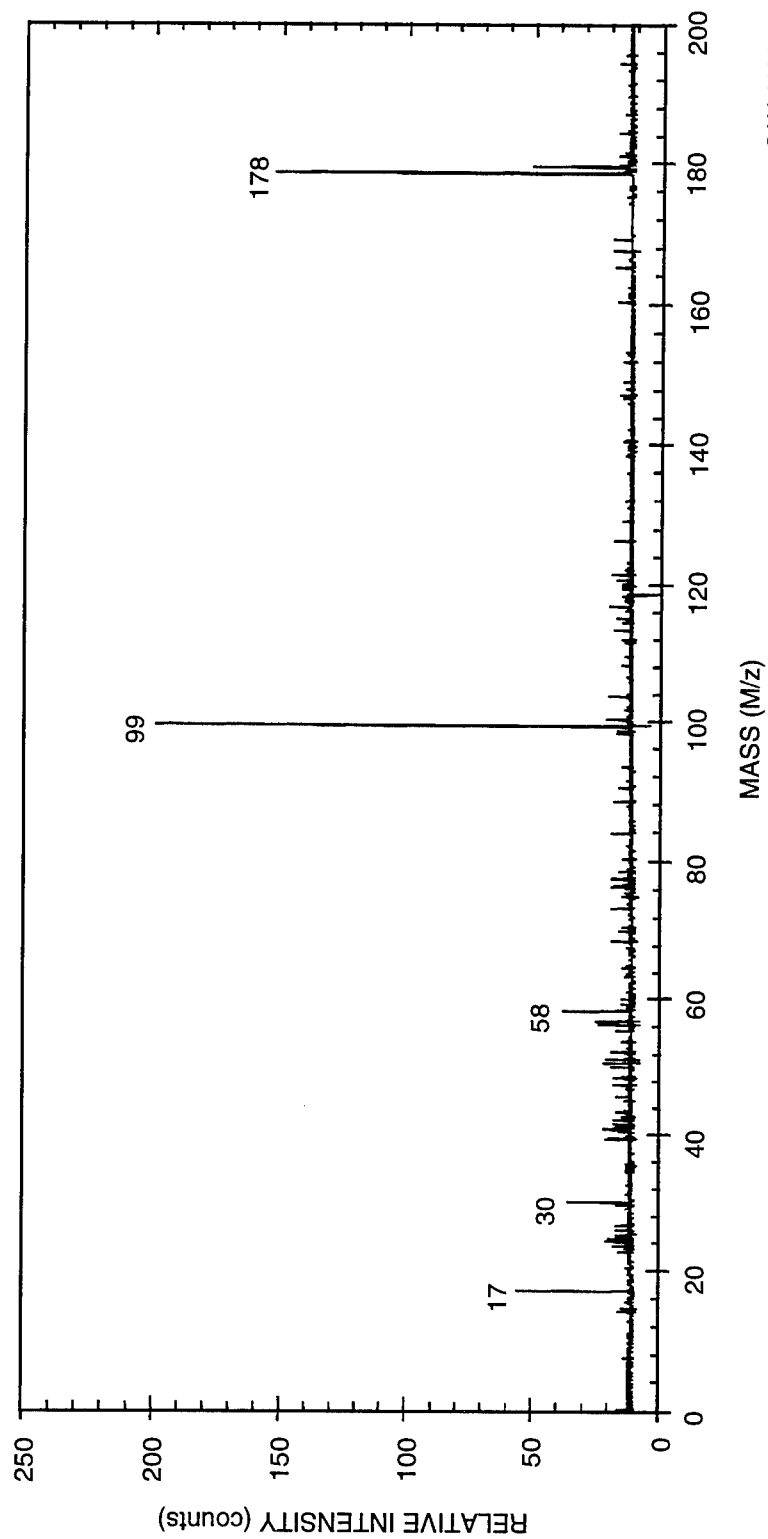


Figure 16. Single-shot SALL spectrum of compressive-impact-induced fragment emission of NTO, with nominal 300- $\mu$ s delay after initial impact.



In contrast, the simple-shear experiments, in generating a "clean" fracture surface, may provide for little opportunity to reabsorb NTO that has been bumped off the surface by a migrating shear band (see discussion below under General Mechanisms of Stress-Induced Chemical Reaction). This explanation would of course require that the lower molecular weight and lower polarity of the mass 99 species be sufficient to make its reabsorption substantially less effective than that of the mass-130 NTO.

### **Laser Desorption After Shear**

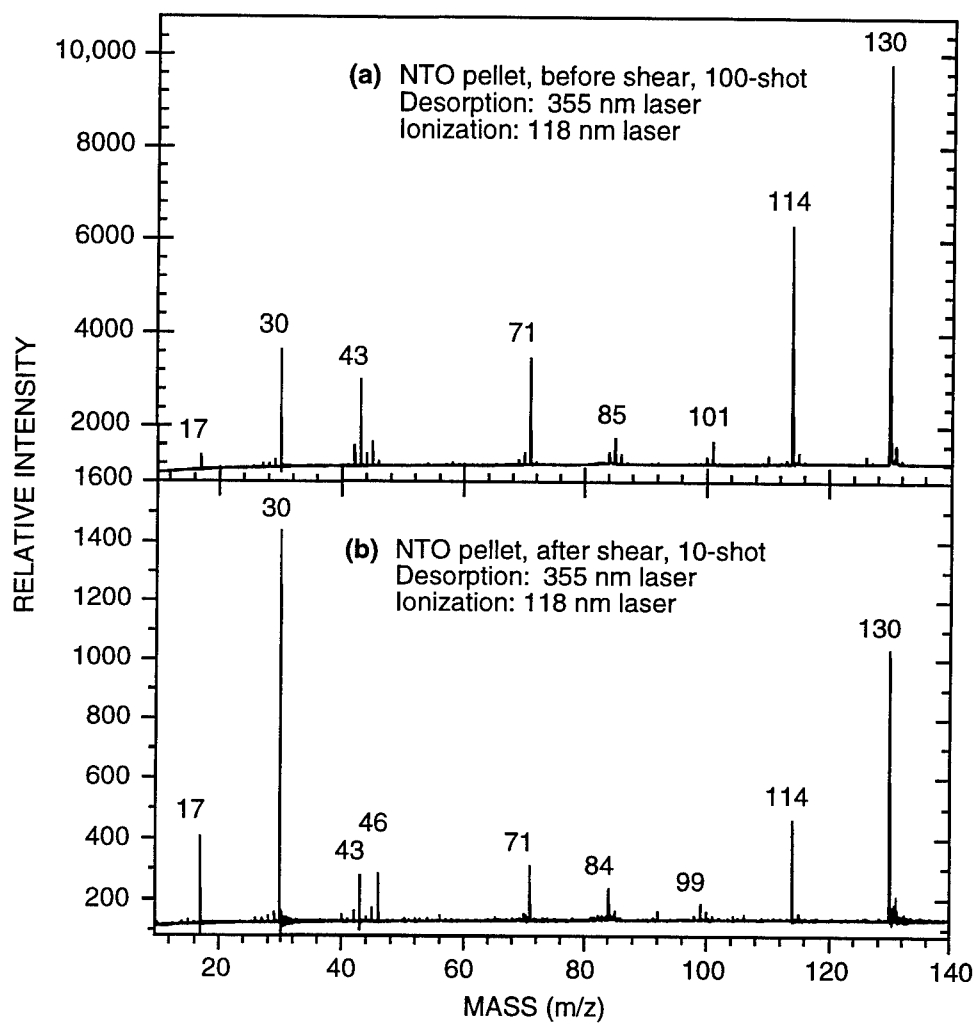
Laser desorption spectra obtained before and after shear are in general terms very similar, but some differences do exist. As Figure 17 shows, significant shear-induced signal intensity persists at  $m/z$  99 even seconds after shearing; although this intensity is quite low relative to the signals induced by laser desorption, it can be clearly seen, in contrast to the laser-desorption spectrum taken before shear, where there is *no*  $m/z$  99 visible.

### **Laser Desorption after Near-Threshold Impact**

For comparison with our real-time stress-induced measurements as well as with the recent work of Beard and Sharma<sup>12</sup> on subcritically impacted NTO, we prepared samples by subjecting them to impact in a standard drop-weight impact apparatus at the threshold of detonation (6 kg @ 55 cm), and then examining the NTO recovered from the sub-critically impacted samples. Figure 18 shows that once again the laser-desorption peaks dominate, so that at first glance they may obscure the very real differences that do exist.

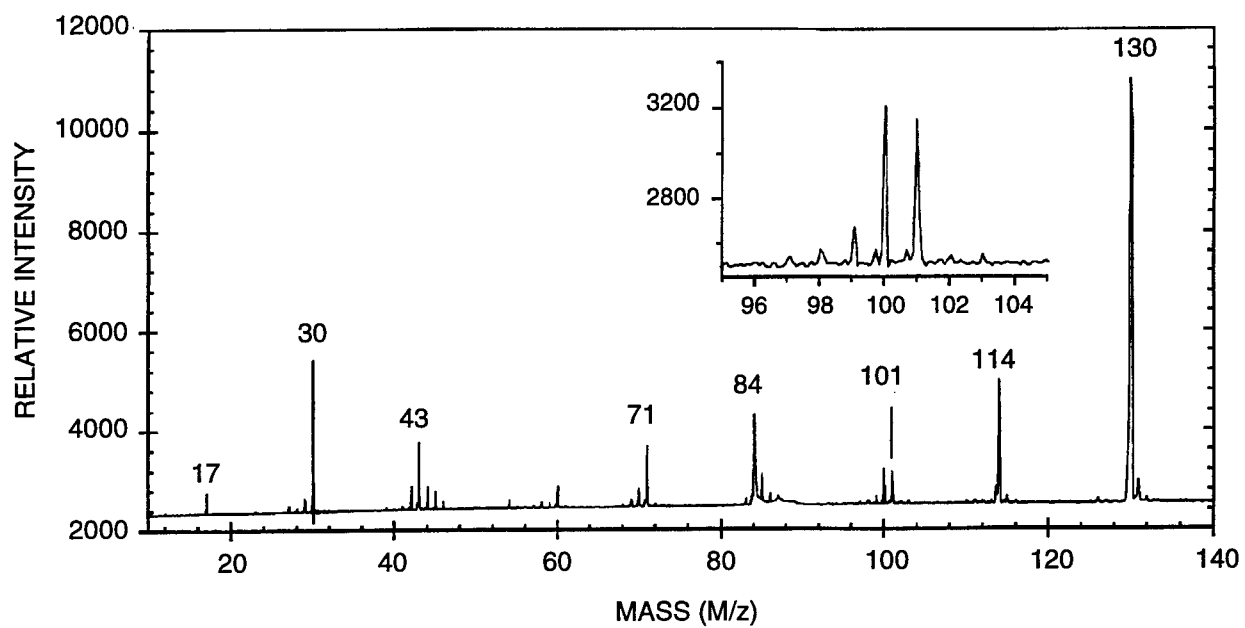
Consistent with the above results on shear- and compression-impact-induced decomposition, laser-desorption spectra of the previously impacted samples (examined about 1 hr after impact and handling in air), now show small peaks at  $m/z$  99, where previously there were none visible in the laser-desorption spectra. The  $m/z$  99 intensity is about 2% of the  $m/z$  130 intensity in the impacted NTO, compared with 1.3% in the post-examination of the sheared pellet (Figure 12b), essentially zero (i.e., <0.05%) for a fresh pellet (Figure 18), and contrasted with ~500% of  $m/z$  130 in the real-time shear-induced spectra themselves (Figures 12, 13).

Thus, the appearance of a new peak at  $m/z$  99 is common to the very modest stress caused during simple shear and to the much larger stresses resulting during marginally subcritical impact. The fact that  $m/z$  99 is stable enough for some of it to survive roughly an hour during transfer to the SALI apparatus and pumpdown is certainly consistent with the suggestion outlined below that its stability as a closed-shell species may represent a bottleneck in the NTO initiation sequence.



CAM-6134-17

Figure 17. Comparison of laser-desorption SALI spectra taken (a) before and (b) 2 s after shear test.



CAM-6134-18

Figure 18. Laser-desorption SALI spectrum of NTO recovered from a sub-critical impact test.

## Mechanistic Implications for NTO Decomposition

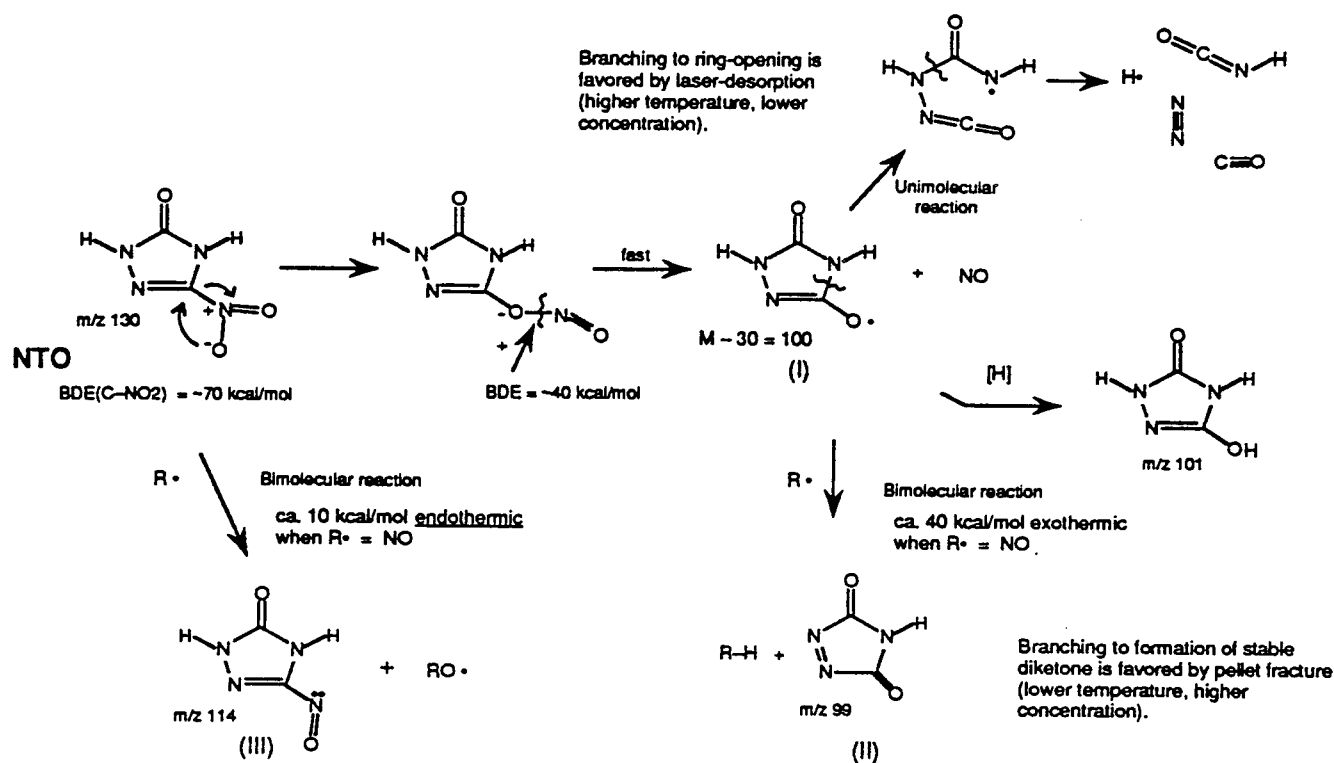
The mass spectra obtained under conditions of slow thermal decomposition, thermal decomposition induced by laser ablation, and decomposition induced by either simple shear stress or compressive impact have allowed us to view a sequence of identifiable intermediates that have not previously been reported for NTO decomposition under any conditions. From this view, we have been able to derive a plausible reconciliation of a substantial amount of literature data on NTO decomposition that previously appeared to be in conflict and to suggest how one of these intermediates may be responsible for the pronounced insensitivity exhibited by NTO.

The shear-induced- and compressive-impact-induced spectra, observed *in-situ* without laser desorption, are dominated by a peak at  $m/z$  99, which is related to peaks in the mass spectra of thermal decomposition induced by laser desorption, but which does not itself appear in those spectra. The laser-desorption mass spectra are dominated by M-16, M-30, M-45, M-46, and M-59 (giving decomposition intermediates/products at 114, 100, 85, 84, and 71 Da).

The fracture-induced and thermally induced decomposition all start with the same nitro-nitrate rearrangement and NO loss.  $M/z$  99 is most probably the closed-shell triaza-diketone resulting from H-atom removal after NO loss. Under higher temperature, lower-pressure conditions (e.g., in a laser plume), unimolecular H-atom loss from the mass 100 alkoxy radical evidently cannot compete with unimolecular ring-opening, followed by additional  $\beta$ -scission reactions to produce CO, N<sub>2</sub> and other low-mass species. However, under the higher-density, but lower-temperature conditions that result from sub-critical mechanical stress, subsequent bimolecular H-atom removal to produce the closed-shell diketone is apparently the preferred process. This relatively stable intermediate constitutes a "dead-end" that may explain the initiation insensitivity of NTO. We discuss this possibility in a forthcoming publication, and also show how this sequence satisfactorily explains earlier literature data, including (1) the "initial" formation of CO<sub>2</sub>,<sup>13</sup> (2) the results of nitrogen double-labeling experiments,<sup>14</sup> and (3) the fact that neither NO<sub>2</sub> nor HONO has been seen as a substantial initial product of NTO decomposition.<sup>15</sup> Scheme 1 is a condensed presentation of the principal reactions in the decomposition sequence.

The preferential formation of the mass 99 intermediate under marginal mechanical stress conditions can be further understood by considering the most likely candidate radicals for the necessary bimolecular H-atom removal. Under marginal conditions, where there are relatively few initial intermediates generated, and where they are constrained to remain in the vicinity of the initial reaction, the most likely candidate is the homolysis partner, the radical NO. Using published data<sup>16</sup> and group additivity procedures,<sup>17</sup> we estimate (Scheme 1) the radical disproportionation to

form HNO and mass 99 to be exothermic by about 40 kcal/mole and therefore to be very fast. On the other hand, the addition-elimination reaction between NO and another NTO molecule to generate  $m/z$  114 (also a relatively stable intermediate) is estimated to be about 10 kcal/mol *endothermic*, and to be substantially slower. Thus, in the absence of radical species that are stronger reducing agents than NO,  $m/z$  114 tends not to be generated, and NO is consumed primarily in the process of forming the mass 99 intermediate.



Scheme 1. Principal reactions in proposed NTO decomposition sequence following a nitro-nitrite rearrangement.

## General Mechanisms of Stress-Induced Chemical Reaction

Data obtained with the apparatus described are not only useful in determining the chemical decomposition mechanism of a particular material, energetic or otherwise, but also in helping to understand the general process(es) by which deposited mechanical energy causes reaction and liberates the chemical decomposition products to the gas phase. As indicated in the introduction, for a long time the question as to how mechanical energy is converted, during the initiation of

explosive decomposition, into the breaking of chemical bonds has remained unanswered. In the case of explosives or other energetic materials, the question is most often elaborated by asking whether the mechanical energy (i.e., nonrandom movement of portions of the macroscopic structure) is degraded to heat (randomized motion of the various bonding elements) within some portion of the structure (such as along a shear band), or whether the mechanical energy remains localized until it causes direct mechanical rupture of chemical bonds. In the case of synthetic polymers and other macromolecules, there is no doubt the latter sequence occurs. However, most explosives are molecular crystals or amorphous (or even liquid) composites of small molecules, where the application of mechanical stress is most likely to be relieved in the breaking of the intermolecular bonds, which are much weaker than the intermolecular bonds.

In order for self-sustaining chemical decomposition to ultimately develop, it is required that enough strong bonds be broken and enough reaction sequences proceed to the secondary (or tertiary, etc.) reactions that are exothermic and can feed energy back (either as a thermal- or shock wave) into the system. It has most commonly been considered that initiation resulting from compressive impact is the result of localized generation of frictional heat in shear bands around collapsing voids or close to an abrading grit particle. However, a substantial body of opinion has held that if the shock front is sufficiently sharp it can directly cause the rupture of bonds far stronger than the weak intermolecular bonds. It is obvious that the study of "fractoemission" processes, with substrates or under conditions that do not involve the development of self-sustaining reaction, can provide insight into this problem.

Dickinson and coworkers<sup>2-4</sup> have monitored the fractoemission phenomenon in a wide range of solid substrates, reporting the emission of neutral fragments, electrons, positive ions, and electromagnetic radiation. They have discussed several general mechanisms, and the results reported here appear to fit one of those categories.

Given that our original minimum delay time (3000  $\mu$ s ) is several thousand times the period required for thermal fragments emitted from a fracture surface to travel to the mass spectrometer ionizing region, it is perhaps surprising that we were able to detect fracture-induced fragments with relatively high single-shot signal/noise ratios (up to 200/1). That is, any fragments generated and emitted from the fracture surface at the time of the crack would, in 3 ms, have traveled far beyond the mass spectrometer sampling region. For some reason, fragments continue to be emitted for a relatively long time after that event. Dickinson and coworkers have suggested<sup>4</sup> that long-lived emission can result from the time required for deeply buried shear bands to migrate to the surface. With this general suggestion in mind, it is useful to consider what we observed when the delay time for observation was moved from milliseconds/seconds to microseconds, or when the nature of the mechanical stress was changed.

We began with no specific expectation about what would be seen with a delay of only a few hundred microseconds after the shear event, but under circumstances where a much less favorable observation angle (almost 90° off-normal) was dictated. Nor could we predict what would be seen with a much more energetic compression event, but one in which most of the new surfaces generated in the crushing are buried in the rubble pile, with little line-of-sight access to the ionization and extraction region. Dickinson et al. had earlier reported<sup>3</sup> that electronic emission from RDX samples was much stronger under compressive impact conditions, but we had no real basis for extrapolation from their conditions or from electronic emission to evolution of neutral fragments. The results described above show that with delay shortened to around 100  $\mu$ s, signals with ca. five-fold higher intensities are seen, as compared with those we saw with delays of 3 to 10,000 ms. The decay time constant shown in Figure 14 above is about 10 s. Spectra that are only five times more intense at these much shorter delays of ca. 100  $\mu$ s are indeed consistent with the long decay times measured at ca. 10 seconds, but are nonetheless intuitively surprising when considered from the following point of view.

Given that the appearance of the new fracture surface is rather monolithic, as if failure had taken place primarily along a single plane, it seems surprising that more total emission (implying more deposited energy in total) could originate from many smaller, buried shear bands than from the one large fracture that ultimately causes failure.\* One might ask if instead long decay times arise from the fact that long times are required for thermally produced decomposition products to be chemically generated. However, any heat generated locally in the shear process will dissipate extremely rapidly. For example, for a 1-mm hot spot, the time constant for conductive accommodation to the bulk temperature will be  $\sim 10$  ms). Therefore, thermally driven chemistry cannot continue for very long.

Similarly, simple vaporization of fragments like m/z 99 from the fracture surfaces should be relatively fast. Taking the cyclic imide succinimide as a model that should have vapor pressure not greatly different from the triazadiketone m/z 99, we estimate that the rate of vaporization of pure m/z 99 from a fracture surface at 20°C would be fast enough to remove one full monolayer in about 2 ms. Although this time is a lower limit, because m/z 99 would actually be desorbing from the more polar NTO surface (rather than vaporizing from a surface of the mass 99 material itself), we would *not* expect chemisorption of the triazodiketone on NTO to increase the desorption time

---

\*If we compare total emission in a presumed initial "burst" at, say 0-100 ms from the instant of completion of the main fracture, with a lower emission intensity over the period of 100 ms to 10 s, the "initial" intensity would have to be higher by a factor of  $10 \text{ s} / 100 \times 10^{-6} \text{ s} = 10^5$  for the total species emitted initially to exceed the total of those emitted over the 100-ms to 10-s time period.

by three orders of magnitude.\* Thus, it appears that slow decay of the intensity of  $m/z$  99 must involve something more than simple slow desorption of decomposition fragments from the fracture surface.

Returning to the suggestion that the decomposition products may be generated within shear bands that are not exactly at the surface, we can readily estimate the diffusion time for such products. Assuming that the depth of such shear bands is typically a maximum of  $10\text{ }\mu\text{m}$ ,<sup>18</sup> a diffusion coefficient typical<sup>19</sup> of organic solute diffusion in solid polymers,  $2 \times 10\text{ cm}^2/\text{s}$ , would lead to a characteristic diffusion time of about 2 s, and a diffusion depth of  $1\text{ }\mu\text{m}$  would lead to a diffusion time of about 0.02 s. Thus, material rising from  $\sim 10\text{-}\mu\text{m}$  depths within the fracture surface could possibly account for the long delay times observed here.

The specific observations of Dickinson et al.<sup>3</sup> on fracto-emission of RDX crystals seem very relevant to our results showing quite long-lived emissions of fractured NTO. These authors note that, when the single-crystal three-point bend fracture surfaces are smooth, the emission tends to be low level and short lived (decay time constant  $\sim 20\text{ ms}$ ), but when the fracture surfaces are rougher, even with the same three-point bend procedure, the emission tends to be substantially more intense and to have a much longer decay time ( $\sim 300\text{ s}$ ). Similarly, the compressive failure of RDX produced more intense, long-lasting emission. A three-point bend that produces a quickly growing crack under pure tensile stress may generate electrons and other decomposition fragments, as Dickinson proposes,<sup>3</sup> via a gaseous electric discharge driven by rapid charge separation on the two parting surfaces. However, when the stress is more complex (e.g., containing a significant shear or compression component), fracture may involve production of shear bands that do not lie exactly at the new fracture surface, and therefore, whose decomposition products require time to diffuse to the surface.

An alternative explanation for the long decay times is that mechanical energy not released in the initial crack formation is stored as strain that is released bit by bit as time goes on. Each release of strain could generate local hot spots and cause additional chemical reaction. However, this latter variation seems less likely because we expect these later releases would have to involve much less energy than the original crack propagation and would lead to a more pronounced decrease in emission intensity with time.

We have not in this work made observations within the flight time ( $\sim 1\text{ }\mu\text{s}$ ) of fragments emitted in the initial crack growth event (which would have provided a direct assessment of intensity decline from the very beginning). The present experimental arrangement allows *in*

---

\*The published "vacuum stability" of NTO corresponds to a vaporization time of about 30 ms per monolayer at  $100^\circ\text{C}$  even for NTO itself.



*principle* for such measurements, but because the repetition rate of the ionizing laser is 10 Hz, all time dependence to be mapped out on a finer than 100-ms time scale requires an entire series of experiments, each with a new pellet introduced separately into the vacuum chamber. Such an approach is time consuming when the time grid is 100  $\mu$ s; it becomes impractical when the time grid is 10  $\mu$ s or less.

At this point, we believe that the most useful application of the techniques developed here involves use at the millisecond time scale (and selectively at the 100  $\mu$ s scale) to study the effects of chemical variations in the material to be fragmented, in order to test the chemical explanations we have put forward for the sequence of observed intermediates and for the origin of NTO's insensitivity. The variations useful for NTO would include (1) isotopic substitution to confirm structures of speculatively identified intermediates, (2) additives that would influence competitive reactions and change branching ratios, (3) other explosive materials, alone and in combination with NTO, and (4) compositions that include either the NTO intermediates identified here or sources of those intermediates other than NTO itself.

## SUMMARY AND CONCLUSIONS

Installation of a spring-driven shearing device in a laser-desorption mass spectrometry apparatus has allowed us to conduct controllable *in-situ* fracture of pellets of the high-explosive NTO and to obtain high-quality spectra of the spontaneous fragment emission that results. We have compared these spectra with standard thermal-desorption and laser-desorption spectra of NTO obtained in the same apparatus. The most pronounced difference between these two categories of spectra is the appearance of  $m/z$  99 as the dominant peak in the fracture-induced spectra, while this peak is entirely absent in the slow thermal and laser-desorption spectra. The laser-desorption spectra themselves have allowed us to identify thermal fragments of NTO not previously reported and to suggest an NTO decomposition sequence that reconciles previously disparate literature data on NTO. The ability to record real-time fracture-induced spectra has allowed us to see the unexpected appearance of  $m/z$  99, which is entirely unobservable in the various thermal desorption spectra. This observation in turn has prompted the suggestion that the origin of the marked initiation insensitivity of NTO may result from an increased tendency to form this relatively stable closed-shell intermediate under conditions of sub-critical mechanical stress: bimolecular hydrogen-transfer processes under condensed phase (i.e., high concentration), low-temperature conditions of mechanical stress may shift the branching ratio in decomposition toward a relative dead end. The capability demonstrated here offers the potential for sensitive and very direct monitoring of the sequence of reactions that occurs as a result of mechanical energy input to various explosive and nonexplosive materials.

## ACKNOWLEDGMENTS

*Support for this research by the Air Force Office of Scientific Research, under AFOSR Contract No. F49620-94-C0055 is gratefully acknowledged. We thank Program Manager Dr. Michael Berman for helping to maximize the connection between this work and other fundamental and applied studies of NTO. We also appreciate the courtesy of Mr. Stephen Aubert and Gary Parsons of Eglin Air Force Base in supplying us with samples of the same material used in the USAF NTO formulation studies, as well as guidance in the hot-pressing of NTO.*

## REFERENCES

1. See, for example, J. Kang, P. B. Butler, and M. R. Baer, *Combustion and Flame* **89**, 117 (1992).
2. K. Y. Lee, L. B. Chapman, M. D. Coburn, *J. Energetic Materials* **5**:27 (1987).
3. J. T. Dickinson, J. T. Miles, W. L. Elban, R. G. Rosemeier, *J. Appl. Phys.* **55**, 3994 (1984).
4. J. T. Dickinson, L. C. Jensen, S. C. Langford, *Phys. Rev. Lett.* **66**, 2120 (1991).
5. C. H. Becker, and K. T. Gillen, *Anal. Chem.* **56**, 1671 (1984).
6. J. B. Pallix, U. Schule, C. H. Becker, and D. L. Huestis, *Anal. Chem.* **61**, 805 (1989).
7. C. He, J. N. Basler, and C. H. Becker, *Nature* **385**, 797.
8. D. F. McMillen, D. C. Erlich, C. He, C. H. Becker, and D. A. Shockey, *Combustion and Flame* **111**, 133.(1997).
9. S. Aubert, "Characterization of the Hydrodynamic Performance Properties for NTO and TNTO Composite Explosives," Final Report WL-TR-94-7037 for Wright Laboratory, Armament Directorate, May 1994.
10. S. Aubert, J. D. Corley, and J. G. Glenn, "Development of TNTO Composite Explosives," Final Report WL-TR-92-7073 for Wright Laboratory, Armament Directorate, June 1993.
11. J. F. Kalthoff and S. Winkler, "Failure Mode Transition at High Rates of Shear Loading," in *Impact Loading and Dynamic Behavior of Materials*, Eds. C. Y. Chiem, H.-D. Kunce, S. W. Meyer, DGM Informationsgesellschaft: Germany, 1988, pp. 185-195.
12. B. C. Beard and J. Sharma, *J. Energetic Materials* **11**, 329 (1993).
13. T. R. Botcher, D. J. Beardall, and C. A. Wight, *J. Phys, Chem.* **100**, 8802 (1996).
14. J. Oxley, J. L. Smith, K. E. Yeager, E. Rogers, and X. X. Dong, *J. Phys, Chem. A* **101**, 3531 (1997).
15. G. K. Williams, S. F. Palopoli, and T. B. Brill, *Combustion and Flame* **98**, 197 (1994).
16. L. Batt., G. N. Robinson, "Thermochemistry of Nitro Compounds, Amines, and Nitroso Compounds," in *Chem. of Functional Groups, Suppl. F*, Ed., S. Patai, John Wiley and Sons, Ltd., London, 1981.
17. S. W. Benson, *Thermochemical Kinetics*, Second Edition, John Wiley and Sons, New York, 1976.
18. V. K. Mohan, V. C. J. Bhasu, and J. E. Field, *Proceedings of the Ninth Symposium (International) on Detonation*, 1988, p. 557.
19. E. L. Cussler, *Diffusion: Mass Transfer in Fluid Systems*, Cambridge University Press, 1984, p.130.